INVESTIGATING AGE-DEPENDENT ARTHROPATHY IN A CIRCADIAN MUTANT MOUSE MODEL

A Dissertation Presented

By

Elizabeth An Yu

Submitted to the Faculty of the
University of Massachusetts Graduate School of Biomedical Sciences, Worcester
in partial fulfillment of the requirements for the degree of

DOCTOR OF PHILOSOPHY

June 9, 2011

MD/PhD Program in Biomedical Sciences

INVESTIGATING AGE-DEPENDENT ARTHROPATHY IN A CIRCADIAN MUTANT MOUSE MODEL

A Dissertation Presented
By

Elizabeth An Yu

The signatures of the Dissertation Defense Committee signifies completion and approval as to style and content of the Dissertation

_____
David R. Weaver, Thesis Advisor

_____
Paul J. Fanning, Member of Committee

_____
Paul R. Odgren, Member of Committee

_____
Janet L. Stein, Member of Committee

_____
Carolyn M. Macica, External Member of Committee

The signature of the Chair of the Committee signifies that the written dissertation meets the requirements of the Dissertation Committee

_____
William J. Schwartz, Chair of Committee

The signature of the Dean of the Graduate School of Biomedical Sciences signifies that the student has met all graduation requirements of the school.

_____
Anthony Carruthers, Ph.D.,
Dean of the Graduate School of Biomedical Sciences

MD/PhD Program in Biomedical Sciences
June 9, 2011

ACKNOWLEDGEMENTS

I would like to thank Dr. David R. Weaver, my mentor, for giving me the opportunity to learn and develop as a scientist in his laboratory. His ability to recognize when I needed help and when it was better to let me stubbornly experiment on my own has enabled me to learn more than I could have imagined. He is an incredible teacher with a fascinating sense of humor. I greatly appreciate his endless support, especially when I opted to pursue a project outside of his expertise. Our tangential conversations were always entertaining and I thank him for being such an easy-going and encouraging mentor. It has been such a pleasure working with him for the past four years.

The development of my thesis project could not have been possible without the collaboration of Dr. Jane. B. Lian, who graciously welcomed me and my crazy project into her lab. She let me fumble around her lab and learn from all of the talented people working there, in particular Sadiq Hussain, Tripti Gaur, Stacey Russell, Kimberly LeBlanc, and Jonathan Gordon. Without Jane's collaboration and insightful suggestions, this project would not have been possible.

Members of my thesis research advisory committee provided me with the guidance and feedback to shape and develop this project. Dr. Paul J. Fanning candidly shared protocols, advice, and assisted in data interpretation that was otherwise totally over my head. Dr. Janet Stein's realistic observations and interpretation of data were invaluable to the development of this project. Dr. William Schwartz, my fearless committee chair, was always straightforward but jovial, and his forthcoming advice

helped quiet my many anxieties about marrying clinical practice and scientific research (for the time being!). Paul, Janet, and Bill all kindly agreed to serve on my dissertation examination committee, in addition to Dr. Paul Odgren and Dr. Carolyn Macica, whom I thank for donating their time to provide feedback and suggestions.

I would also like to thank Dr. Steven M. Reppert, our department chair, for his academic support and generosity, and Dr. Peter Newburger, my MD/PhD advisor, for his helpful suggestions, assistance, and encouragement. Drs. Robert Dallmann and Jason DeBruyne, past members of the Weaver and Reppert labs, were the first to observe arthropathy in *Clock*$^{-/-}$*;Npas2*$^{m/m}$ double mutant mice and without their astute observations I would never have had a thesis project. Dr. J.P. Etchegaray and Christopher Lambert, past and present members of our lab, were an invaluable source of guidance and an entertaining distraction at times. Drs. Christine Merlin, Stanley Heinze, and Patrick Guerra of the Reppert lab, were always supportive, helpful, and encouraging. I thank all of these people for their advice and time, without which I would have been lost in the fog of science.

There are multiple people who helped me along the way with other protocols and procedures: Rubing Zhao-Shea (Tapper lab), Cathy Whittle (Akbarian lab), Keith Reddig (Li lab), Dr. Paul Furcinitti, and Dr. Kip Sluder. My brief stint in studying Alzheimer's disease was buoyed by Dr. Jianhua Zhou, Ming Chung Kan (Richter lab), and members of my qualifying committee: Dr. William Schwartz, Dr. Paul Dobner, Dr. Neil Aronin, and Dr. Zuoshang Xu.

I would also like to thank the MD/PhD program, the Program of Neuroscience, and all of its faculty and administrators for making this training program possible and for keeping me on track.

For emotional support, I turned to my family and friends who were always there with sympathetic smiles and encouraging words. Jeffrey Hsiao, Dr. Jehan Ghany, Dr. Michelle Trivedi, my tennis ladies, and countless others were unrelenting in their support and humor to make me smile, which I relied on more than once to make it through this training. I thank my godfather, Dr. Yen Li, who helped me find my very first summer research internship, which fostered my interest in bench research. I thank my parents, Ko and Lee Chun-Ma Yu, for always believing in me and supporting my choices, and my brother, Gene, for serving as a lifelong role model. I thank my future mother-in-law, Dr. Nancy DeTora, for copious home cooked meals, compassionate conversation, and priceless dog-sitting services. Lastly, I thank my unbelievably understanding and loving fiancé, Adam, who tolerated my late-nights in lab, early mornings at tennis before lab, and general absence as I worked on this dissertation. Thank you all for your generosity, understanding, and support – I would not have made it this far without you standing behind me, urging me toward the finish line.

ABSTRACT

Ectopic calcification can cause pain and limit mobility. Studies suggest that circadian genes may play a role in the calcification process. Core circadian genes *Clock*, *Npas2*, and *Bmal1* are transcription factors that form CLOCK:BMAL1 or NPAS2:BMAL1 transactivator complexes that drive the rhythmic expression of circadian oscillator genes and output genes. Circadian oscillator genes *Period1-3* and *Cryptochrome1-2* encode proteins that form transcription repressor complexes that feedback to inhibit CLOCK/NPAS2:BMAL1 activity, thus completing the feedback loop that is the basis of the molecular circadian clockwork. Arrhythmic *Bmal1*$^{-/-}$ mice exhibit site-specific, age-dependent arthropathy. While studying the circadian phenotype of *Clock*$^{-/-}$*;Npas2*$^{m/m}$ double mutant mice, we discovered that these double mutant mice develop site-specific arthropathy similar to the arthropathy described in *Bmal1*$^{-/-}$ mice. Based on the circadian clockwork mechanism, we hypothesized that CLOCK/NPAS2:BMAL1 transactivator complexes drive the expression of a gene (or genes) that prevents age-dependent arthropathy. To investigate *Clock*$^{-/-}$*;Npas2*$^{m/m}$ double mutant mouse arthropathy, we evaluated mutant mice using X-ray, micro-computed tomography, and histology, and found that *Clock*$^{-/-}$*;Npas2*$^{m/m}$ double mutant mice exhibit age-dependent, site-specific arthropathy that phenocopies that of *Bmal1*$^{-/-}$ mice. The costosternal junction and calcaneal tendon are most prominently affected, in that calcification of those tissues is detectable as early as 4-5 weeks and 11-12 weeks, respectively. The arthropathic lesions in these tissues consist of calcium phosphate

deposits, and in *Bmal1*$^{-/-}$ costosternal junction calcifications, the deposits contain calcium pyrophosphate dihydrate crystals. Mechanical stress, disregulation of centrally-regulated circadian rhythms, and systemic serum mineral imbalances likely do not contribute to this pathology. *In vitro* micromass cultures generated from *Clock*$^{-/-}$*;Npas2*$^{m/m}$ double mutant mouse embryonic fibroblasts do not exhibit irregular chondrocyte differentiation compared to wild-type cultures, suggesting that chondrocyte cell-autonomous mechanisms are insufficient to induce this arthropathy. Analysis of *Clock*$^{-/-}$*;Npas2*$^{m/m}$ double mutant intersternebral tissue RNA did not reveal significant changes in chondrocyte or calcification-related gene expression. Histological stains showed an absence of osteoblasts and osteoclasts around costosternal junction calcifications, suggesting that these cell types are not contributing to this pathology. Instead, chondrocytes are localized to the costosternal junction but there were no significant changes in the distribution of chondrocyte markers in this tissue, as evaluated by immunohistochemistry. These findings suggest that *Clock* or *Npas2*, and *Bmal1*, regulate ectopic calcification through a combination of systemic and local factors, and that the cells affected by *Clock* and *Npas2*, or *Bmal1*, disruption are a subset of the cells distributed in specific tissues that develop age-dependent arthropathy. The significance of these findings is that “circadian genes” play a role in the regulation of ectopic calcification in a non-oscillator capacity. Understanding this new mechanism by which ectopic calcification is controlled could lead to novel approaches for the treatment of some human calcification diseases.

TABLE OF CONTENTS

LIST OF TABLES

LIST OF FIGURES

Chapter I: *Introduction*

Chapter II: *Characterizing arthropathy in* Clock$^{-/-}$;Npas2$^{m/m}$ *double mutant mice*

LIST OF ABBREVIATIONS

Age-dep.	age-dependent
ALP	alkaline phosphatase
ALT	alanine aminotransferase
ANK	ankylosis protein
ANKH	ankylosis protein homolog
ANOVA	analysis of variance
ARNT	aryl hydrocarbon receptor nuclear translocator
AS	ankylosing spondylitis
Bmal1	brain and muscle ARNT-like protein-1
BMP2	bone morphogenic protein 2
BSA	bovine serum albumin
BSI	backscatter electron imaging
BFR/TV	bone formation rate/tissue volume
C5	cervical vertebra 5
CA1-CA3	caudal vertebra 1 – caudal vertebra 3
CC	chondrocalcinosis
Clock	circadian locomotor output cycles kaput
COG	clock output gene
CPPD	calcium pyrophosphate dihydrate
CPPD-CDD	calcium pyrophosphate dihydrate crystal deposition disease
Chromatin-IP	chromatin-immunoprecipitation
Cry	cryptochrome
CT	calcaneal tendon
Dbp	D-element-binding protein
DD	constant darkness
DISH	diffuse idiopathic skeletal hyperostosis
DMEM	Dulbecco's modified eagle medium
DMEM+15%FBS	DMEM supplemented with 15% FBS
EC	ectopic calcification
EDTA	ethylenediaminetetraacetic acid
EGTA	ethylene glycol tetraacetic acid
Enpp1	ectonucleotide pyrophosphatase phosphodiesterase 1
F12	1X Nutrient Mixture F12 Ham's
F12+15%FBS	F12 media supplemented with 15% FBS
FBS	fetal bovine serum
FGF23	fibroblast growth factor 23
FGFR3	fibroblast growth factor receptor 3
GABA	gamma-aminobutyric acid
GAPDH	glyceraldehyde-3-phosphate dehydrogenase

HA	hydroxyapatite
HBM	high bone mass
HDAC	histone deacetylase
HIF-1α	hypoxia-inducible factor-1α
HIF-2α	hypoxia-inducible factor-2α
HO	heterotopic ossification
IC	inconclusive data
IHC	immunohistochemistry
Ihh	Indian hedgehog
Inflamm.	inflammatory
ISH	*in-situ* hybridization
ISS	intersternebral space
kl	*Klotho* mutation
L2, L5, etc.	lumbar vertebra 2, lumbar vertebra 5, etc.
LD	light:dark
M	muscle
MEF	mouse embryonic fibroblast
Mgp	matrix gla protein
Micro-CT	micro-computed tomography
N/A	not applicable
NC	no change
Npas2	neuronal PAS domain-containing protein-2
NPP1	(ecto)nucleotide pyrophosphatase phosphodiesterase 1
nt	nucleotides
OA	osteoarthritis
Ocn	osteocalcin
OU	our unpublished data
OPLL	ossification of the posterior longitudinal ligament (of the spine)
P0, P1, etc.	passage-0, passage-1, etc.
PBS	phosphate buffered saline
PC-1	plasma cell membrane glycoprotein-1
Per	period
PFA	paraformaldehyde
PHEX	phosphate-regulating gene with homology to endopeptidases on the X chromosome
P_i	orthophosphate
PLP	paraformaldehyde-lysine-periodate
PP_i	inorganic pyrophosphate
PTHrP	parathyroid hormone-related peptide
R	rib cartilage
RNAi	RNA interference
ROI	region of interest
RT-PCR	real-time polymerase chain reaction
S1-4	sacral vertebrae 1-4

SCN	suprachiasmatic nucleus
SEI	secondary electron imaging
SEM	scanning electron microscope/microscopy
ST	sternebral trabeculae
T3, T5, etc.	thoracic vertebra 3, thoracic vertebra 5, etc.
TNAP	tissue-nonspecific alkaline phosphatase
TSPC	tendon stem/progenitor cell
TUNEL	terminal deoxynucleotidyl transferase dUTP nick end labeling
UMMS	University of Massachusetts Medical School
Vgat	vesicular GABA transporter
XLH	X-linked hypophosphatemia

LIST OF GENE & PROTEIN SYNONYMS

ALP	*Alp1, Akp2, TNAP, TNSALP*
Bmal1	*Arntl, Mop3, Arnt3*
Npas2	*Mop4*
NPP1	ENPP1, PC-1
Runx2	*Cbfa1, Aml3*

PREFACE

In addition to my thesis project, I also contributed to other projects in the Weaver Laboratory that resulted in three publications on which I am a co-author (see below). These publications are publicly available online.

Etchegaray, JP, Machida, KK, Noton, E, Constance, CM, Dallmann, R, Di Napoli, MN, DeBruyne, JP, Lambert, CM, **Yu, EA**, Reppert, SM, Weaver, DR. Casein Kinase 1 delta regulates the pace of the mammalian circadian clock. Mol Cell Biol. 29: 3853-3866. 2009.

Etchegaray, JP, **Yu, EA**, Indic, P, Dallmann, R, Weaver, DR. Casein kinase 1 delta regulates period length in the suprachiasmatic circadian clock in vitro. PLoS One. 5:e10303. 2010.

Yu, EA, Weaver, DR. Disrupting the circadian clock: Gene-specific effects on aging and other phenotypes. (Review.) Aging. 2011.

CHAPTER I

Introduction

An arrhythmic, circadian mutant mouse model was created in our laboratory to study circadian rhythms and unexpectedly these mice develop site-specific ectopic calcification. These initial findings formed the basis of my thesis project. The purpose of this introduction is to familiarize the reader to the two topics bridged together in this dissertation: calcification and circadian rhythms. Relevant mutant mouse models are also discussed, as are select genes involved in the regulation of calcification and possible mechanisms of this pathology.

Calcification

Ectopic calcification and ossification.

Ectopic calcification is the abnormal calcification of soft tissues and can be a sign of aging [1, 2]. Ectopic calcifications are typically composed of calcium phosphate salts, such as hydroxyapatite (HA) or calcium pyrophosphate dihydrate (CPPD), and can arise by two mechanisms: metastatic and dystrophic calcification. Metastatic calcification is widespread ectopic mineralization that occurs secondary to systemic mineral imbalances, such as hyperparathyroidism. In the absence of systemic mineral imbalances, ectopic calcification is localized and referred to as dystrophic calcification, which typically occurs as a result of trauma, disease, or aging.

Ossification, on the other hand, is the formation of true bone tissue, which is organized into cortical bone and medullary space. Calcification occurs in ossification, but not vice versa. The main cells responsible for true bone tissue formation are osteoprogenitor cells, chondrocytes, osteoblasts, osteocytes, and osteoclasts. Osteoprogenitor cells are immature progenitor cells derived from undifferentiated mesenchymal stem cells and are located in the periosteum. They can differentiate into osteoblasts, which form bone, or chondrocytes, which form cartilage [3, 4]. Once osteoblasts become trapped in the bone matrix that they secrete, they are termed osteocytes [5]. Osteoclasts originate from a mononuclear, hematopoetic cell lineage and are responsible for resorbing bone [5]. Healthy bone depends upon constant turnover; a homeostasis between osteoblast (bone formation) and osteoclast (bone resorption) activity. There are three types of ossification: endochondral, intramembranous, and heterotopic (or ectopic) ossification. Endochondral and intramembranous ossification are normal physiologic processes resulting in the appropriate formation of healthy bone tissue. Endochondral ossification is marked by the presence of a hyaline cartilage scaffolding intermediate on which bone is formed, while intramembranous ossification does not incorporate a cartilage intermediate. Heterotopic ossification (HO) is pathological endochondral ossification in soft tissue where bone does not normally exist. HO is commonly associated with trauma, such as neurological injury, major joint surgery, or burns [6, 7]. Although the exact mechanisms of HO remain unclear, it is thought that mesenchymal stem cells present in soft tissue transform into osteogenic cells after appropriate inducing events, leading to bone formation in abnormal locations. An example is Achilles tendon

ossification in humans, which is rare but can occur secondary to injury [8].

Cartilage is a connective tissue closely associated with bone. It provides a cushioning effect in joints, and structure and support in other tissues. In endochondral ossification, the hyaline cartilage scaffold on which osteoblasts deposit bone matrix is created by chondrocytes. Chondrocytes are normally present in cartilage and growth plates and originate from the same mesenchymal stem cell as osteoblasts. As part of their physiologic differentiation, chondrocytes transition through four stages: resting, proliferating, pre-hypertrophic, and hypertrophic chondrocytes (Figure 1.1). All four stages are present in the growth plate of long bones, where endochondral ossification occurs, and there are well-described gene expression patterns at each stage of differentiation. Resting and proliferating chondrocytes express *Sox9* and *Col2a1*, pre-hypertrophic chondrocytes express *Indian hedgehog* (*Ihh*), and hypertrophic chondrocytes express *Col10a1* and *alkaline phosphatase* (*ALP, Akp2, or TNAP*). *Runx2* is expressed in all four stages, although to a lesser extent in hypertrophic chondrocytes. [3, 4, 9-11]. SOX9 is a transcription factor that regulates the expression of *Col2a1*, which encodes Type II collagen, the main cartilage matrix protein in hyaline cartilage. *Sox9* expression is essential for chondrocyte differentiation and cartilage formation, as $Sox9^{+/-}$ mice die perinatally and suffer from a variety of skeletal abnormalities, including hypoplasia of nearly all skeletal elements formed via endochondral ossification and premature mineralization of the vertebrae and some craniofacial bones [12, 13]. *Ihh* regulates the proliferation of chondrocytes in the prehypertrophic zone by way of a local feedback loop involving parathyroid hormone-related peptide (PTHrP). IHH stimulates the

expression of PTHrP, which then stimulates chondrocyte proliferation [9]. *Runx2* (also known as *Cbfa1* or *Aml3*) is the master gene of osteoblast differentiation but it also plays a role in chondrogenesis: it is expressed in chondrocytes and stimulates chondrocyte hypertrophy [4]. Alkaline phosphatase (ALP) is responsible for mineralizing extracellular matrix and is expressed in hypertrophic chondrocytes as well as osteoblasts [14, 15]. Hypertrophic chondrocytes calcify the surrounding cartilage and eventually apoptose, leaving enlarged lacunal spaces into which osteoblasts and blood vessels can migrate. In osteoarthritis (OA), aging articular cartilage becomes progressively calcified. Apoptotic chondrocytes in OA cartilage have been proposed to contribute to these abnormal, age-related calcifications [16-18]. It has also been reported that chondrocyte apoptosis increases with age in rodent models, both in calcified and uncalcified regions of articular cartilage [19]. Taken together, these findings suggest that abnormal chondrocyte apoptosis, which is age-dependent, could contribute to ectopic calcifications.

Hydroxyapatite (HA) and calcium pyrophosphate dihydrate (CPPD)

The two main types of calcium phosphate salts are hydroxyapatite (HA) and calcium pyrophosphate dihydrate (CPPD). HA is present in normal, healthy bone and makes up the majority of inorganic material in bone matrix [20]. HA has a P:Ca atomic weight ratio of 0.45 and its chemical formula is $Ca_{10}(PO_4)_6(OH)_2$ [21]. CPPD, on the other hand, is typically only present pathologically, has a P:Ca atomic weight ratio of 0.75, and its chemical formula is $Ca_2O_7P_2 \bullet 2H_2O$ [21]. Several calcification diseases, such as OA and CPPD crystal deposition disease (CPPD-CDD), are characterized by the deposition of

calcium phosphate salts in joints [21-23]. In OA, chondrocytes produce matrix vesicles, which are extracellular vesicles that bud from the surface membrane of chondrocytes [21]. Matrix vesicles contain enzymes that produce inorganic pyrophosphate (PP_i) and orthophosphate (P_i) [24]. At low concentrations, PP_i is an inhibitor of HA formation but at high concentrations can induce CPPD crystal deposition [25]. The key molecules involved in regulating extracellular PP_i levels, and thus the balance between HA versus CPPD deposition, are nucleotide pyrophosphatase phosphodiesterase 1 (NPP1 or PC-1, encoded by *Enpp1*), tissue-nonspecific alkaline phosphatase (TNAP, encoded by *Akp2*), and progressive ankylosis protein (ANK, encoded by *Ank*) [26] (Figure 1.2). NPP1 generates PP_i from the hydrolysis of ATP and TNAP hydrolyzes PP_i to yield P_i, which crystallizes with calcium to form HA [25-27]. ANK is a multiple-pass transmembrane protein that mediates intracellular to extracellular channeling of PP_i [28-30]. Careful homeostasis between the activities of these three proteins dictates whether or not there is calcification, and if there is, whether HA or CPPD crystals are deposited (Figure 1.2).

Circadian rhythms

Overview of circadian rhythms

Circadian rhythms are self-sustaining, endogenous, biological rhythms with a cycle length of approximately 24 hours. They respond to external cues but are maintained under constant conditions. For instance, human corticosteroid release is rhythmic (peaks after waking and decreases at the onset of sleep) and maintains its rhythmicity under

constant conditions, such as constant darkness [31]. Circadian rhythms govern changes in physiology and behavior in most organisms and their disruption can impair health and well-being. Shift work is a common cause of disrupted circadian rhythms and can increase the risk of heart disease and other major diseases in people [32].

The mammalian circadian clockwork consists of a central pacemaker in the hypothalamus and peripheral pacemakers in other tissues [33]. The central pacemaker in the mammalian brain is bilateral suprachiasmatic nuclei (SCN), which receive photic input from the retina and send signals to synchronize peripheral tissues. The SCN are responsible for generating behavioral rhythmicity, which can be visualized by running wheel actograms, while peripheral rhythms govern changes in physiology and behavior in their respective tissues. It has been shown that circadian oscillators are present within individual cells, such as fibroblasts [34, 35], neurons [36], and osteoblasts [37].

Actograms

Mice can be individually housed in cages with running wheels and every revolution of the wheel is documented electronically and plotted in an actogram. While in a 12 hour light:dark cycle, wild-type mice will entrain to the external light source by being inactive during the light phase and active during the dark phase (Figure 1.3A, left). Arrhythmic circadian mutant mice will also be inactive during the light phase but active in the dark phase, but this seemingly normal activity pattern is due to masking effects of light (Figure 1.3A, right). Arrhythmic circadian mutants lack a functioning circadian clock and so are unable to truly entrain to any external cues.

In constant darkness, wild-type mice maintain rhythmicity with a slightly less than 24-hour period length (Figure 1.3A, left). Arrhythmic mice are unable to maintain rhythms in the absence of an external light cue and so exhibit irregular activity patterns when put into constant darkness (Figure 1.3A, right).

Mammalian circadian clockwork model

The molecular basis of circadian rhythms involves interconnected transcriptional feedback loops (Figure 1.3B). Basic helix-loop-helix-PAS-containing transcription factors *Clock* (*Circadian Locomotor Output Cycles Kaput*), *Npas2* (*Neuronal PAS domain-containing protein 2*, also known as *Mop4*), and *Bmal1* (*Brain and Muscle Arnt-like protein-1*, also known as *Mop3*) encode proteins that are part of the transcriptional activator complex of the circadian oscillator. CLOCK, NPAS2, and BMAL1 heterodimerize to form CLOCK:BMAL1 or NPAS2:BMAL1 complexes that drive rhythmic expression of core clock and clock output genes (COGs) [33, 38, 39]. Core clock genes are part of the circadian oscillator feedback loop while most COGs do not feed back into the oscillator. Core clock genes include two period genes (*mPer1 & 2*), two cryptochrome genes (*mCry1 & 2*), *Rev-Erbα*, and *Rorα*. PER and CRY form heterotypic complexes that translocate into the nucleus and repress transcription by inhibiting the activity of CLOCK/NPAS2:BMAL1, thus completing a negative feedback loop [40]. REV-ERBα suppresses *Bmal1* transcription through a response element on the *Bmal1* promoter [41] while RORα drives *Bmal1* transcription [42], thus completing the other feedback loop. COGs are rhythmically expressed and initiate changes in physiology. For instance, D-

binding protein (*Dbp*) is a rhythmically expressed clock output gene [43] that regulates the expression of liver enzymes [44].

Disrupting the clock

Several mice with mutations in core clock genes have been generated to study circadian rhythms. Combinations of double mutant mice have been generated as well. Arrhythmic mutant mice discussed here have mutations in *Bmal1*, *Clock*, *Crys*, *Pers*, and/or *Npas2* [39, 45-49]. Mice lacking both *Crys* (*Cry1*$^{-/-}$;*Cry2*$^{-/-}$) or both *Pers* (*Per1*$^{-/-}$;*Per2*$^{-/-}$) are arrhythmic under constant darkness, as are *Bmal1*$^{-/-}$ mice. *Clock*$^{\Delta 19/\Delta 19}$ mutants express a dominant negative form of CLOCK that is capable of binding BMAL1 and DNA, but unable to drive transcription [38, 46, 50]. *Clock*$^{\Delta 19/\Delta 19}$ mutant mice are arrhythmic under constant darkness, and so it was concluded that *Clock*, in addition to *Bmal1*, are essential components of the circadian oscillator. Thus, it was a surprise to learn that *Clock*$^{-/-}$ mice are still rhythmic under constant darkness [51]. In the SCN, *Clock* and *Npas2* are functionally redundant and both genes must be disrupted in order to disrupt behavioral rhythmicity [39]. A different story is told for peripheral tissue, however. In liver tissue of *Clock*$^{-/-}$ mice, core clock proteins, such as PERs and CRYs, continue to be rhythmically expressed *in vivo* due to imposed rhythmicity from the SCN [51]. However, when *Clock*$^{-/-}$ liver and lung tissue are cultured *ex vivo*, they are arrhythmic [52]. *Npas2*$^{m/m}$ liver and lung tissue are rhythmic *ex vivo* just like wild-type tissue. These findings show that in *Clock*$^{-/-}$ mice, functioning SCN (due to the ability of NPAS2 to functionally substitute for CLOCK in the SCN) are able to impose rhythmicity upon peripheral tissue

oscillators, but once liver or lung tissue is disconnected from the central pacemaker, those peripheral tissues are unable to maintain synchronized rhythms. Thus, peripheral circadian oscillators require CLOCK, but not NPAS2, in order to function properly.

These arrhythmic genotypes illustrate the necessity of functioning *Bmal1*, *Clock* or *Npas2*, *Crys*, and *Pers* for the regulation of circadian rhythms in the SCN. Many studies investigating the effects of core clock gene disruption in peripheral tissues have been performed. In $Clock^{\Delta 19/\Delta 19}$ mutant and $Bmal1^{-/-}$ mice, pancreatic islets are altered leading to impaired glucose tolerance, reduced insulin secretion, and diabetes mellitus [53]. Pancreas-specific *Bmal1* disruption causes severe glucose intolerance and defective insulin production despite normal activity and feeding behavior [53, 54]. Disrupting *Bmal1* in retina causes visual defects, similar to retinal pathology observed in whole body $Bmal1^{-/-}$ mice [55]. Liver-specific $Bmal1^{-/-}$ mice are unable to properly regulate glucose homeostasis and exhibit metabolism defects in a circadian manner [56]. Mice exhibit rhythmic responses to a variety of drugs, which can be explained by the rhythmic expression of cytochrome P450, an enzyme important for metabolism of xenobiotics, in the liver [57, 58]. $Clock^{\Delta 19/\Delta 19}$ mutant and $Bmal1^{-/-}$ mice are hypersensitive to cyclophosphamide, an anti-cancer drug, and $Clock^{-/-}$ mice have altered responses to pentobarbital and ethanol [59, 60]. Clearly, peripheral oscillator genes regulate peripheral tissue physiology, as disruption of these genes can cause drastic phenotypes.

Musculoskeletal phenotypes of circadian mutant mice

There is mounting evidence that circadian genes are involved in musculoskeletal phenotypes. Core clock genes are rhythmically expressed in osteoblasts, chondrocytes, bone, and teeth, as well as osteoblastic and chondrogenic cell lines [37, 61-63].

Bmal1$^{-/-}$ mice

Bmal1$^{-/-}$ mice display dramatic age-progressive non-inflammatory arthropathy [64]. These mice develop joint ankylosis due to calcification of ligaments and tendons. By 35 weeks of age, essentially all *Bmal1*$^{-/-}$ animals have complete immobilization of weight-bearing and non-weight-bearing joints. These effects are site-specific; the areas primarily affected in *Bmal1*$^{-/-}$ mice are the calcaneal tendon, longitudinal ligaments of the vertebrae, and costosternal junctions while articular cartilage is spared. *Bmal1*$^{-/-}$ mice have also been shown to have altered skeletal muscle structure and function [65].

Per and *Cry* mutant mice

Per1$^{-/-}$;*Per2*$^{-/-}$ double knockout and *Cry1*$^{-/-}$;*Cry2*$^{-/-}$ double knockout mice display subtle skeletal defects. Starting at six weeks of age, these mice display age-progressive high bone mass (HBM) in both vertebrae and long bones [37]. *Per2*$^{-/-}$ and *Cry2*$^{-/-}$ single knockout mice also display subtle HBM in vertebrae and long bones [66]. However, soft tissue calcification has not been noted in *Per1*$^{-/-}$;*Per2*$^{-/-}$ or *Cry1*$^{-/-}$;*Cry2*$^{-/-}$ double mutants, or *Per2*$^{-/-}$ or *Cry2*$^{-/-}$ single mutants, even in animals of advanced age (our lab's

unpublished data)[37, 67].

Bmal1$^{-/-}$ versus *Per1*$^{-/-}$*;Per2*$^{-/-}$ double knockout mice

Clearly core clock genes are involved in the regulation of calcification. However, the effects of *Bmal1* disruption are most likely **not** related to its role in circadian rhythms because other arrhythmic circadian mutants, namely the *Per1*$^{-/-}$*;Per2*$^{-/-}$ and *Cry1*$^{-/-}$*;Cry2*$^{-/-}$ mutant mice, do not exhibit the same phenotype. If this arthropic phenotype were due to disruption of the circadian oscillator, one would expect to see the same phenotype regardless of how the oscillator was broken. Instead, arrhythmic *Bmal1*$^{-/-}$ mice exhibit calcification in specific soft tissues [64], while arrhythmic *Per1*$^{-/-}$*;Per2*$^{-/-}$ and *Cry1*$^{-/-}$*;Cry2*$^{-/-}$ double knockout and *Per2*$^{-/-}$ or *Cry2*$^{-/-}$ single mutant mice exhibit increased calcification within vertebrae and long bone [37, 66].

Also, the phenotype of *Bmal1*$^{-/-}$ mice is much more dramatic than the subtle phenotype of *Per1*$^{-/-}$*;Per2*$^{-/-}$ and *Cry1*$^{-/-}$*;Cry2*$^{-/-}$ double knockout mice. *Bmal1*$^{-/-}$ mice exhibit gross calcifications detectable by X-ray, a rather insensitive tool, while *Per1*$^{-/-}$*;Per2*$^{-/-}$ and *Cry1*$^{-/-}$*;Cry2*$^{-/-}$ double knockout mice reveal subtle increases in bone volume detected by micro-computed tomography (micro-CT), a very sensitive method. These phenotypic differences suggest the mechanism of calcification in these mouse strains is different and unrelated to circadian rhythms.

Tissue-specific rescue of *Bmal1* lends additional evidence to support this idea [68]. In this study, *Bmal1* expression was rescued in brain or muscle of *Bmal1*$^{-/-}$ mice. Brain-specific *Bmal1* rescue restored behavioral circadian rhythmicity but did not prevent

calcaneal tendon calcification. This result shows that restoration of central circadian rhythms is not sufficient to prevent peripheral ectopic calcification. Muscle-specific *Bmal1* rescue was not sufficient to prevent ectopic calcification either, further supporting the finding that ectopic calcification in *Bmal1*$^{-/-}$ mice is site- and tissue-specific [68].

Clock$^{-/-}$*;Npas2*$^{m/m}$ double mutant mice

In the course of studying *Clock*, *Npas2*, and *Bmal1*, our laboratory observed that *Clock*$^{-/-}$*;Npas2*$^{m/m}$ double mutant mice develop severe, site-specific arthropathy similar to that observed in *Bmal1*$^{-/-}$ mice. Due to the overlapping roles of *Clock* and *Npas2* in the SCN clock [39], the emergence of such a similar phenotype is not surprising from a molecular standpoint. Disrupting *Clock* and *Npas2*, or *Bmal1*, leads to the same molecular effect: lack of CLOCK/NPAS2:BMAL1 transcription factor heterodimers. My hypothesis is that **CLOCK or NPAS2, and BMAL1, drive the expression of a gene or genes that prevents age-dependent ectopic calcification** in a pathway separate from the one in which PER and CRY act, because disruption of *Per1/2* and *Cry1/2*, the circadian oscillator repressors, leads to a different skeletal phenotype.

Musculoskeletal phenotypes of other mutant mice

Multiple mutant mouse lines have been developed to study bone development. While many exhibit robust calcification phenotypes, none phenocopy *Bmal1*$^{-/-}$ mice to the same extent as *Clock*$^{-/-}$*;Npas2*$^{m/m}$ double mutant mice (Table 1.1). Nevertheless, mutant

mice with varying degrees of phenotypic similarity to *Bmal1*$^{-/-}$ and *Clock*$^{-/-}$*;Npas2*$^{m/m}$ double mutant mice can be used to identify genes possibly involved in the ectopic calcification observed in *Clock*$^{-/-}$*;Npas2*$^{m/m}$ double mutant mice. Of the three molecules central to PP_i regulation, *Enpp1*$^{-/-}$ and *Ank*$^{-/-}$ mice exhibit interesting ectopic calcification phenotypes that mirror aspects of the arthropic phenotype observed in *Bmal1*$^{-/-}$ and *Clock*$^{-/-}$*;Npas2*$^{m/m}$ double mutant mice. *Akp2*$^{-/-}$ mice do not develop ectopic calcification, but the combined roles of *Enpp1*, *Ank,* and *Akp2* in extracellular PP_i regulation make *Akp2* a gene of interest as well.

<u>*Enpp1*$^{-/-}$ mice</u>

Enpp1$^{-/-}$ mice, also known as "tiptoe walking" (or *ttw/ttw*) mice, are an animal model for ossification of the posterior longitudinal ligament (OPLL) of the spine, which is a common form of human myelopathy that results from the ectopic ossification of spinal ligaments [69]. *Enpp1*$^{-/-}$ mice develop progressive ankylosing intervertebral and peripheral joint hyperostosis, as well as arterial and articular cartilage calcification and increased vertebral cortical bone formation [26, 69-72]. There is a dramatic decrease in extracellular PP_i in *Enpp1*$^{-/-}$ mice and the calcification observed in these mutants is consistent with both membranous and endochondral ossification, rather than dystrophic calcification [72]. Of particular interest is the finding that *Enpp1*$^{-/-}$ mice display ectopic calcification of their calcaneal tendon [26], a site-specific effect also observed in *Bmal1*$^{-/-}$ mice [64]. If *Enpp1* gene dysregulation is involved in the arthropic pathogenesis of *Bmal1*$^{-/-}$ and *Clock*$^{-/-}$*;Npas2*$^{m/m}$ double mutant mice, we would expect to see down regulation of

Enpp1 and/or decreased NPP1 activity in the circadian mutant mice.

ank/ank and *Ank*$^{-/-}$ mice

Mice carrying the *ank* mutation have been studied as a model of arthritis and this autosomal recessive mutation causes loss of joint mobility that spreads to most joints throughout the limbs and vertebral column as the animals age, ultimately leading to complete rigidity and death around six months of age [73]. These animals exhibit an inflammatory arthropathy with HA crystals deposited in joints [74, 75]. Although the distribution of phenotypes in *ank/ank* mutant mice does not precisely resemble any single form of human arthritis, many pathologic features in *ank/ank* mutant mice mirror classic features of other arthritic diseases, such as ectopic calcification seen in mineral deposition disease, cartilage erosion and osteophyte formation seen in OA, and vertebral fusion seen in ankylosing spondylitis [28, 76]. The *ank/ank* mutant carries a single nucleotide nonsense mutation in the *Ank* locus and it has been shown that *Ank*$^{-/-}$ mice exhibit the same phenotype as *ank/ank* mutant mice, suggesting that ANK is required to inhibit ectopic calcification [73, 77]. The human form of this protein is called ankylosis protein homolog (ANKH). There is striking similarity between *Enpp1*$^{-/-}$ and *ank/ank* mutant mice in terms of their enthesopathy, ankylosing hyperostosis of the spine, articular cartilage calcification, and peripheral joint fusion. This similarity is consistent with their shared ability to generate extracellular PP_i: ANK transports PP_i from the intracellular to extracellular environment and NPP1 cleaves ATP to generate PP_i (Figure 1.2). Therefore, PP_i regulation is critical to the regulation of ectopic calcification. Similarly with *Enpp1*

gene dysregulation, if *Ank* is involved in the arthropic phenotype of *Bmal1*$^{-/-}$ and *Clock*$^{-/-}$*;Npas2*$^{m/m}$ double mutant mice, we would expect to see down regulation of *Ank* expression and/or ANK activity in *Bmal1*$^{-/-}$ and *Clock*$^{-/-}$*;Npas2*$^{m/m}$ double mutant mice.

Akp2$^{-/-}$ mice

The *Akp2*$^{-/-}$ mouse is a mutant model of infantile hypophosphatasia, a human disease marked by osteomalacia associated with reduced serum TNAP activity [78, 79]. *Akp2*$^{-/-}$ mice lack functional TNAP, leading to hypomineralized cartilage and bone, and increased extracellular PP_i. It is unclear why the increase in PP_i does not lead to ectopic calcification in this mutant mouse model. Mutations in *Enpp1* and *Ank* lead to decreased extracellular PP_i levels while mutating *Akp2* increases extracellular PP_i levels, so it seems logical that inhibiting TNAP activity could rescue the bone mineralization phenotype in *Enpp1*$^{-/-}$ and *Ank*$^{-/-}$ mice. Interestingly, *Akp2*$^{-/-}$;*Enpp1*$^{-/-}$ double mutant mice have normal bone mineralization and extracellular PP_i levels [27], and *Akp2*$^{-/-}$*;ank/ank* double mutant mice have partial normalization of mineralization and PP_i levels [26], showing that these three molecules are key regulators of bone mineralization. If PP_i dysregulation is involved in age-dependent arthropathy of *Bmal1*$^{-/-}$ or *Clock*$^{-/-}$*;Npas2*$^{m/m}$ double mutant mice, we could see changes in ALP activity, in addition to *Enpp1* and *Ank* expression levels.

HDAC4$^{-/-}$ mice

Another gene of interest is histone deacetylase (HDAC) 4, which is a class II

HDAC capable of responding to a variety of signal transduction pathways [80]. Histone deacetylases favor chromatin condensation and transcriptional repression, counterbalancing the transcriptional activation of histone acetylation, which promotes gene transcription by relaxing chromatin structure by facilitating access of the transcriptional machinery to DNA target sequences [81]. It has been shown that H3 histone acetylation is rhythmic and under the influence of core circadian oscillator genes, namely *Cry*, in regulating the circadian negative feedback loop. CRY disrupts the CLOCK-BMAL1-coactivator complex and this disruption reduces histone acetyltransferase activity, which reduces transcriptional activation [82]. In the case of *Bmal1*$^{-/-}$ and *Clock*$^{-/-}$*;Npas2*$^{m/m}$ double mutant mice, the lack of a transcriptional activator complex leads to decreased levels of *Per* and *Cry* expression and thus decreased transcriptional repression. Because *Per* expression is decreased in *Bmal1*$^{-/-}$ mice [45], it is possible that the subtle HBM phenotype characteristic of *Per1*$^{-/-}$*;Per2*$^{-/-}$ and *Cry1*$^{-/-}$*;Cry2*$^{-/-}$ double knockout mice is included among the more impressive ectopic calcifications observed in *Bmal1*$^{-/-}$ and *Clock*$^{-/-}$*;Npas2*$^{m/m}$ double mutant mice.

HDAC4 is expressed in prehypertrophic chondrocytes and regulates chondrocyte hypertrophy and endochondral bone formation by inhibiting *Runx2* expression [80]. *HDAC4*$^{-/-}$ mice display premature ossification of developing bones secondary to ectopic and precocious chondrocyte hypertrophy and do not survive to weaning. *HDAC4*$^{-/-}$ mice phenocopy *Runx2*-overexpressing mice, and overexpression of *HDAC4* results in a phenotype similar to that of dominant-negative *Runx2* mutants [80, 83]. Of particular interest is the finding that *HDAC4*$^{-/-}$ mice display costosternal junction calcification [80] similar to

that observed in *Bmal1*$^{-/-}$ mice [64]. Because HDACs favor transcriptional repression, it is possible that the lack of transcriptional repression in *HDAC4*$^{-/-}$ mice relates to the lack of transcriptional activation in *Bmal1*$^{-/-}$ and *Clock*$^{-/-}$*;Npas2*$^{m/m}$ double mutant mice. Perhaps HDAC4 represses a molecule that promotes arthropathy, whereas CLOCK/NPAS2:BMAL1 complexes drive the expression of a competing molecule that prevents arthropathy. If HDAC4 is involved in the development of arthropathy in *Bmal1*$^{-/-}$ and *Clock*$^{-/-}$*;Npas2*$^{m/m}$ double mutant mice, we would expect to see less HDAC4 activity in our circadian mutant mice.

Mglap$^{-/-}$ mice

The fourth mutant mouse that exhibits a possibly related ectopic calcification phenotype is the *Mglap*$^{-/-}$ mouse. Matrix GLA protein (MGP) is an inhibitor of ectopic calcification expressed predominantly by chondrocytes and vascular smooth muscle cells and is encoded by *Mglap* in mice and *MGP* in humans [84, 85]. *Mglap*$^{-/-}$ mice exhibit spontaneous calcification of arteries and cartilage and die within two months of birth due to blood vessel rupture secondary to arterial calcification. The extent of their ectopic calcification extends to various cartilages, including the growth plate, which leads to short stature, osteopenia, and fractures [84]. MGP is a part of a small family of proteins that contain γ-carboxylated glutamate residues. The carboxylation of glutamate residues on MGP is dependent on vitamin K and confers a high affinity for mineral ions, thus inhibiting mineral deposition [85]. In humans, nonsense mutations in *MGP* cause Keutel syndrome, a rare autosomal recessive disorder characterized by ectopic calcification in

cartilage (including the costosternal junctions), the spinal column, and epiphyses of long bones [86]. People with Keutel syndrome additionally suffer from tracheobronchial and pulmonary stenosis and midfacial hypoplasia. The idea that pathological extracellular matrix calcification could be due to the lack of inhibitors of calcification [85], such as MGP, raises the possibility that the site-specificity of arthropathy observed in *Bmal1*$^{-/-}$ and *Clock*$^{-/-}$*;Npas2*$^{m/m}$ double mutant mice could be due to site-specific loss of MGP function. *Mglap* expression could be expressed in tissues unaffected by ectopic calcification, while tissues like costosternal junction and calcaneal tendon lack the transcription factors necessary to drive the expression of *Mglap*. If this is the case, then we would expect to see down regulation of *Mglap* function in tissues undergoing ectopic calcification in *Bmal1*$^{-/-}$ and *Clock*$^{-/-}$*;Npas2*$^{m/m}$ double mutant mice.

The mutant mouse models discussed here are merely a subset of the many mutant lines created to study bone formation and homeostasis. Many other genes could also be involved in the pathogenesis of ectopic calcification in *Bmal1*$^{-/-}$ and *Clock*$^{-/-}$*;Npas2*$^{m/m}$ double mutant mice, but the genes and mutant lines discussed here are highlighted due to the similarities in their calcification phenotypes to those of *Bmal1*$^{-/-}$ and *Clock*$^{-/-}$*;Npas2*$^{m/m}$ double mutant mice.

Possible mechanisms of age-dependent arthropathy in circadian mutant mice

Dysfunctional chondrocyte maturation

As previously stated, chondrocytes are responsible for cartilage formation and calcification during endochondral ossification. However, inappropriate chondrocyte activity can lead to abnormal calcification. One possible mechanism of abnormal calcification is the inappropriate differentiation of resting chondrocytes into osteogenic cells, which then calcify the surrounding tissue. For example, chondrocytes are normally found in the costal cartilage but if they become dysregulated, they could inappropriately differentiate into hypertrophic chondrocytes and calcify the costal cartilage. This mechanism could be applicable to tendon because chondrocytes are found, albeit in small numbers, at the enthesis of tendon and bone [87]. In this mechanism, chondrocytes would also undergo apoptosis, which is part of the physiologic maturation program of chondrocytes. While apoptosing, hypertrophic chondrocytes could release apoptotic bodies that contribute to calcification of surrounding tissue, which is a proposed mechanism of OA [18].

Progenitor cell dysfunction

Another possible mechanism involves adult progenitor cells. Progenitor cells could inappropriately differentiate into osteogenic cells that then calcify the surrounding tissue, which is the hypothesized mechanism of HO [7]. Progenitor cells are present in adult cartilage [88, 89] and tendons [90], so it is possible that progenitor cells in these tissues

inappropriately differentiate into osteogenic cells secondary to disruption of *Clock* and *Npas2* expression and cause HO.

De-differentiation and systemic dysregulation

A third possible mechanism is the de-differentiation of chondrocytes or tenocytes followed by differentiation into an osteogenic cell; this mechanism is not experimentally separable from the others described above. A fourth possible mechanism is systemic dysregulation, either of circadian rhythms or serum minerals that could cause abnormal calcification in these mice. However, the site-specific phenotype observed in *Clock*$^{-/-}$*;Npas2*$^{m/m}$ double mutant and *Bmal1*$^{-/-}$ mice, the lack of phenotypic similarity with other arrhythmic mutant mice (namely, the *Per1*$^{-/-}$*;Per2*$^{-/-}$ and *Cry1*$^{-/-}$*;Cry2*$^{-/-}$ double knockout mice), and the lack of serum calcium and phosphorous changes in *Bmal1*$^{-/-}$ mice [64] do not support systemic dysregulation; instead these characteristics suggest a more localized mechanism. Nevertheless, it is possible that an interaction between site-specific mechanisms and systemic hormonal or mineral imbalances could contribute to this age-dependent, site-specific arthropathy.

Extracellular PP_i dysregulation

A fifth possible mechanism involves extracellular PP_i dysregulation. *Enpp1*$^{-/-}$ [70] and *Ank*$^{-/-}$ mice [73] have abnormal extracellular PP_i levels and exhibit ectopic calcification phenotypes of varying similarity to that described for *Bmal1*$^{-/-}$ mice [64]. If there is too much extracellular PP_i, then CPPD crystals precipitate in tissue. If there is too little

extracellular PP_i, then HA crystals precipitate. Thus, depending on the type of crystals deposited in *Clock*$^{-/-}$;*Npas2*$^{m/m}$ double mutant mice, it could suggest that disruption of extracellular PP_i homeostasis contributes to site-specific arthropathy.

Osteoclast or osteoblast dysfunction

Lastly, an imbalance in bone homeostasis could cause abnormal calcification. If osteoblast activity is inappropriately high or osteoclast activity is inappropriately low, bone formation would be favored. *Bmal1*$^{-/-}$ mice exhibit increased bone formation rate/tissue volume (BFR/TV) ratios, mineral apposition rates, and number of osteoblasts per square millimeter, all suggestive of an increase in osteoblast function [37].

Concluding remarks

Through the course of this dissertation, these possible mechanisms will be discussed and it will be shown that local factors, possibly interacting with systemic factors, likely cause the dramatic arthropic phenotype in *Clock*$^{-/-}$;*Npas2*$^{m/m}$ double mutant mice, and that the local effects are anatomically very specific.

Ectopic calcification and ossification are abnormal (and in the case of ectopic calcification, age-related) processes that can limit mobility. Abnormal calcifications can cause discomfort and, in extreme cases, severe pain for patients. Recent data suggest that an absence of *Clock* and *Npas2*, or *Bmal1* leads to the formation of ectopic calcifications. The studies outlined in this dissertation aim to characterize and investigate mechanisms

of age-related arthropathy observed in *Clock*$^{-/-}$*;Npas2*$^{m/m}$ double mutant mice. Understanding these mechanisms will not only identify a novel pathway connecting circadian clock genes and genes of matrix mineralization, but may also identify possible therapeutic targets to treat some types of age-related ectopic calcification.

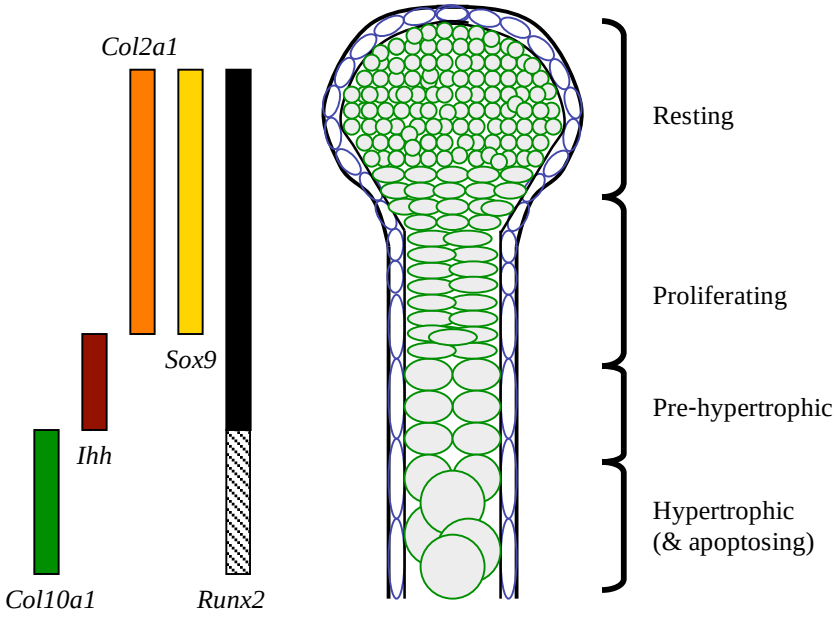

Figure 1.1. Chondrocyte maturation. Chondrocytes go through the following stages of maturation: resting, proliferating, pre-hypertrophic, and hypertrophic chondrocytes. There are characteristic gene expression patterns at each of these stages, as discussed in the text. The hatched box represents decreased *Runx2* expression in hypertrophic chondrocytes.

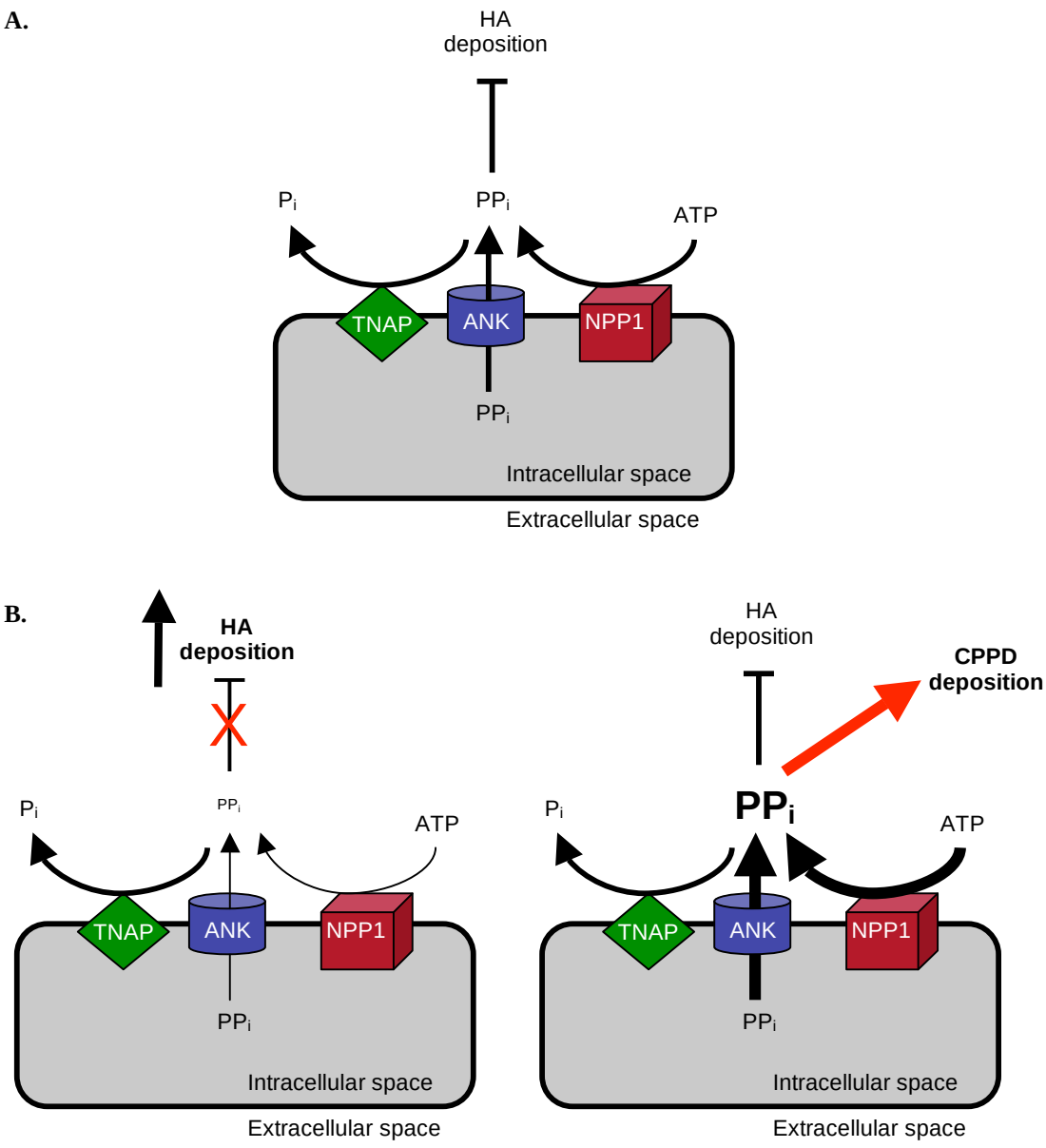

Figure 1.2. Diagrammatic representation of TNAP, ANK, and NPP1 in the regulation of extracellular PP_i levels. (A) Normal, low, physiologic levels of PP_i inhibit HA crystal deposition. NPP1 hydrolyzes ATP to form PP_i. ANK transports intracellular PP_i to the extracellular space. TNAP hydrolyzes PP_i to form P_i, which crystallizes with calcium to form HA. (B) Too little PP_i leads to HA crystal deposition (left) while too much PP_i leads to CPPD crystal deposition (right). Careful homeostasis among these three proteins dictate extracellular PP_i levels.

A.

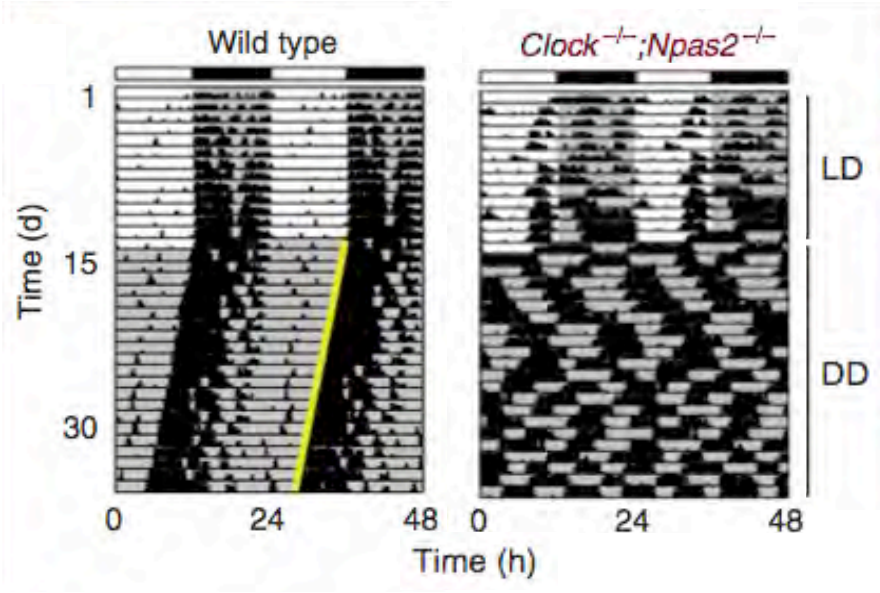

B.

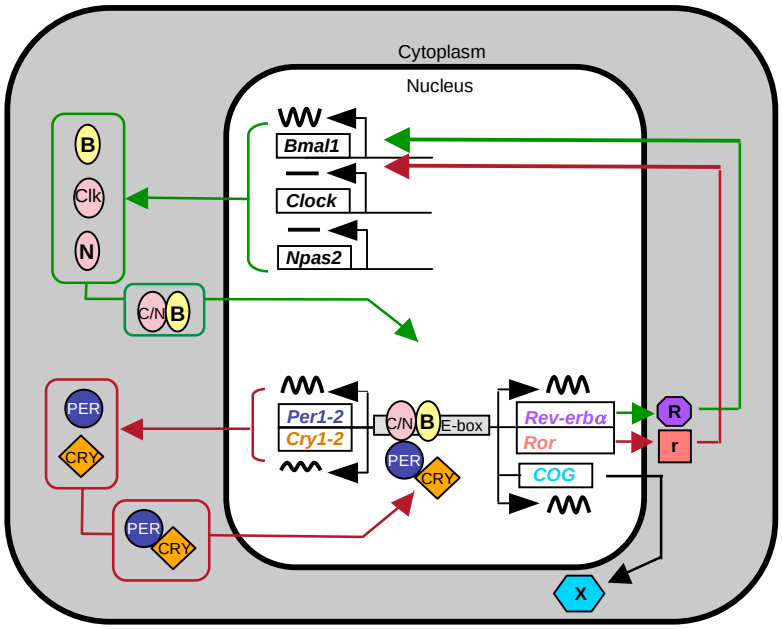

Figure 1.3. **Locomotor actograms and the mammalian circadian clockwork model.** (A) Double plotted locomotor activity records (also known as actograms) of rhythmic wild-type and arrhythmic *Clock*$^{-/-}$;*Npas2*$^{m/m}$ double mutant mice. Horizontal white bars represent when lights are on and horizontal black bars represent when lights are off. Activity is documented as revolutions of the running wheel and represented as black marks on the actogram. The yellow line is drawn to emphasize the slightly less than 24-hour period length of the wild-type mouse. Note the arrhythmic activity of the *Clock*$^{-/-}$;*Npas2*$^{m/m}$ double mutant mouse in DD. Adapted from DeBruyne et al., 2007 (ref. 39). (B) Model of the mammalian circadian clock. See text for details. Red lines represent transcriptional inhibition, green lines represent transcriptional activation. Adapted from Yu et al., 2011 (ref. 126). (LD: light:dark; DD: constant darkness Clk: Clock; N: Npas2; C/N: Clock or Npas2; B: Bmal1; R: Rev-erbα; r: Rorα; COG: clock output gene; X: unknown clock output protein.

Table 1.1. Summary of calcification-related mutant mouse models.

	Bone mass	Age-dep	Inflamm	Ectopic calcification	Crystal deposits	Serum Ca^{2+} or P changes	Premature death
Bmal1$^{-/-}$	NC (64)	Yes (64)	No (64)	Yes (64)	CPPD (OU)	No (64, 95)	Yes (95, 96)
Clock$^{-/-}$; *Npas2*$^{m/m}$	IC (OU)	Yes	Probably no (OU)	Yes	Unknown	No	Yes (OU)
Enpp1$^{-/-}$	No change (70)	Yes (70)	No (26)	Yes (69, 26)	HA (147)	Unknown	Yes (70)
Ank$^{-/-}$ & *ank/ank*	Increase (29)	Yes (73)	Yes (74, 75)	Yes (73)	HA (74, 75)	Unknown	Yes (73)
Akp2$^{-/-}$	Decrease (78, 79)	Yes (79)	No (78, 79)	No (78, 79)	N/A	No (79)	Yes (78, 79)
Mgp$^{-/-}$	NC (84)	Yes (84)	No (84)	Yes (84)	HA (84)	Unknown	Yes (84)
HDAC4$^{-/-}$	Unknown	Yes (80)	No (80)	Yes (80)	Unknown	Unknown	Yes (80)
Prrx1$^{-/-}$	Decrease (114)	Yes (114)	Probably no (114)	No (114)	N/A	Unknown	Yes (114)
Hyp mice	Decrease (148)	Yes (148)	No (135)	Yes (135)	Unknown	Yes (148, 130)	No (148)
kl/kl	Decrease (93)	Yes (93)	Probably no (93)	Yes (93)	Unknown	Yes (93)	Yes (93)
FGF23$^{-/-}$	Decrease (98)	Yes (98)	Unknown	Yes (99)	Unknown	Yes (98)	Yes (98)
Runx2$^{-/-}$	Decrease (149)	No (149)	Probably no (149)	No (149)	N/A	Unknown	Yes (149)
Sox9$^{+/-}$	Both* (13)	Yes (13)	Unknown	Yes – heart valves (152)	Unknown	Unknown	Yes (13)
Ihh$^{-/-}$	Decrease (150)	Yes (150)	No (150)	No (150)	N/A	Unknown	Yes {(150)
Col10a1$^{-/-}$	NC (151)	N/A	Unknown	No (151)	N/A	Unknown	No (151)
Per1$^{-/-}$; *Per2*$^{m/m}$	Increase (37)	Yes (37)	Unknown	No (37)	Unknown	No (37)	No (37, OU)
Cry1$^{-/-}$; *Cry2*$^{-/-}$	Increase (37)	Yes (37)	Unknown	No (37)	Unknown	Probably no (37)	No (37, OU)

Age-dep: age-dependent; Inflamm: inflammatory; NC: no change; OU: our unpublished data/observations; N/A: not applicable; IC: inconclusive data; HA: hydroxyapatite; CPPD: calcium pyrophosphate dihydrate. *$Sox9^{+/-}$ mice exhibit hypoplasia of most bones derived from endochondral ossification but also display premature mineralization of vertebrae & craniofacial bones

Chapter II

Characterizing arthropathy in *Clock*$^{-/-}$;*Npas2*$^{m/m}$ double mutant mice

Summary

Clock$^{-/-}$;*Npas2*$^{m/m}$ double mutant and *Bmal1*$^{-/-}$ mice are arrhythmic circadian mutant mice used to study circadian rhythms. CLOCK and NPAS2 are functionally redundant in the SCN, in that either can bind to BMAL1 to form a heterodimer transcription factor complex that drives rhythmic gene expression. In the course of other studies, it was found that 35+ week-old *Clock*$^{-/-}$;*Npas2*$^{m/m}$ double mutant mice exhibit calcification similar with that of 35 week-old *Bmal1*$^{-/-}$ mice. Here we further explore that finding and show that *Clock*$^{-/-}$;*Npas2*$^{m/m}$ double mutant mice manifest an overall arthropathy similar to that of *Bmal1*$^{-/-}$ mice. This arthropathy is site-specific, age-progressive, and consists of ectopic calcifications. In *Clock*$^{-/-}$;*Npas2*$^{m/m}$ double mutant mice, several different sites are affected, both weight-bearing and non-weight-bearing. The sites with the most prominent arthropathy in *Clock*$^{-/-}$;*Npas2*$^{m/m}$ double mutant mice are the calcaneal tendon and costosternal junction. These calcifications contain calcium and phosphate, and in *Bmal1*$^{-/-}$ costosternal junction consist of CPPD crystal deposits. The consistency of phenotypes between *Clock*$^{-/-}$;*Npas2*$^{m/m}$ double mutant and *Bmal1*$^{-/-}$ mice strongly suggests that disruption of the transcriptional activator complex leads to gene dysregulation that causes age-dependent, site-specific ectopic calcification.

Acknowledgements

This chapter is a result of collaboration between our laboratory and the laboratories of Jane Lian and Paul Fanning in the Department of Cell Biology at the University of Massachusetts Medical School (UMMS). As such, I would like to acknowledge the appropriate people for their contribution to the work presented here.

Drs. Robert Dallmann and Jason DeBruyne were responsible for first recognizing arthropathy in *Clock*$^{-/-}$*;Npas2*$^{m/m}$ double mutant mice, and Robert performed the first X-rays to identify ectopic calcification in 44-48 week-old mutant mice. Stacey Russell performed all of the micro-CT scans and showed me how to create 3-D reconstructed images. Sadiq Hussain and April Mason-Savas taught me everything I know about histology, and also performed some of the histological stains. Sadiq performed toluidine blue stains of decalcified 11-12 week-old tissues and April performed von Kossa and safranin-O stains of non-decalcified sterna tissues, and von Kossa, safranin-O, and alizarin red stains of non-decalcified calcaneal tendon. Jennifer Colby and Sadiq also showed me how to collect, dissect, and X-ray mice. Sadiq additionally taught me how to use the microscope and software associated with imaging slides. Lastly, Dr. Gregory Hendricks of the Core Electron Microscopy Facility operated the scanning electron microscope (SEM) to calculate P:Ca atomic weight ratios and stoichiometric analysis of crystal deposits in ectopic calcification and bone.

Figure 2.1. Distribution of ectopic calcification in 41-42 week-old *Clock*$^{-/-}$*;Npas2*$^{m/m}$ double mutant mice.
Elizabeth Yu – Department of Neurobiology, UMMS
Stacey Russell – Musculoskeletal Center Imaging Core, Department of Cell Biology, UMMS

Figure 2.2. X-ray images of *Clock*$^{-/-}$*;Npas2*$^{m/m}$ internal organs do not reveal ectopic calcification.
Elizabeth Yu – Department of Neurobiology, UMMS

Figure 2.3. *Clock*$^{-/-}$*;Npas2*$^{m/m}$ double mutant mice exhibit age-dependent weight loss.
Elizabeth Yu – Department of Neurobiology, UMMS

Figure 2.4. Age-progressive calcification of calcaneal tendon in *Clock*$^{-/-}$*;Npas2*$^{m/m}$ double mutant mice.
Elizabeth Yu and Dr. David Weaver – Department of Neurobiology, UMMS

Figure 2.5. Age-progressive calcification of costosternal junction in *Clock*$^{-/-}$*;Npas2*$^{m/m}$ double mutant mice.
Elizabeth Yu and Dr. David Weaver – Department of Neurobiology, UMMS

Figure 2.6. No ectopic calcification in calcaneal tendon or costosternal junction of 76 week-old *Per1*$^{-/-}$*;Per2*$^{-/-}$ double mutant mice.
Elizabeth Yu and Dr. David Weaver – Department of Neurobiology, UMMS

Figure 2.7. Ectopic calcification of costosternal junction and calcaneal tendon in 11-12 week-old *Clock*$^{-/-}$*;Npas2*$^{m/m}$ double mutant mice.
Stacey Russell – Musculoskeletal Center Imaging Core, Department of Cell Biology, UMMS

Figure 2.8. Acellular lesions in decalcified costosternal sections of young *Clock*$^{-/-}$*;Npas2*$^{m/m}$ double mutant mice.
Elizabeth Yu – Department of Neurobiology, UMMS
Sadiq Hussain – Department of Cell Biology, UMMS

Figure 2.9. Lesions in costosternal junction and calcaneal tendon of *Clock*$^{-/-}$*;Npas2*$^{m/m}$ double mutant mice contain calcium phosphate deposits.
Elizabeth Yu – Department of Neurobiology, UMMS
April Mason-Savas – Department of Cell Biology, UMMS

Figure 2.10. Calcaneal tendon of 6-7 and 11-12 week-old *Clock*$^{-/-}$*;Npas2*$^{m/m}$ double mutant mice.
Elizabeth Yu – Department of Neurobiology, UMMS

Figure 2.11. Ectopic calcification in the sternum of a 53 week-old *Bmal1*$^{-/-}$ mouse contains CPPD crystal deposits.

Elizabeth Yu – Department of Neurobiology, UMMS
Dr. Gregory Hendricks – Core Electron Microscopy Facility

Introduction

The mammalian circadian clock is based on interconnected feedback loops that take approximately 24 hours to complete [33]. At the center of these feedback loops are the transcription factors *Clock*, *Npas2*, and *Bmal1*, which form a transcription activator complex to drive the expression of *Period 1-3* and *Cryptochrome 1-2*. PERs and CRYs form transcriptional repressor complexes that inhibit CLOCK:BMAL1 or NPAS2:BMAL1, and thus their own transcription [40]. Disruption of these core clock genes causes arrhythmicity in constant darkness. Specifically, *Bmal1*$^{-/-}$ mice are arrhythmic [45]. *Bmal1*$^{-/-}$ mice also exhibit age-dependent arthropathy, characterized by ectopic calcification of the costosternal junction, calcaneal tendon, and longitudinal spinal ligaments [64].

While using *Clock*$^{-/-}$*;Npas2*$^{m/m}$ double mutant mice to study the roles of *Clock* and *Npas2* in behavioral circadian rhythmicity, our lab discovered an arthropic phenotype in 35+ week-old *Clock*$^{-/-}$*;Npas2*$^{m/m}$ double mutant mice. These double mutant mice exhibit gross motor deficits, such as severe stiffness of the hind legs and distorted tail postures (our unpublished data). They are also unable to balance on a raised beam or hang upside down from a wire cage, which are indicative of diminished motor coordination and paw grip strength, respectively (our unpublished observations) [91]. Upon closer inspection of appendicular and axial skeletons using X-ray, it was discovered that 35+ week-old *Clock*$^{-/-}$*;Npas2*$^{m/m}$ double mutant mice exhibited site-specific arthropathy similar to that of 35 week-old *Bmal1*$^{-/-}$ mice [64].

NPAS2 can substitute for CLOCK in the SCN: either molecule can bind to BMAL1 to form a heterodimer transcription complex that binds to E-box elements and drives rhythmic gene expression. This complex can drive core circadian oscillator genes, such as the *Pers* and *Crys*, or clock output genes, such as *Dbp* [33, 43]. Given the functional redundancy of *Clock* and *Npas2* in the SCN and their shared ability to bind to BMAL1, we postulated that disruption of the transcriptional activator (CLOCK:BMAL1 or NPAS2:BMAL1) causes site-specific arthropathy. To investigate this phenotype, we used a combination of X-ray, micro-computed tomography (micro-CT), and histological techniques to characterize the extent of arthropathy in *Clock*$^{-/-}$*;Npas2*$^{m/m}$ double mutant mice and mice of other circadian genotypes.

Experimental procedures

Generation and maintenance of study animals

All animal studies were reviewed and approved by the Institutional Animal Care and Use Committee at the University of Massachusetts Medical School. Mice used for these studies had been backcrossed at least 10 generations to the C57BL/6J background, except for *Per* mutant and respective control mice, which were on the 129/sv background. Wild-type controls were studied simultaneously in each experiment. Unless otherwise stated, multiple mice were housed in gender-segregated, ventilated 191x279x127mm cages in a pathogen-free barrier facility maintained on a 12-hour light/12-hour dark cycle with food and water *ad libitum*. Light was provided by fluorescent tubes and was ~200 lux at the level of the cages. Dim red light from fluorescent tubes was on continuously, including periods referred to as constant darkness.

Clock$^{-/-}$ mice were generated by our lab, as previously described [51]. *Bmal1* founder mice were a kind gift from Dr. Christopher A. Bradfield (University of Wisconsin) [45]. *Npas2* founder mice were a kind gift from Dr. Steven L. McKnight (University of Texas – Southwestern Medical Center) [92]. To generate *Clock*$^{-/-}$*;Npas2*$^{m/m}$ double mutant mice, *Clock*$^{+/-}$*;Npas2*$^{m/m}$ three-allele mutant mice were crossed to one another to obtain *Clock*$^{-/-}$*;Npas2*$^{m/m}$ double mutant mice. *Clock*$^{-/-}$*;Npas2*$^{+/m}$ three-allele mutant mice were also intercrossed to obtain *Clock*$^{-/-}$*;Npas2*$^{m/m}$ double mutant mice, although with less success than *Clock*$^{+/-}$*;Npas2*$^{m/m}$ three-allele mutant mice intercrosses. *Clock*$^{+/-}$*;Npas2*$^{m/m}$ three-allele mutant mice intercrosses also generated *Clock*$^{+/-}$*;Npas2*$^{m/m}$

three-allele and (*Clock*$^{+/+}$*;)Npas2*$^{m/m}$ mice. *Clock*$^{-/-}$ mice were obtained by crossing *Clock*$^{-/-}$ or *Clock*$^{+/-}$ heterozygote with *Clock*$^{+/-}$ heterozygote mice. *Npas2*$^{m/m}$ mice were obtained by intercrossing *Npas2*$^{m/m}$ mice. *Clock*$^{-/-}$*;Npas2*$^{+/-}$ three-allele mutant mice were generated by crossing *Clock*$^{+/-}$*;Npas2*$^{m/m}$ three-allele mutant mice with *Clock*$^{-/-}$ mice. *Bmal1*$^{+/-}$ heterozygote mice were intercrossed to generate *Bmal1*$^{-/-}$ mice. With the exception of *Bmal1*$^{-/-}$ crosses, the crosses did not generate wild-type littermates, necessitating separate wild-type C57BL/6J mouse crosses to generate age-matched controls.

Genotyping

For polymerase chain reaction (PCR) genotyping at the *Clock* locus, a three-primer set was used to distinguish wild-type, floxed, and deleted alleles [51]. This primer set consists of two forward primers (Clock 5F3, CAGCTTCATTTGAAATCTGCAT; Clock 3loxF2: AGCTGGGGTCTATGCTTCCT) and a common reverse primer (Clock 3loxR, CGCTGAGAGCCAAGACAAT). Reactions were performed using the following cycling protocol: 95^{o}C for 3 minutes, 35 cycles of 95^{o}C for 30 seconds, 53^{o}C for 60 seconds, and 72^{o}C for 60 seconds, followed by a final extension phase at 72^{o}C for 7 minutes. Product sizes were 220 nucleotides (nt) for wild-type, 380 nt for floxed, and 450 nt for *Clock*$^{-/-}$.

For PCR genotyping at the *Npas2* locus, a three-primer set was used to distinguish wild-type and deleted alleles [39]. This primer set consists of two forward primers (LacZ.4: GTGCTGCAAGGCGATTAAGTTGGGT; NP2.5' intron:

GGAACCTCTGCGGCATGACAAAGCCTTCGTG) and a common reverse primer (NP2.3' exon: GGTGGTTTTGTCCATTTTCCGAGTGTT). Reactions were performed using the following touch-down cycling protocol: 95^{o}C for 3 minutes, 20 cycles of 95^{o}C for 30 seconds, 63^{o}C (-0.5^{o}C/cycle) for 60 seconds, 72^{o}C for 60 seconds, then 20 cycles of 95^{o}C for 30 seconds, 53^{o}C for 60 seconds, and 72^{o}C for 60 seconds, followed by a final extension phase at 72^{o}C for 7 minutes. Product sizes were 185 nt for wild-type and 250 nt for *Npas2*$^{m/m}$.

For PCR genotyping at the *Bmal1* locus, a three-primer set was used to distinguish wild-type and deleted alleles. This primer set consists of two forward primers (Forward 2 at 3': CAGAGAAGCAAACTACAAGCC; Neo6-2: TGCCCCAAAGGCCTACCCGCTTCC) and a common reverse primer (Reverse 2 at 3': ATGTGCACCTCATGTGTCTGG). Reactions were performed using the same touch-down cycling protocol as for *Npas2*. Product sizes were 700 nt for wild-type and 470 nt for *Bmal1*$^{-/-}$.

For PCR genotyping at the *Per1* locus, a three-primer set was used to distinguish wild-type and deleted alleles [49]. This primer set consists of a common forward primer (Per1AA-F: ATTAGTCAGCCCTCAGAGACAGGCGTC) and two reverse primers (Per1AA-R: TGAGTCCTTGCCATTGCCAGAAGAGG; Neo3B: CCAGCTCATTCCTCCACTCATGATCTA). Reactions were performed using the same cycling protocol as for *Clock*. Product sizes were 363 nt for wild-type and 235 nt for *Per1*$^{-/-}$.

For PCR genotyping at the *Per2* locus, a three-primer set was used to distinguish wild-type and deleted alleles [49]. This primer set consists of two forward primers (Per2i5FC: GTATAGTCACCCGATCATACTCTCC; Neo6-2: TGCCCCAAAGGCCTACCCGCTTCC) and a common reverse primer (Per2-6eR: AAGATGCTGCAGTCAGGACCTCACC). Reactions were performed using the same cycling protocol as for *Clock*. Product sizes were 259 nt for wild-type and 403 nt for *Per2*$^{-/-}$.

PCR products were separated on 1.5% agarose gels and visualized with ethidium bromide.

Animal collection and fixation

Animals were collected during the daytime, typically mid to late afternoon. Mice were asphyxiated in a CO_2 chamber, decapitated, skinned, and eviscerated. Some animals were weighed in a scale (CS200, Ohaus, Pine Brook, NJ, USA) prior to decapitation (Table 2.1 and Table 2.2). The skeleton was dissected into the following sections: forelimbs (including scapula), forepaws, hind limbs, pelvis (including proximal 1/3 of tail, caudal spinal column, and hip joints), ribcage with sternum, and the remaining spinal column. Sterna and forepaws were flattened between two slides and all tissues were fixed by immersion in freshly made periodate-lysine-paraformaldehyde solution (PLP: 2% paraformaldehyde (PFA) containing 0.075M lysine and 0.01M sodium periodate solution, pH 7.4, stored at 4^{o}C) for three days at 4^{o}C under vacuum before being transferred to 1X

phosphate buffered saline (PBS) and stored at 4^{o}C. This PLP fixative is compatible with all subsequent analysis techniques: X-ray, micro-CT, and histology.

X-rays

Once skeletal tissues were collected and fixed, they were X-rayed with a high resolution MX-20 Faxitron on mammography film (Table 2.3). Organs were dissected into the following groups and also X-rayed: heart and lung, liver, spleen, kidneys, and stomach and intestines (Table 2.4). Depending on the body part being X-rayed, settings were 20kV for 6-20 seconds.

Micro-computed tomography (micro-CT)

After skeletal tissues were fixed and X-rayed, a subset was analyzed using micro-computed tomography (micro-CT, Table 2.5).

Two wild-type and 2 *Clock*$^{-/-}$*;Npas2*$^{m/m}$ double mutant mice, 11-12 weeks old, were subjected to micro-CT analysis. The scanning of the limbs and sternum was performed in air on a Scanco MicroCT 40 at 70kV$_{p}$, 114μA and a resolution of 15 um. The forelimb regions of interest (ROIs) included the metacarpals and the wrist joint in the neutral position. The hindlimb ROI included the metatarsals and the lower tibia/ankle joint. The sternum and ribs were scanned in air as flat as possible in the ventral-dorsal plane. The sternum ROI included the manubrium to the xiphoid cartilage. The spinal vertebrae were scanned whole in air in the rostral-caudal plane at a resolution of 6 um. The lumbar ROI included the whole trabeculae from the rostral end of L5 to caudal end

of L2. The thoracic ROI included the whole trabeculae from the rostral end of T3 to caudal end of T5. The cervical ROI included the whole trabeculae from the rostral end of C5 to caudal end of T7.

Two wild-type and 2 *Clock*$^{-/-}$*;Npas2*$^{m/m}$ double mutant mice, 41-42 weeks old, were also subjected to micro-CT analysis. In these animals, the scanning of the limbs and sternum was performed in air on a Scanco MicroCT40 at 70kV$_p$, 114µA and a resolution of 15 um. The forelimb ROI included the elbow joint in midway flexion, the shoulder joint in the standing position, and the metacarpals. The hindlimb ROIs included the knee in midway flexion, and the metatarsals and ankle joints. The sternum and ribs were scanned in air as flat as possible in the ventral-dorsal plane. The sternum ROI included the manubrium to the xiphoid cartilage. The spinal vertebrae were scanned in three sections in air in the rostral-caudal plane at a resolution of 6 um. The lumbar ROI included the whole trabeculae from the rostral end of L5 to caudal end of L2. The thoracic ROI included the whole trabeculae from the rostral end of T3 to caudal end of T5. The cervical ROI included the whole trabeculae from the rostral end of C5 to caudal end of T7. The tail vertebrae and hip were scanned together at a resolution of 8 um intact in air in the rostral-caudal plane. A larger diameter sample holder was utilized due to the width of the hip. The hip ROI included the pelvic girdle and the sacrum (S1-4). The tail vertebrae ROI included the caudal vertebrae CA1-CA3.

For ectopic bone imaging, each ROI was utilized with no delineation between cortical or trabecular bone. The segmentation parameters included the values 0.8 Gauss sigma, and 1.0 Gauss support, and a threshold of 220-1000 (density range of >500mg of

HA/cm^3) in all joints except the knee and sternum. The 11-12 week-old sterna were imaged at a threshold of 170-1000 (density range of >400mg HA/cm^3), while the 41-42 week-old sterna and knees were imaged at a threshold of 212-1000 (density range of >450mg of HA/cm^3). The appropriate thresholds were selected by visually comparing the gray-level images to the binarized image both in 2-D and 3-D.

Histologic analysis of decalcified tissues

After being fixed and X-rayed, a subset of sternal (Table 2.6) and hindlimb (Table 2.7) tissues were decalcified in 18% EDTA, pH 7.4, at 4^{o}C with agitation for two weeks. During the first week 18% EDTA was changed daily and during the second week 18% EDTA was changed every two days. After decalcification, tissues were dehydrated in the following solutions for one hour each: 70% ethanol, 80% ethanol, 95% ethanol (twice), 100% ethanol (three times), xylene (three times), paraffin (twice). After dehydration, samples were immediately subjected to vacuum wax infiltration and then embedded in paraffin. Samples were sectioned at 6 um and processed for staining. For toluidine blue staining, slides were deparaffinized, rehydrated, and stained in 1% toluidine blue, either made in isopropanol or distilled water, for one minute and then rinsed in tap water, dehydrated, and coverslipped. Toluidine blue made in isopropanol stains everything blue. Toluidine blue made in distilled water stains bone and muscle blue but cartilage pink/purple. Histological images were captured using a Zeiss Axioskop 40 microscope, Zeiss AxioCam HRc camera, and Zeiss AxioVision 4 (version 4.7.2.0) software.

Histologic analysis of non-decalcified tissues

Another subset of tissues was not decalcified prior to histological analysis (Table 2.8). These tissues were fixed and X-rayed, then embedded in glycol methacrylate and sectioned at 3 um. Slides from non-decalcified tissues were used for safranin-O, von Kossa, and alizarin red staining.

For safranin-O staining, slides were placed in Weigert's iron hematoxylin working solution for ten minutes, then washed in tap water and stained with fast green solution for five minutes. Slides were then rinsed with 1% acetic acid solution for 10-15 seconds and then stained in 0.1% safranin-O solution for 10-25 minutes (until red staining was visible under the microscope), before being dehydrated and coverslipped. Safranin-O stains proteoglycans red/pink.

For von Kossa staining, slides were placed in 1% silver nitrate for 1.5 hours at room temperature under ambient bench top light. Slides were then rinsed in distilled water and placed in 5% sodium thiosulfate for five minutes, rinsed again and counterstained with 1% toluidine blue made in distilled water for five minutes. After being rinsed in tap water, slides were coverslipped. Von Kossa stains phosphate brown/black.

For alizarin red staining, slides were placed in 2% alizarin red for five minutes and then rinsed in tap water and coverslipped. Alizarin red stains calcium red.

For each genotype, there were four to six mice and for each mouse at least one slide with three serial sections was examined. Histological images were captured using a

Zeiss Axioskop 40 microscope, Zeiss AxioCam HRc camera, and Zeiss AxioVision 4 (version 4.7.2.0) software.

Scanning electron microscopy (SEM) analysis

To collect tissue for scanning electron microscopy analysis, a 53 week-old female *Bmal1*$^{-/-}$ mouse was asphyxiated in a CO_2 chamber, decapitated, eviscerated, skinned, and dissected into the following parts: forelimbs (including scapula), forepaws, hind limbs, pelvis (including proximal 1/3 of tail, caudal spinal column, and hip joints), ribcage with sternum, and the remaining spinal column. Forepaws and sternum were flattened between two slides and tissues, including organs, were fixed by immersion in freshly made 4% PFA in 0.2M cacodylate buffer, pH 7.2 overnight at 4^{o}C. The next day, the sternum was embedded in O.C.T. mounting media and sectioned in a cryostat at 60 um. Sections were kept at 4^{o}C until SEM processing, which involved air drying the slides and then scoring and breaking the slides to isolate one entire section of tissue. This portion of the slide was mounted on an aluminum scanning stud with conductive carbon tape and colloidal graphite. The specimen was then carbon coated (3 nm) in a vacuum evaporator and examined with a FEI Quanta 200 FESEM at 10 KV accelerating voltage at spot size 3. Images were acquired in both secondary electron imaging (SEI) and backscatter electron imaging (BSI) modes as well as combined imaging mode. X-ray spectroscopy was performed using an Oxford-link EDS system with a 30 mm^2 detector window. All scans were collected for 120 seconds in a point and identification. All spectra were normalized and analyzed for weight %, atomic %, and stoichiometry. Identification of crystal

composition was based on P:Ca ratios and phosphate, calcium, and oxygen stoichiometry, as compared to an internal library of standards and best-fit chemical composition in the Oxford-link software package. The atomic % for each element was multiplied by its atomic weight (P = 30.97, Ca = 40.08) to calculate P:Ca atomic weight ratios.

Statistical analysis

Male and female weights were analyzed by two-way ANOVA (Prism 5 for Mac OS X software). Bonferroni post-tests were done for comparisons among ages and genotypes. P-values less than 0.05 were considered statistically significant.

Results and discussion

Anatomical distribution of arthropathy

A first step in characterizing a new calcification phenotype in a mutant mouse line is to identify the affected areas. To do this, micro-computed tomography (micro-CT), an extremely sensitive method to detect calcification, was performed on two 41-42 week-old wild-type and two *Clock*$^{-/-}$;*Npas2*$^{m/m}$ double mutant mice (Table 2.5). Major joints were analyzed and the following areas in *Clock*$^{-/-}$;*Npas2*$^{m/m}$ double mutant mice exhibited ectopic calcification: elbows, stifles (knee joints), forepaws, hindpaws, calcaneal tendon, cervical vertebrae, proximal caudal vertebrae, costovertebral junctions, and costosternal junctions (Figure 2.1A and 2.1B). Surprisingly, the shoulder and hip joints were spared (Figure 2.1C). Distal femurs were examined to determine if *Clock*$^{-/-}$;*Npas2*$^{m/m}$ double mutant mice develop high bone mass like *Per1*$^{-/-}$;*Per2*$^{-/-}$ double mutant mice [37], but there was striking variability in bone mass within genotypes, such that conclusions could not be drawn from such a small sample size (data not shown). A larger sample size is necessary to compare distal femur bone mass of *Clock*$^{-/-}$;*Npas2*$^{m/m}$ double mutant and wild-type mice.

Most of the joints containing ectopic calcification are weight-bearing joints in quadrupeds. Aside from ectopic joint calcification, it is possible that other soft tissues, such as organs, in *Clock*$^{-/-}$;*Npas2*$^{m/m}$ double mutant mice could also be inappropriately calcified. Several other mutant mouse lines exhibit abnormal calcification of soft tissues, such as internal organs and arterial blood vessels [84, 93, 94]. Diffuse calcification of organs

would suggest metastatic calcification as a mechanism. The internal organs of 37-49 week-old wild-type and *Clock*$^{-/-}$;*Npas2*$^{m/m}$ double mutant mice were X-rayed, but no visible calcifications were detected (Figure 2.2, Table 2.4).

Age-dependent changes in body weight

At this advanced age, gross motor deficits are readily apparent in *Clock*$^{-/-}$;*Npas2*$^{m/m}$ double mutant mice. *Clock*$^{-/-}$;*Npas2*$^{m/m}$ double mutant mice are also noticeably smaller than their wild-type counterparts. Statistical analyses revealed a significant effect of age and genotype on weight as well as a significant interaction between age and genotype. In other words, *Clock*$^{-/-}$;*Npas2*$^{m/m}$ double mutant mice lose weight as they age while wild-type mice gain weight with age (Figure 2.3, Tables 2.1 and 2.2). This age-dependent weight loss was also observed in *Bmal1*$^{-/-}$ mice, consistent with previously published studies (Figure 2.3) [64, 95, 96].

Age-dependent development of arthropathy

Given the age-progressive nature of arthropathy in *Bmal1*$^{-/-}$ mice, we wanted to assess age-dependenct of arthropathy in *Clock*$^{-/-}$;*Npas2*$^{m/m}$ double mutant mice. To do this, animals were X-rayed across a wide range of ages (Table 2.3). In order to obtain clear X-ray images of joints, animals were sacrificed and joints were isolated. Despite being a somewhat insensitive tool, X-ray is both an efficient and cost-effective method to assess gross tissue calcification in a large number of animals. *Clock*$^{-/-}$;*Npas2*$^{m/m}$ double mutant mice exhibit age-dependent arthropathy in both the calcaneal tendon (Figure 2.4)

and costosternal junction (Figure 2.5), similar to *Bmal1*$^{-/-}$ mice. There is 100% penetrance of gross phenotypic abnormalities and arthropathy, the latter confirmed by X-ray, in *Clock*$^{-/-}$*;Npas2*$^{m/m}$ double mutant mice 35 weeks and older (our unpublished data). *Per1*$^{-/-}$*;Per2*$^{-/-}$ double mutant mice do not develop arthropathy even at advanced ages (Figure 2.6, our unpublished observations). Like *Bmal1*$^{-/-}$ mice [64, 96], *Clock*$^{-/-}$*;Npas2*$^{m/m}$ double mutant mice usually do not survive past 60 weeks of age and so there are no X-ray images for 64+ week-old *Clock*$^{-/-}$*;Npas2*$^{m/m}$ double mutant or *Bmal1*$^{-/-}$ mice.

There does not appear to be a gender-related difference in arthropathy development. *Clock* and *Npas2* three-allele (*Clock*$^{+/-}$*;Npas2*$^{m/m}$ and *Clock*$^{-/-}$*;Npas2*$^{+/m}$) and single mutant (*Clock*$^{-/-}$ and *Npas2*$^{m/m}$) animals do not develop costosternal junction calcification (Figure 2.5). However, in the calcaneal tendon, three-allele and single mutant mice all develop an attenuated age-dependent ectopic calcification (Figure 2.4). The attenuated calcaneal tendon calcification in three-allele and single mutants could be due to a gene dosage effect. Curiously, wild-type mice eventually develop calcaneal tendon calcification at advanced ages (64+ weeks) but never develop calcification of costosternal junction within the age range examined. Because calcaneal tendon calcification eventually appears in very old wild-type mice, it is possible that the calcaneal tendon calcification in *Clock*$^{-/-}$*;Npas2*$^{m/m}$ double mutant mice is due to accelerated aging and the later onset of calcaneal tendon calcification in three-allele and single mutants is a reflection of an intermediate phenotype. The hypothesis of accelerated aging is consistent with sterility, weight loss, and premature death observed in *Clock*$^{-/-}$*;Npas2*$^{m/m}$ double mutant mice (our unpublished observations, Figure 2.3). An

accelerated aging phenotype has been described in *Bmal1*$^{-/-}$ mice [96]. *Bmal1*$^{-/-}$ mice exhibit ectopic calcification, sarcopenia, cataracts, reduced subcutaneous fat stores, organ shrinkage, and altered levels of immune cells in peripheral blood, and undergo premature death [64, 95, 96]. BMAL1 is the binding partner of either CLOCK or NPAS2, such that disruption of *Bmal1*, or *Clock* and *Npas2* expression leads to disruption of CLOCK/NPAS2:BMAL1-mediated transcription. Given this molecular interaction and the similarity of arthropathy, sterility, weight loss, and premature death in *Clock*$^{-/-}$*;Npas2*$^{m/m}$ double mutant and *Bmal1*$^{-/-}$ mice, it is very possible that *Clock*$^{-/-}$*;Npas2*$^{m/m}$ double mutant mice exhibit the same symptoms of accelerated aging as *Bmal1*$^{-/-}$ mice.

Micro-CT analysis of young adult mice

An important aspect of ectopic calcification in *Clock*$^{-/-}$*;Npas2*$^{m/m}$ double mutant mice is the age at which these calcifications first appear. Is ectopic calcification a developmental process or does it occur post-natally? Identification of the rough age of onset also facilitates the design of future experiments. By studying *Clock*$^{-/-}$*;Npas2*$^{m/m}$ double mutants at the age at which ectopic calcifications are just beginning to form, we can be more certain that any molecular changes observed cause the arthropathy, rather than occur as a result of it.

In *Bmal1*$^{-/-}$ mice, calcifications are detectable as early as eight weeks of age [64]. To assess arthropathy in young adult *Clock*$^{-/-}$*;Npas2*$^{m/m}$ double mutant mice, micro-CT was performed on 11-12 week-old *Clock*$^{-/-}$*;Npas2*$^{m/m}$ double mutant and wild-type mice. At this younger age, calcifications are clearly visible at the costosternal junction and

calcaneal tendon (Figure 2.7). Other sites that are affected in 41-42 week-old *Clock*$^{-/-}$*;Npas2*$^{m/m}$ double mutant mice (forepaws, hindpaws, vertebrae) are not as severely calcified as compared to the costosternal junction and calcaneal tendon. All future studies focused on these two sites for two reasons: first, these are the main sites affected in *Bmal1*$^{-/-}$ mice and second, these are the sites with the earliest visible arthropathy in *Clock*$^{-/-}$*;Npas2*$^{m/m}$ double mutant mice. Studying sites that first develop pathology aids in the management of the mouse colony and also reduces any possible interaction with other sites of developing pathology.

Histological characterization of arthropathy

To investigate arthropathy in even younger animals, tissues were analyzed histologically. Sternal samples were decalcified, paraffin-embedded, and sectioned. At 4-5 weeks of age, small lesions are barely noticeable at the costosternal junction of *Clock*$^{-/-}$*;Npas2*$^{m/m}$ double mutant mice. These small lesions appear in about 50% 4-5 week-old *Clock*$^{-/-}$*;Npas2*$^{m/m}$ double mutant mice (Figure 2.8A, data not shown). By 6-7 weeks and definitely by 11-12 weeks of age large acellular regions are visible across 85% and 100% of *Clock*$^{-/-}$*;Npas2*$^{m/m}$ double mutant mice, respectively (Figure 2.8B, data now shown). Upon closer inspection, these acellular regions startlingly do not appear to contain cells, but possibly contain extracellular matrix-related debris (Figure 2.8C). These histological samples were decalcified prior to sectioning and staining so calcification in the acellular lesions were removed. However, the lesions are anatomically in the same location as the ectopic calcification visible on X-ray.

To identify the components of the lesions and confirm the hypothesis that the lesions contained ectopic calcification, sternal and hind limb tissues of 6-7 week-old *Clock*$^{-/-}$;*Npas2*$^{m/m}$ double mutant mice were not subjected to decalcification, embedded in glycol methacrylate, and sectioned, thereby preserving any calcified tissue. As expected, the acellular costosternal junction lesions stain positive for alizarin red and von Kossa, indicative of the presence of calcium and phosphate, respectively (Figure 2.9A&B). The lesions do not, however, stain positive for safranin-O, which stains proteoglycans that are a main component in cartilage. Notably, there is a layer of calcified, non-cartilage tissue on the sternebral surface that faces the intersternebral cartilage. Lesions in the calcaneal tendon of 19-22 week-old *Clock*$^{-/-}$;*Npas2*$^{m/m}$ double mutant mice also stain positive for alizarin red and von Kossa, but negative for safranin-O (Figure 2.9C). Older animals were chosen to study calcaneal tendon calcification because toluidine blue stains of 6-7 and 11-12 week-old calcaneal tendon did not reveal consistent lesions (Figure 2.10). In one 11-12 week-old calcaneal tendon, an abnormal lesion is visible (Figure 2.10), but in the other *Clock*$^{-/-}$;*Npas2*$^{m/m}$ double mutant calcaneal tendon, the mutant tendon looks like wild-type tissue tendon (data not shown). However, 100% of 11-12 week-old *Clock*$^{-/-}$;*Npas2*$^{m/m}$ double mutant calcaneal tendon contain calcifications on X-ray (data not shown). The discrepancy between the histology and X-ray results of *Clock*$^{-/-}$;*Npas2*$^{m/m}$ double mutant calcaneal tendon could be due to variation in tissue section depth. Histologically prepared 11-12 week-old calcaneal tendons were not sectioned completely through, so it is possible that the histology images of 11-12 week-old *Clock*$^{-/-}$;*Npas2*$^{m/m}$

double mutant calcaneal tendon that do not exhibit abnormalities were simply not sectioned at the correct depth at which to observe ectopic calcification.

Characterization of crystal deposits

The presence of calcium and phosphate in the costosternal junction and calcaneal tendon ectopic calcification of *Clock*$^{-/-}$;*Npas2*$^{m/m}$ double mutant mice has been confirmed by histology, but the exact type of crystal within the lesions remains unclear. The two most likely possibilities are hydroxyapatite (HA) or calcium pyrophosphate dihydrate (CPPD) crystals. HA crystals have a phosphate:calcium (P:Ca) atomic weight ratio of 0.45 while CPPD crystals have a P:Ca atomic weight ratio of 0.75. By assessing the P:Ca atomic weight ratio of ectopic calcification in costosternal junction and calcaneal tendon, it is possible to identify the chemical forms within the deposits.

Due to limited availability of *Clock*$^{-/-}$;*Npas2*$^{m/m}$ double mutant mice, a 53 week-old *Bmal1*$^{-/-}$ mouse with severe gross motor abnormalities was used to evaluate the P:Ca atomic weight ratio of ectopic costosternal junction calcification. Our hypothesis that disruption of the CLOCK/NPAS2:BMAL1 complex leads to age-dependent arthropathy insinuates that either *Clock* and *Npas2*, or *Bmal1*, disruption can cause age-dependent arthropathy, and we have shown that *Clock*$^{-/-}$;*Npas2*$^{m/m}$ double mutant mice phenocopy the arthropathy observed in *Bmal1*$^{-/-}$ mice. Thus, it is expected that the crystal deposits in *Bmal1*$^{-/-}$ mice are of the same composition as crystal deposits in *Clock*$^{-/-}$;*Npas2*$^{m/m}$ double mutant mice. To calculate the P:Ca atomic weight ratio, 60 um sections of sterna were subjected to scanning electron microscopy (SEM) and X-ray microscopy. Sternebral

trabecular tissue and ectopic calcifications were measured to assess bone mineral content (Figure 2.11A). The X-ray spectra of the ectopic calcifications were similar to one another but distinct from the X-ray spectrum of trabecular bone (Figure 2.11B). *Bmal1*$^{-/-}$ costosternal junction ectopic calcifications consist of deposits with a P:Ca atomic weight ratio, and phosphate, calcium, and oxygen stoichiometry consistent with CPPD crystals (Figure 2.11C). This ratio and stoichiometry are unlike that of trabecular bone, which has a P:Ca atomic weight ratio, and phosphate, calcium, and oxygen stoichiometry consistent with tricalcium phosphate, the main crystal found in bone ash, which is the expected composition of trabecular bone (Figure 2.11C). This finding suggests that *Clock*$^{-/-}$*;Npas2*$^{m/m}$ double mutant and *Bmal1*$^{-/-}$ mice develop CPPD crystal deposition disease (CPPD-CDD). Because this experiment included only one study animal, measuring the P:Ca atomic weight ratios of ectopic calcification in multiple *Clock*$^{-/-}$*;Npas2*$^{m/m}$ double mutant mice is necessary to confirm these initial findings.

Concluding remarks

The findings from these studies show that *Clock*$^{-/-}$*;Npas2*$^{m/m}$ double mutant mice exhibit site-specific, age-dependent ectopic calcification. Several different joints and entheses develop ectopic calcification by 41-42 weeks of age, including the forepaws, hindpaws, elbows, stifles, calcaneal tendon, costosternal junctions, costovertebral junctions, and cervical, thoracic, and proximal caudal vertebrae. Costosternal junction and calcaneal tendon calcification is visible as early as 11-12 weeks on X-ray, and costosternal junction calcification is histologically visible as early as 4-5 weeks. The

ectopic calcification in *Bmal1*$^{-/-}$ costosternal junction contain CPPD crystal deposits. As a whole, the arthropic phenotype of *Clock*$^{-/-}$*;Npas2*$^{m/m}$ double mutant mice appears to phenocopy that of *Bmal1*$^{-/-}$ mice [64]. The distribution of arthropathy in *Clock*$^{-/-}$*;Npas2*$^{m/m}$ double mutant and *Bmal1*$^{-/-}$ mice [64] is inconsistent with that of *Per1*$^{-/-}$*;Per2*$^{-/-}$ and *Cry1*$^{-/-}$*;Cry2*$^{-/-}$ double mutant mice [37]. The findings presented here suggest that disruption of the transcriptional activator complex leads to an arthropic phenotype distinct from the modest increase in bone mass specific to disruption of the transcriptional repressor complex. The next step from these findings is to identify possible mechanisms of arthropathy and genes dysregulated due to disruption of the CLOCK:BMAL1 or NPAS2:BMAL1 transcriptional activator complex.

Table 2.1. Sample sizes for male body weight data.

	4-5 wks	6-7 wks	15-22 wks	35-57 wks
Wild-type	2	17	17	8
Clock$^{-/-}$;*Npas2*$^{m/m}$	2	14	9	7
Bmal1$^{-/-}$	2	14	4	2

Table 2.2. Sample sizes for female body weight data.

	6-7 wks	10-13 wks	15-22 wks	35-57 wks
Wild-type	14	5	18	8
Clock$^{-/-}$;*Npas2*$^{m/m}$	11	2	9	2
Bmal1$^{-/-}$	1	1	3	4

Table 2.3. Sample sizes for skeletal X-ray data.

	6-7 wks	10-13 wks	15-22 wks	35-57 wks	64-80 wks
B6 wild-type	M: 8 F: 8	M: 11 F: 7	M: 14 F: 12	M: 11 F: 8	M: 5 F: 3
Clock$^{-/-}$;*Npas2*$^{m/m}$	M: 7 F: 6	M: 4 F: 3	M: 4 F: 7	M: 10 F: 6	-
Bmal1$^{-/-}$	M: 6 F: 1	M: 2 F: 3	M: 4 F: 3	M: 1 F: 5	-
Clock$^{-/-}$	M: 4 F: 3	M: 3 F: 3	M: 4 F: 4	M: 3 F: 4	M: 4 F: 2
Npas2$^{m/m}$	M: 4 F: 6	M: 4 F: 4	M: 4 F: 4	M: 4 F: 4	M: 3 F: 3
Clock$^{+/-}$;*Npas2*$^{m/m}$	M: 4 F: 4	M: 3 F: 3	M: 3 F: 3	M: 3 F: 3	M: 4 F: 2
Clock$^{-/-}$;*Npas2*$^{+/m}$	M: 4 F 4	M: 3 F: 4	M: 3 F: 4	M: 3 F: 4	M: 4 F: 3
129/sv wild-type	-	-	-	-	M: 1
Per1$^{-/-}$;*Per2*$^{-/-}$	-	-	-	-	M: 1

- : did not collect; M: males; F: females

Table 2.4. Sample sizes for organ X-ray data.

	37-49 wks
Wild-type	M: 5
Clock$^{-/-}$;*Npas2*$^{m/m}$	M: 5

M: males

Table 2.5. Sample sizes for micro-CT data.

	11-12 wks	41-42 wks
Wild-type	M: 3 F: 0	M: 1 F: 1
Clock$^{-/-}$;*Npas2*$^{m/m}$	M: 2 F: 0	M: 1 F: 1

M: males; F: females

Table 2.6. Sample sizes for decalcified sternal tissue data.

	4-5 wks	6-7 wks	10-12 wks
Wild-type	M: 2 F: 2	M: 4 F: 1	M: 3 F: 0
Clock$^{-/-}$;*Npas2*$^{m/m}$	M: 2 F: 2	M: 5 F: 4	M: 3 F: 0

M: males; F: females

Table 2.7. Sample sizes for decalcified calcaneal tendon tissue data.

	6-7 wks	11-12 wks
Wild-type	M: 2	M: 2
Clock$^{-/-}$;*Npas2*$^{m/m}$	M: 2	M: 2

M: males

Table 2.8. Sample sizes for non-decalcified tissue data.

	6-7 wks (sterna)	19-22 wks (calcaneal tendon)
Wild-type	M: 1 F: 2	M: 3 F: 0
Clock$^{-/-}$;*Npas2*$^{m/m}$	M: 2 F: 2	M: 2 F: 1

M: males; F: females

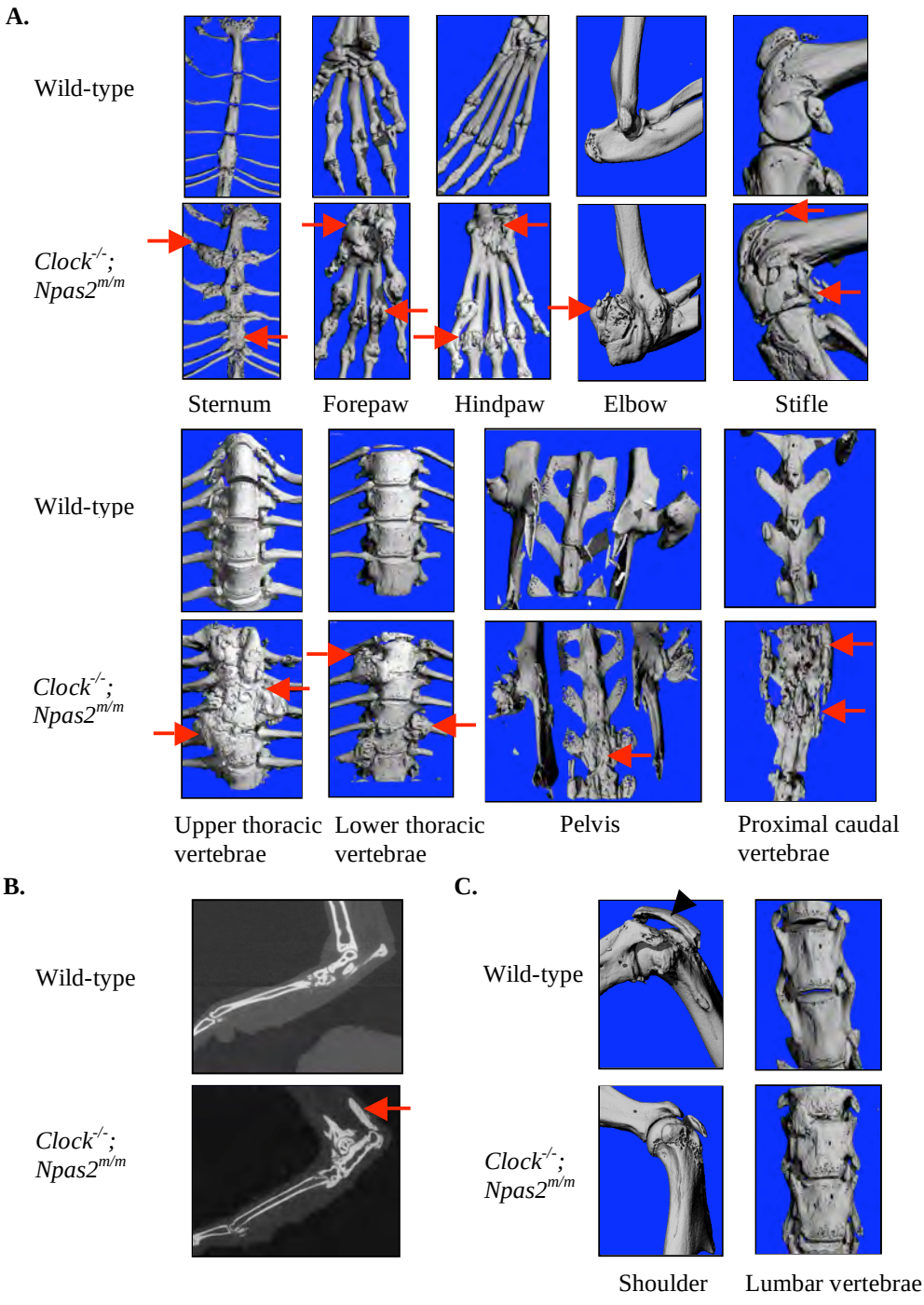

Figure 2.1. Distribution of ectopic calcification in 41-42 week-old *Clock*$^{-/-}$;*Npas2*$^{m/m}$ double mutant mice. (A) 3-D reconstructed micro-CT images illustrating distribution of ectopic calcification in *Clock*$^{-/-}$;*Npas2*$^{m/m}$ double mutant mice. (B) Sagittal 2-D micro-CT images of ectopic calcification in calcaneal tendon of *Clock*$^{-/-}$;*Npas2*$^{m/m}$ double mutant mice. (C) 3-D micro-CT images illustrating lack of visible ectopic calcification in shoulders and lumbar vertebrae of *Clock*$^{-/-}$;*Npas2*$^{m/m}$ double mutant mice. Note that the clavicle was included in the imaging of wild-type shoulder but not *Clock*$^{-/-}$;*Npas2*$^{m/m}$ shoulder (black arrow head). Red arrows highlight ectopic calcification.

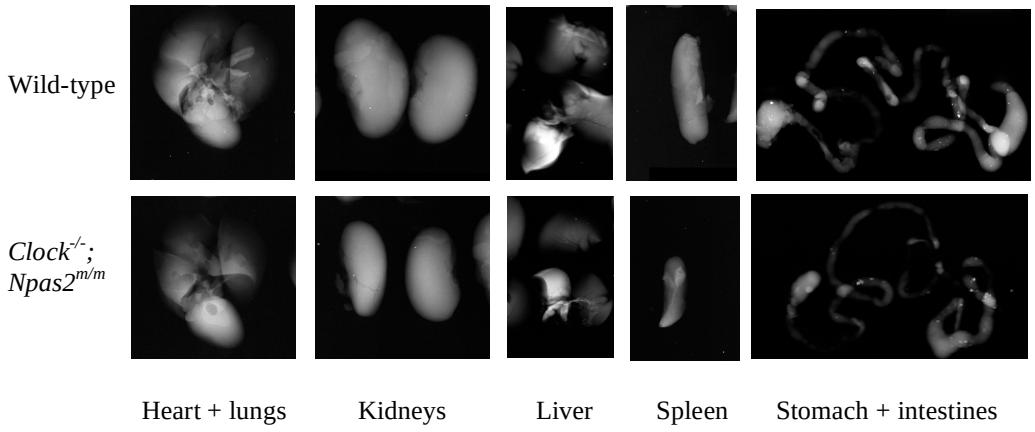

Figure 2.2. X-ray images of *Clock*$^{-/-}$;*Npas2*$^{m/m}$ internal organs do not reveal ectopic calcification. Representative X-ray images from a 37 week-old *Clock*$^{-/-}$;*Npas2*$^{m/m}$ double mutant and a 43 week-old wild-type mouse show no visible difference between mutant and wild-type tissues. Radio-opacities observed in liver, stomach, and intestines are most likely due to the thickness of the tissue or, in the case of the stomach and intestines, the presence of undigested food pellets.

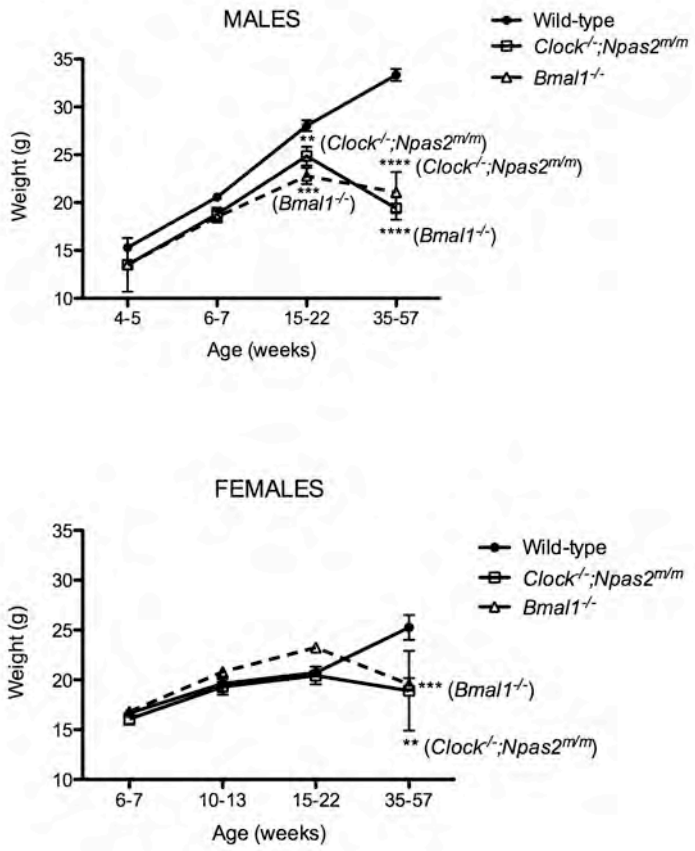

Figure 2.3. *Clock*$^{-/-}$*;Npas2*$^{m/m}$ double mutant mice exhibit age-dependent weight loss. Both male and female *Clock*$^{-/-}$*;Npas2*$^{m/m}$ double mutant and *Bmal1*$^{-/-}$ mice lose weight as they age compared to wild-type mice. **p < 0.01, ****p < 0.0001

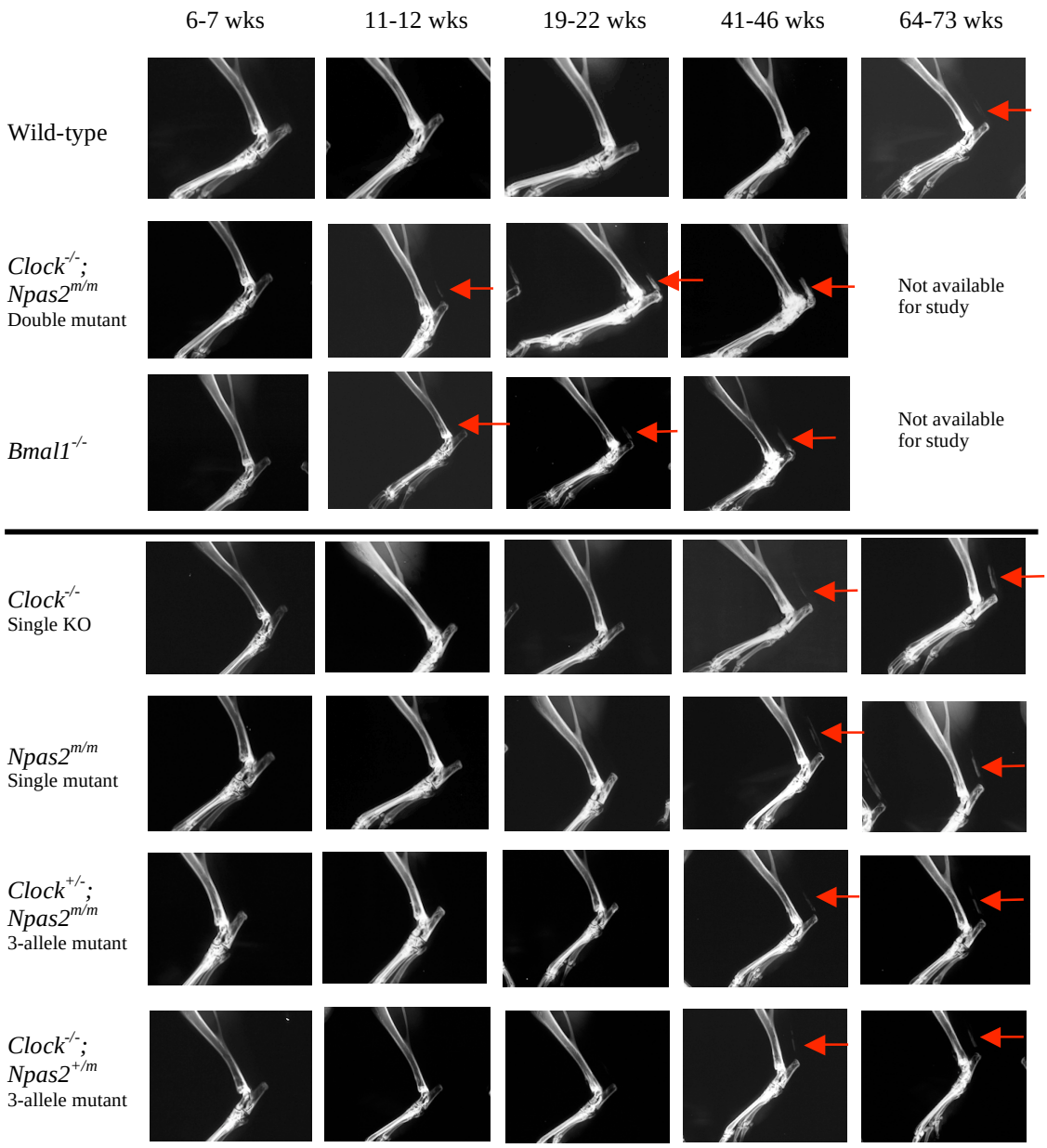

Figure 2.4. Age-progressive calcification of calcaneal tendon in *Clock*$^{-/-}$;*Npas2*$^{m/m}$ double mutant mice. Representative X-ray images of wild-type, *Clock*$^{-/-}$;*Npas2*$^{m/m}$ double mutant, *Bmal1*$^{-/-}$, single mutants (*Clock*$^{-/-}$ and *Npas2*$^{m/m}$), and three-allele mutant (*Clock*$^{+/-}$;*Npas2*$^{m/m}$ and *Clock*$^{-/-}$;*Npas2*$^{+/m}$) calcaneal tendon across age groups, illustrating age-dependent progression of calcification at these sites. Note the appearance of calcaneal tendon calcification in elderly single mutant and three-allele mutants. Red arrows highlight ectopic calcification.

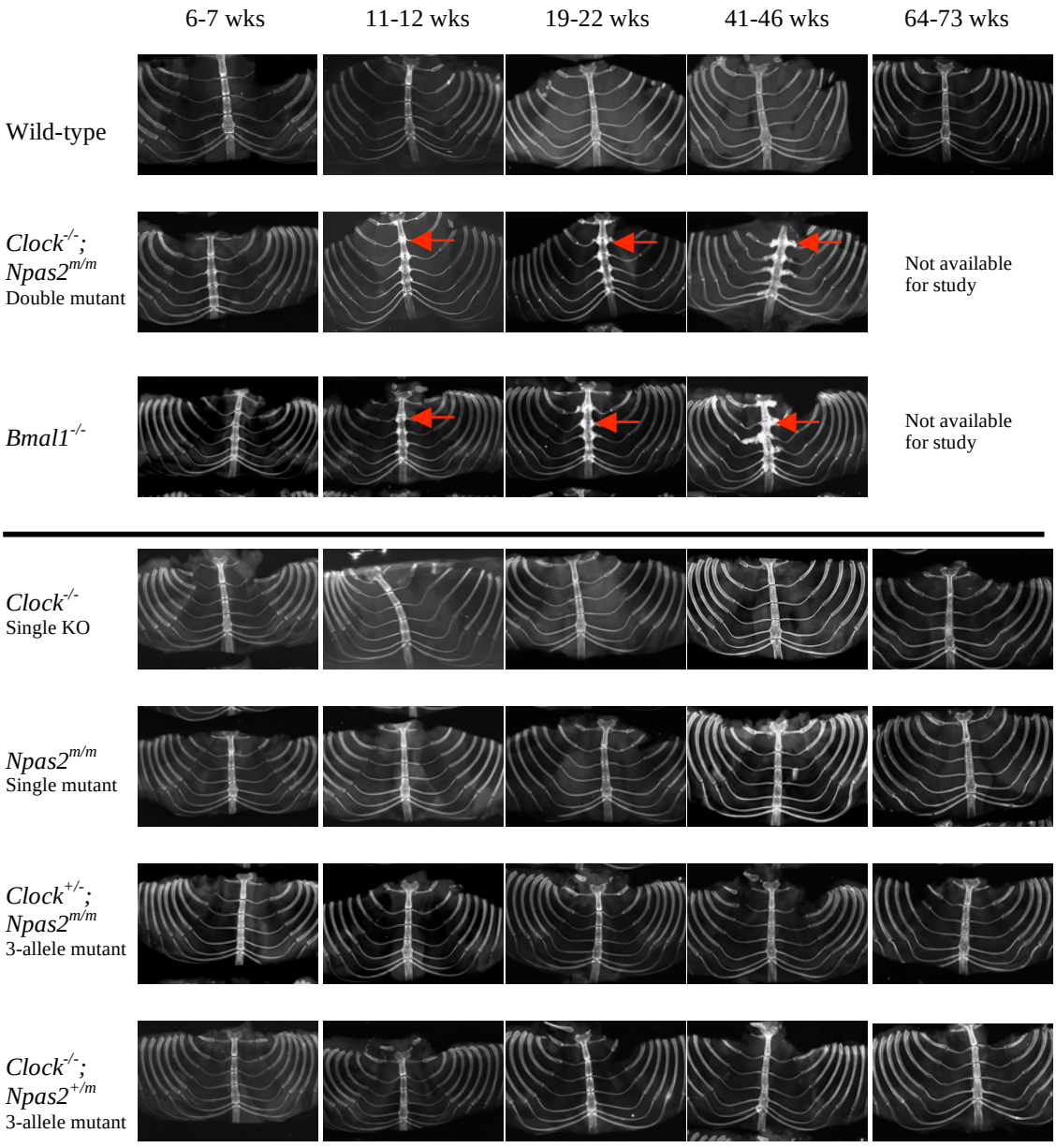

Figure 2.5. Age-progressive calcification of costosternal junction in *Clock*$^{-/-}$;*Npas2*$^{m/m}$ double mutant mice. Representative X-ray images of wild-type, *Clock*$^{-/-}$;*Npas2*$^{m/m}$ double mutant, *Bmal1*$^{-/-}$, single mutants (*Clock*$^{-/-}$ and *Npas2*$^{m/m}$), and three-allele mutant (*Clock*$^{+/-}$;*Npas2*$^{m/m}$ and *Clock*$^{-/-}$;*Npas2*$^{+/m}$) costosternal junction across age groups, illustrating age-dependent progression of calcification at these sites. Note the lack of calcification in any of the single mutant or three-allele costosternal junctions. Red arrows highlight ectopic calcification.

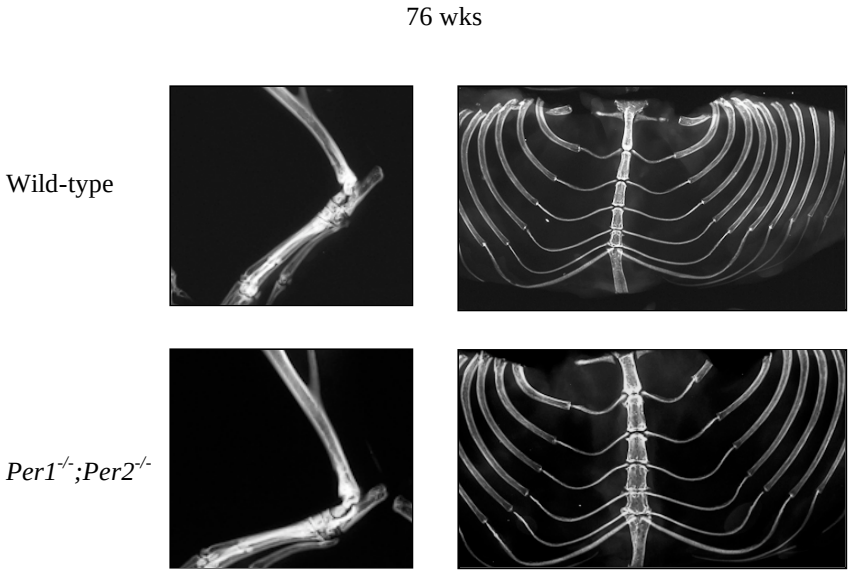

Figure 2.6. No ectopic calcification in calcaneal tendon or costosternal junction of a 76 week-old *Per1*$^{-/-}$;*Per2*$^{-/-}$ double mutant mouse. X-ray images of *Per1*$^{-/-}$;*Per2*$^{-/-}$ double mutant calcaneal tendon and costosternal junction, illustrating a lack of calcification at these sites even at advanced age.

A.

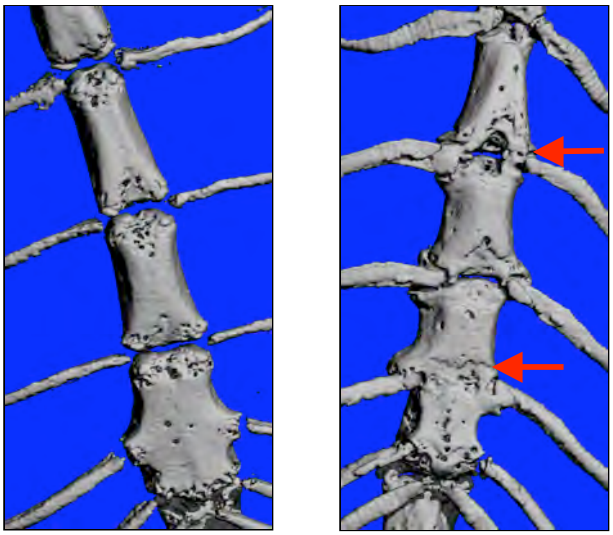

Wild-type *Clock*$^{-/-}$;*Npas2*$^{m/m}$

B.

Clock$^{-/-}$;*Npas2*$^{m/m}$

Figure 2.7. Ectopic calcification of costosternal junction and calcaneal tendon in 11-12 week-old *Clock*$^{-/-}$;*Npas2*$^{m/m}$ double mutant mice. 3-D reconstructed micro-CT images of 11-12 week-old wild-type and *Clock*$^{-/-}$;*Npas2*$^{m/m}$ double mutant costosternal junction (A) and *Clock*$^{-/-}$;*Npas2*$^{m/m}$ double mutant calcaneal tendon (B). Red arrows highlight calcification.

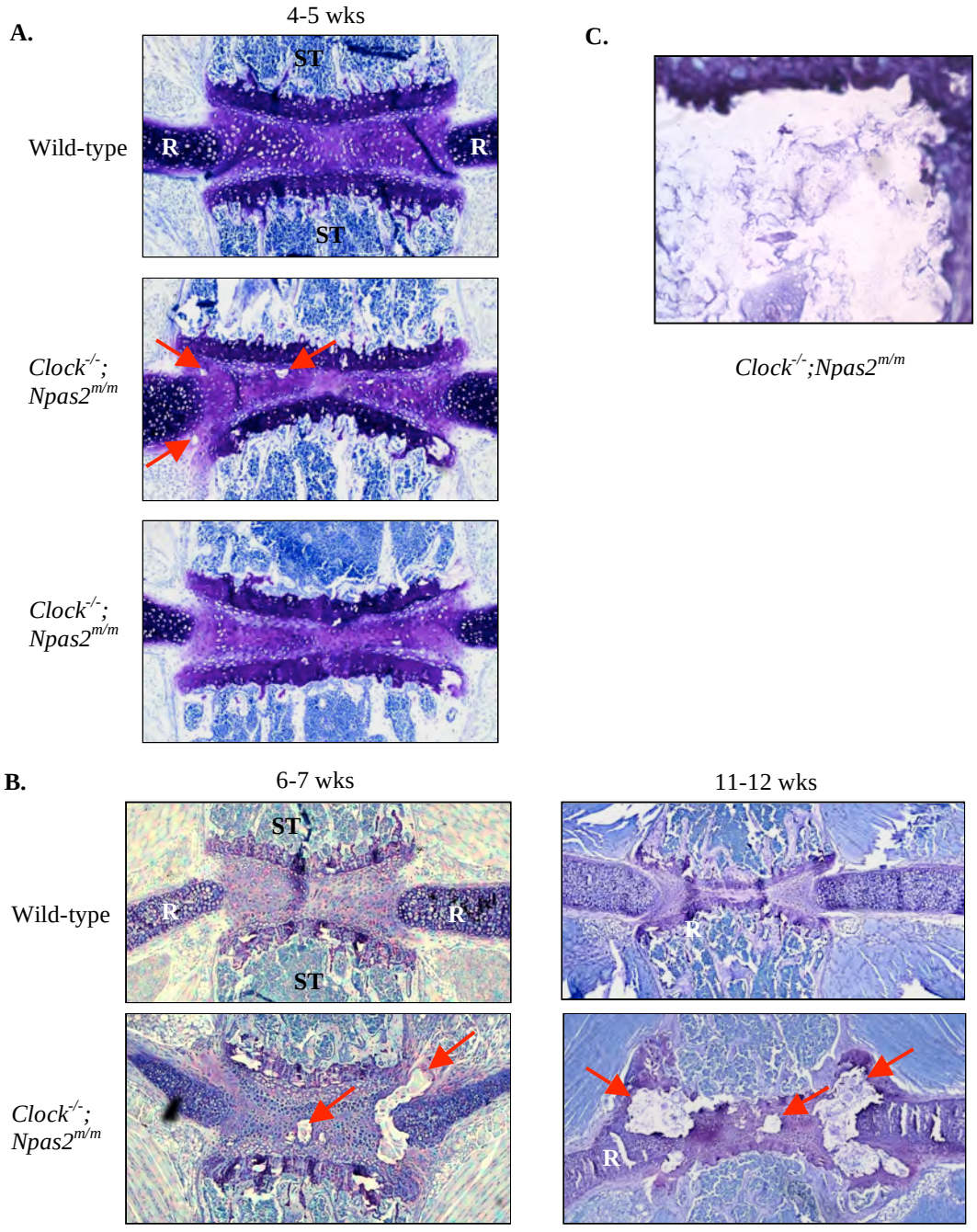

Figure 2.8. Acellular lesions in decalcified costosternal sections of young *Clock*$^{-/-}$;*Npas2*$^{m/m}$ double mutant mice. (A) Toluidine blue (made in water) stain of 4-5 week-old *Clock*$^{-/-}$;*Npas2*$^{m/m}$ double mutant sternum showing inconsistent, small acellular lesions in the costosternal junction. 5X magnifications. (B) Toluidine blue (made in isopropanol) stain of 6-7 and 11-12 week-old *Clock*$^{-/-}$;*Npas2*$^{m/m}$ double mutant sternum illustrating age-dependent increase in acellular lesion size at the costosternal junction. 5X magnifications. (C) Higher magnification of the edge of an acellular lesion from the costosternal junction of an 11-12 week-old *Clock*$^{-/-}$;*Npas2*$^{m/m}$ double mutant mouse. Note the lack of identifiable cells. 40X image. Red arrows highlight acellular lesions. ST: sternebral trabeculae; R: rib cartilage.

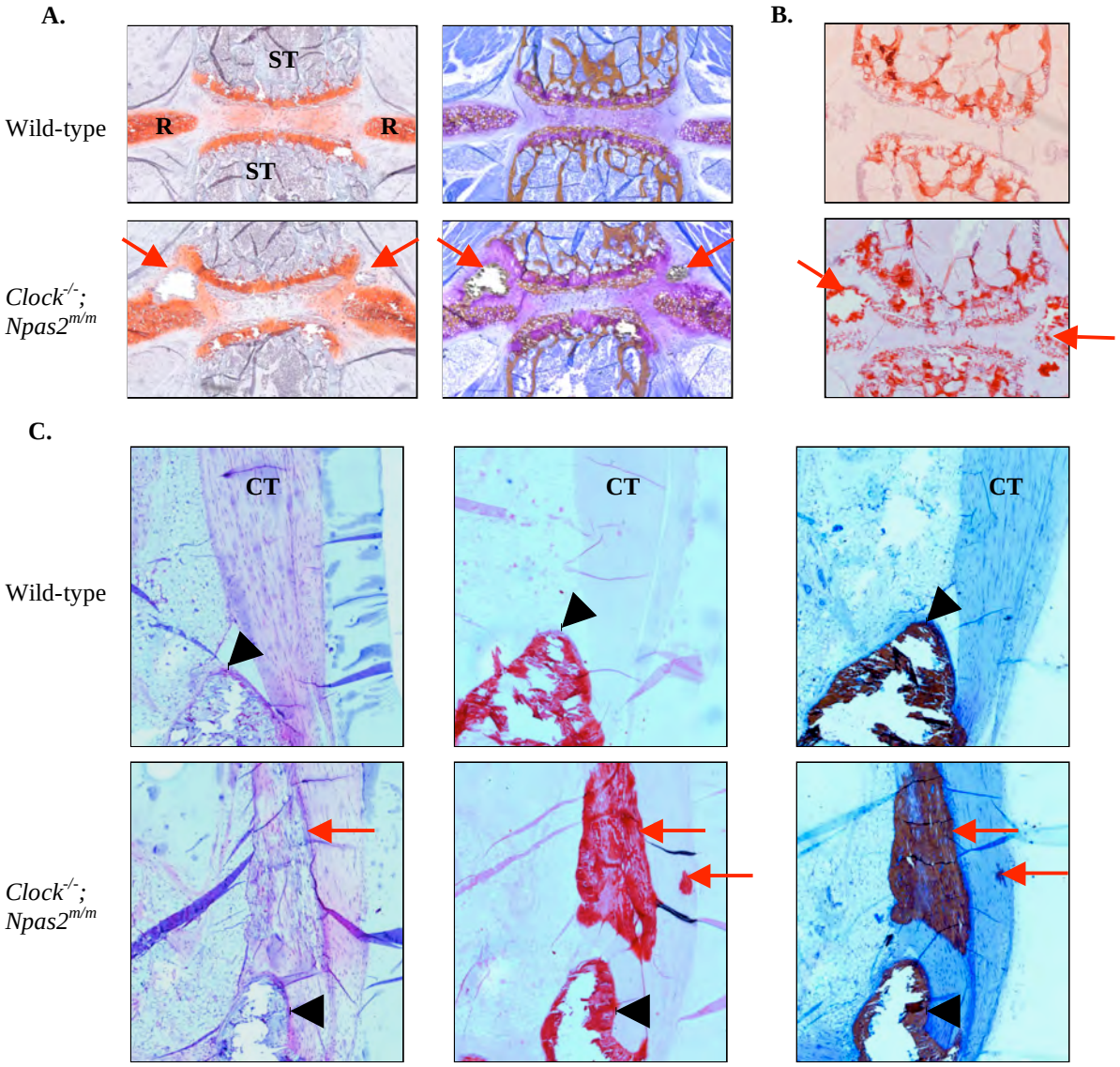

Figure 2.9. Lesions in costosternal junction and calcaneal tendon of *Clock*$^{-/-}$;*Npas2*$^{m/m}$ double mutant mice contain calcium phosphate deposits. (A) Serial sections of non-decalcified, 6-7 week-old wild-type and *Clock*$^{-/-}$;*Npas2*$^{m/m}$ double mutant sternal tissue stained with safranin-O (left) and von Kossa (right), the latter of which is counterstained with toluidine blue made up in distilled water. (B) Alizarin red stain of non-decalcified, 6-7 week-old wild-type and *Clock*$^{-/-}$;*Npas2*$^{m/m}$ double mutant sternal tissue. (C) Serial sections of non-decalcified, 19-22 week-old wild-type and *Clock*$^{-/-}$;*Npas2*$^{m/m}$ double mutant calcaneal tendon stained with safranin-O (left), alizarin red (middle), and von Kossa (right), the last of which is counterstained with toluidine blue made up in distilled water. Note the absence of safranin-O stain but the positive von Kossa and alizarin red stains in the lesions, which are denoted by red arrows. All images are 5X magnifications. Black arrowheads identify the calcaneus bone, the insertion site of the calcaneal tendon. ST: sternebral trabculae; R: rib cartilage; CT: calcaneal tendon.

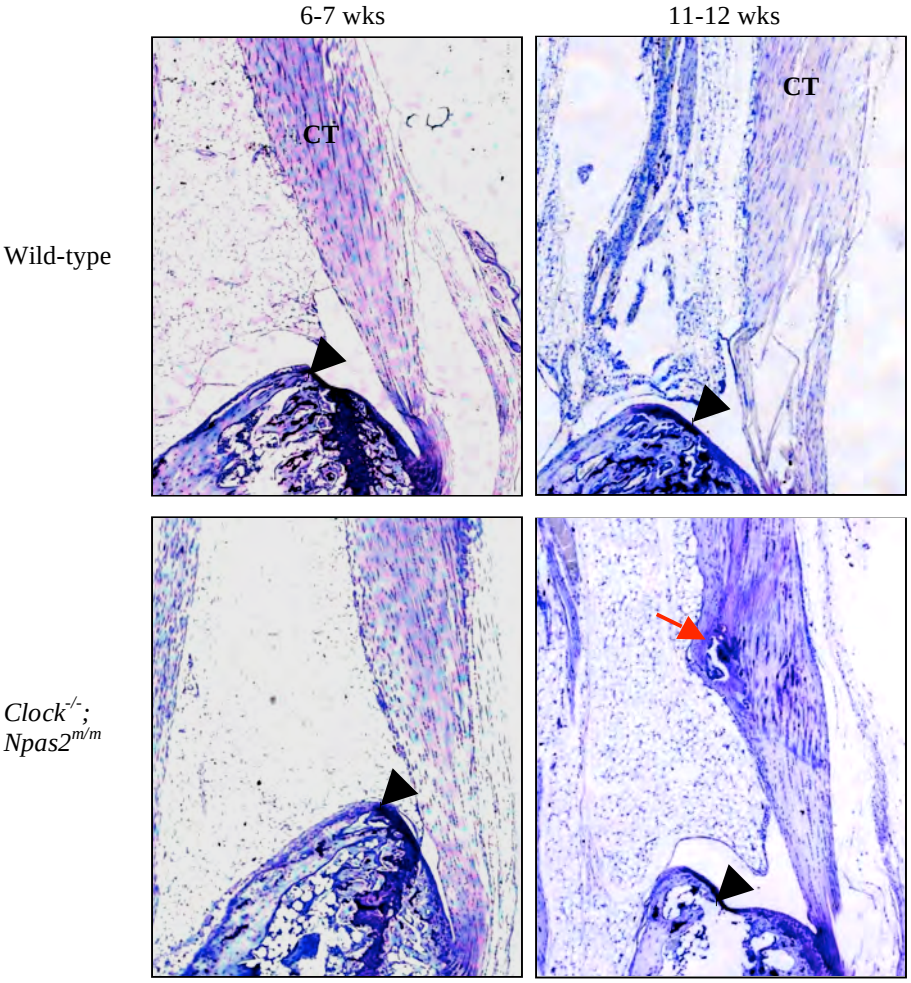

Figure 2.10. Calcaneal tendon histology of 6-7 and 11-12 week-old *Clock*$^{-/-}$;*Npas2*$^{m/m}$ double mutant mice. Toluidine blue (made in isopropanol) stains of decalcified 6-7 week-old *Clock*$^{-/-}$;*Npas2*$^{m/m}$ double mutant calcaneal tendon do not reveal lesions, which is consistent with the lack of visible calcification of these same animals on X-ray. In some 11-12 week-old *Clock*$^{-/-}$;*Npas2*$^{m/m}$ double mutant mice, calcaneal tendon exhibit lesions but this phenotype is inconsistent across double mutants of this age. 5X magnifications. Red arrow highlights probable calcification. Black arrowheads identify calcaneus bone. CT: calcaneal tendon.

A.

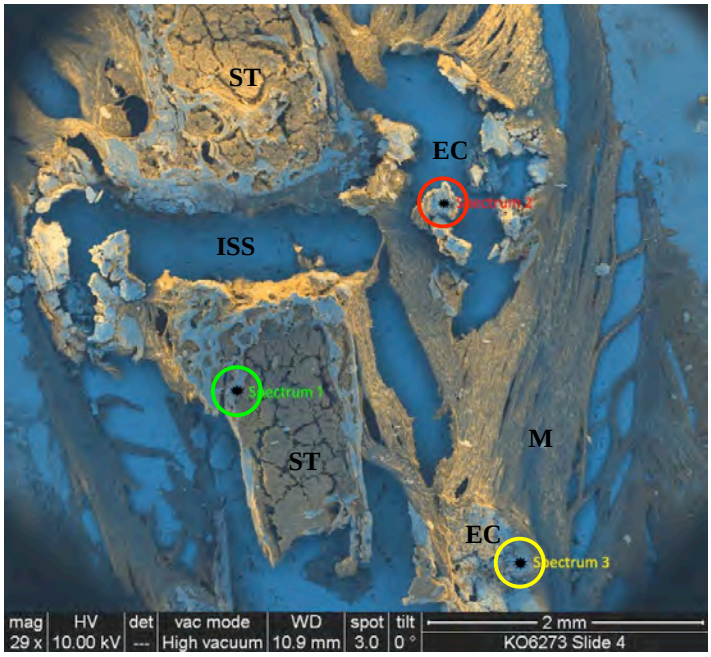

B.

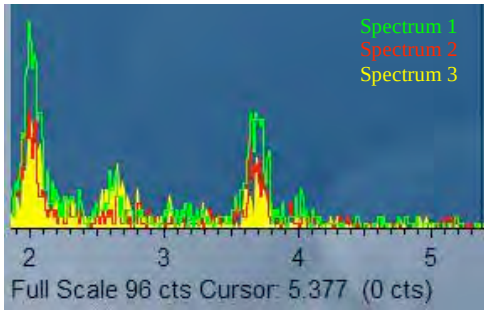

C.

	Element	Atomic %	P:Ca ratio	Crystal
Spectrum 1	P	10.27	0.666	Tricalcium
	Ca	11.50		phosphate (bone ash)
Spectrum 2	P	11.59	0.700	Calcium pyrophosphate
	Ca	12.41		
Spectrum 3	P	3.64	0.855	Calcium pyrophosphate
	Ca	3.19		

Figure 2.11. Ectopic calcification in the sternum of a 53 week-old *Bmal1*$^{-/-}$ mouse contains CPPD crystal deposits. (A) A mixed SEI+BSI image of sternum. Carbon appears brown while heavier elements, such as calcium (calcifications) and silicon (the slide) appear blue. Spectra refer to locations sampled to calculate P:Ca ratios. (B) X-ray spectra graph of the three sampled locations. (C) Raw values of calcium and phosphate atomic % in sampled tissue locations. Note that Spectra 2 & 3 (ectopic calcifications) have P:Ca ratios characteristic of CPPD while Spectrum 1 (bone) does not, and this difference is reflected in the X-ray spectra results. ST: sternebral trabeculae; ISS: intersternebral space; EC: ectopic calcification; M: muscle.

Chapter III

Investigating possible systemic mechanisms of age-dependent arthropathy in *Clock*$^{-/-}$;*Npas2*$^{m/m}$ double mutant mice

Summary

Age-dependent arthropathy in *Clock*$^{-/-}$;*Npas2*$^{m/m}$ double mutant mice could be due to a number of different mechanisms. Three systemic possibilities are mechanical stress, disrupted circadian rhythms, and metastatic calcification. Each of these mechanisms affects the entire mouse and could explain the broad distribution of ectopic calcification observed in *Clock*$^{-/-}$;*Npas2*$^{m/m}$ double mutant mice. Weight-bearing joints develop ectopic calcification, which supports the hypothesis that musculoskeletal-related mechanical stress contributes to the development of arthropathy. The fact that *Clock* and *Npas2* are critical components of the SCN circadian oscillator suggests that arrhythmicity could cause arthropathy in *Clock*$^{-/-}$;*Npas2*$^{m/m}$ double mutant mice. Lastly, the site-specificity of ectopic calcification insinuates metastatic calcification. To study these three possibilities, *Clock*$^{-/-}$;*Npas2*$^{m/m}$ double mutant mice were subjected to a series of studies. Some were given access to running wheels and then X-rayed to assess ectopic calcification development in the presence of increased mechanical stress. There is no visible difference in arthropathy of *Clock*$^{-/-}$;*Npas2*$^{m/m}$ double mutant mice with access to running wheels compared to *Clock*$^{-/-}$;*Npas2*$^{m/m}$ double mutant mice without access to running wheels, suggesting that mechanical stress does not contribute to the development of age-

dependent arthropathy in these mutants. In the next experiment, *Clock* and *Npas2* were both knocked out in the SCN of transgenic mice, rendering them arrhythmic in constant darkness. These arrhythmic transgenic mice do not develop ectopic calcification, showing that disruption of centrally regulated circadian rhythms is not sufficient to cause age-dependent arthropathy. In the last experiment, serum chemistry analyses were performed on *Clock*$^{-/-}$*;Npas2*$^{m/m}$ double mutant mice. Calcium and phosphorus levels are not significantly different in the serum of *Clock*$^{-/-}$*;Npas2*$^{m/m}$ double mutant mice compared to wild-type serum. This result suggests that metastatic calcification is an unlikely mechanism of age-dependent arthropathy in *Clock*$^{-/-}$*;Npas2*$^{m/m}$ double mutant mice.

Acknowledgments

Part of this chapter was a result of work performed by the Department of Animal Medicine at the University of Massachusetts Medical School (UMMS). As such, I would like to acknowledge the appropriate people for their contribution to the work presented here.

Michelle Bombard and the technicians in the Department of Animal Medicine performed the serology analyses. Dr. David Weaver generated *Vgat-Cre+/-;Clock*$^{fl/fl}$*;Npas2*$^{m/m}$ mice and set up the running wheel cages for those mice. Dave also assisted in setting up running wheel cages for *Clock*$^{-/-}$*;Npas2*$^{m/m}$ double mutant and wild-type mice.

Figure 3.1. Mechanical stress does not seem to contribute to arthropathy development in *Clock*$^{-/-}$*;Npas2*$^{m/m}$ double mutant mice.
Elizabeth Yu and Dr. David Weaver – Department of Neurobiology, UMMS

Figure 3.2. Disruption of centrally regulated circadian rhythms is not sufficient to cause age-dependent arthropathy.
Elizabeth Yu and Dr. David Weaver – Department of Neurobiology, UMMS

Figure 3.3. Normal serum calcium and phosphorus levels in *Clock*$^{-/-}$*;Npas2*$^{m/m}$ double mutant mice.
Elizabeth Yu – Department of Neurobiology, UMMS
Michelle Bombard – Supervisor of Veterinary Services, Department of Animal Medicine, UMMS

Introduction

The site-specificity of arthropathy in *Clock*$^{-/-}$*;Npas2*$^{m/m}$ double mutant mice leads to an obvious question: why do calcifications develop at these specific sites but not others? One possibility is mechanical. The main sites affected in 41-42 week-old *Clock*$^{-/-}$*;Npas2*$^{m/m}$ double mutant mice are considered weight-bearing. In quadrupeds, a large portion of an animal's weight is supported by the forepaws, hindpaws, stifles (knees), and elbows. The sternum and costosternal junctions undergo repetitive movement during respiration. The tarsus is a joint that undergoes ubiquitous movement, as contraction of the calf muscles (the gastrocnemius and soleus) lifts the calcaneus via the calcaneal tendon, which is essential to walking, running, and jumping. It is possible that sheer mechanical stress on these joints causes ectopic calcification over time.

A second possible explanation for the extensive joint calcification in *Clock*$^{-/-}$*;Npas2*$^{m/m}$ double mutant mice is disruption of circadian rhythms. *Clock*, *Npas2*, and *Bmal1* are all core components of the circadian oscillator. Disruption of *Clock* and *Npas2*, or *Bmal1* expression is sufficient to cause arrhythmicity in constant darkness [39, 45]. It is possible that disruption of circadian rhythms affects peripheral tissues such that they are not able to function properly and calcification ensues. Such is the case with liver physiology and rhythmicity. In the liver, transcription factors *Dbp*, *Tef*, and *Hlf* are transcriptionally regulated by CLOCK:BMAL1 (and thus are rhythmically expressed) and are involved in detoxification and drug metabolism [58]. Mice lacking all three of these transcription factors are hypersensitive to xenobiotic compounds and suffer from

premature aging [58]. *Clock*$^{\Delta 19/\Delta 19}$ mutant and *Bmal1*$^{-/-}$ mice are similarly hypersensitive to cyclophosphamide, an anti-cancer drug [59]. Disrupting liver-specific oscillators has also been shown to disrupt rhythmicity in pentobarbital metabolism [60]. Therefore, in the case of *Clock*$^{-/-}$*;Npas2*$^{m/m}$ double mutant mice, it is possible that disruption of centrally regulated circadian rhythms in the SCN causes desynchronization of peripheral oscillators in joints, leading to the development of ectopic calcification. Peripheral tissues still contain oscillators, but the disruption of centrally regulated rhythms could trickle down to disrupt peripheral oscillator function.

However, an elegant study using brain-specific *Bmal1* rescue suggests that the arthropathy in *Bmal1*$^{-/-}$ mice is not related to SCN-related circadian rhythms [68]. In this study, the authors constitutively expressed *Bmal1* in the SCN (and other non-SCN brain regions) of *Bmal1*$^{-/-}$ mice. This brain-rescued line employed a tetracycline transactivator system that enabled the authors to reversibly remove *Bmal1* expression by feeding the mice doxycycline. These *Bmal1*$^{-/-}$ mice spent the majority of their lives with *Bmal1* constitutively expressed in the SCN, and when *Bmal1* was expressed these mutants displayed rhythmic locomotor behavior in constant darkness. Rhythmic locomotor activity is indicative of rhythmically functioning SCN, which impose rhythmicity upon peripheral tissues and drive rhythmic expression of peripheral oscillator proteins, even if a core clock component, such as *Clock*, is missing from that peripheral tissue [51]. In other words, in these *Bmal1*$^{-/-}$ mice with *Bmal1* expression in brain, peripheral tissues are presumably rhythmic due to imposed rhythmicity from normal, rhythmic SCN. Interestingly, four to six month-old *Bmal1*$^{-/-}$ mice with *Bmal1* expression in brain

continue to exhibit profound calcaneal tendon calcification. This finding shows that restoration of SCN rhythms, and thus peripheral tissue rhythmicity, is not sufficient to rescue peripheral tissue arthropathy, suggesting that circadian rhythms do not play a role in age-dependent ectopic calcification. It is more likely that *Bmal1* is driving the expression of non-oscillator genes to regulate ectopic calcification, in a manner unrelated to circadian rhythms.

A third possible systemic mechanism of arthropathy in *Clock*$^{-/-}$;*Npas2*$^{m/m}$ double mutant mice is serum electrolyte dysfunction. Abnormal calcium and/or phosphorus levels can cause metastatic calcification and commonly occur secondary to systemic hormone imbalances. For example, people suffering from hyperparathyroidism generate excessive parathyroid hormone, which leads to hypercalcemia and metastatic calcification [97]. A mutant mouse model with ectopic calcification secondary to systemic mineral imbalances is the *FGF23*$^{-/-}$ mouse [98, 99]. *FGF23*$^{-/-}$ mice have elevated serum calcium and phosphorus levels that cause the organ ectopic calcification.

An imbalance of calcium and/or phosphate in the blood can lead to nonspecific calcium phosphate deposition in various soft tissues, such as lungs and blood vessels. Because *Clock* and *Npas2* are important regulators of SCN rhythmicity and the SCN regulate rhythmic hormone production, it is possible that dysfunctional hormone production leads to abnormal serum calcium and phosphorus levels in *Clock*$^{-/-}$;*Npas2*$^{m/m}$ double mutant mice, ultimately leading to ectopic calcification.

To investigate these three systemic mechanisms, *Clock*$^{-/-}$;*Npas2*$^{m/m}$ double mutant mice were subjected to a series of experiments. In the first experiment, *Clock*$^{-/-}$;*Npas2*$^{m/m}$

double mutant mice were placed in cages with running wheels to test the effect of musculoskeletal stress on joints. Mice of the C57BL/6J background are compulsive runners and will spend a large portion of their time awake on the running wheel [100]. In the second experiment, *Clock* expression was exclusively knocked out of the SCN (and other non-SCN brain regions) of $Npas2^{m/m}$ mice. These transgenic mice are denoted $Clock^{fl/fl};Npas2^{m/m}$, meaning they carry two *Clock* alleles with loxP sites flanking exon 5 and 6, as well as two mutated, nonfunctional *Npas2* alleles. By crossing these mice with a Cre-recombinase mouse, we can knockout *Clock* expression in a tissue-specific manner, depending on the promoter that drives Cre-recombinase expression. Vesicular GABA transporter (Vgat)-Cre recombinase was chosen in this study because Vgat is exclusively expressed in GABAergic neurons, which includes every SCN neuron as well as some non-SCN brain regions [101]. By generating $Vgat\text{-}Cre+;Clock^{fl/fl};Npas2^{m/m}$ mice, we effectively knock out *Clock* and *Npas2* expression in GABA-expressing brain tissue, including the SCN, while the rest of the tissues are $Npas2^{m/m}$. In the last experiment, serum samples from 37-49 week-old $Clock^{-/-};Npas2^{m/m}$ double mutant mice were analyzed for calcium and phosphate content.

Experimental procedures

Generation, maintenance, and genotyping of study animals

Clock$^{fl/fl}$ mice were generated in our laboratory, as previously described [51]. *Vgat-Cre+* mice were a kind gift from Dr. Linh Vong in the laboratory of Dr. Brad Lowell (Beth Israel Deaconess Medical Center). *Vgat-Cre+* mice were not backcrossed to the C57BL/6J background prior to conducting these studies.

For *Cre-recombinase* PCR genotyping, a two-primer set was used to identify the expression of *Cre*. This primer set consists of a forward primer (Crelil-F: ACCTGAAGATGTTCGCGATTATCT) and a reverse primer (Crelil-R: ACCGTCAGTACGTGAGATATCTT). A two-primer set to identify the expression of wild-type *Clock* as an internal control was also included, which consists of a forward primer (ClockGTF-63B: GCAAGAAGAACTAAGGAAAATTCAAGAGCAACTTCA GATGGTCCATGGTCAAGGGCTACAGTT) and a reverse primer (ClockGTR-inB: TAGTGCCCTAGATGGCCCTGTTGG). Reactions were performed using the same cycling protocol as for *Clock*. *Cre* product size was 370 nt. Wild-type *Clock* product size was 410 nt.

Please see “Chapter II: Experimental procedures” for additional information on generation, maintenance, and genotyping of mutant and wild-type mice used in this chapter.

Behavioral analysis (running wheels)

Five *Clock*$^{-/-}$*;Npas2*$^{m/m}$ double mutant and six wild-type mice of both genders were used in this study. Mice were 4-5 weeks old at the start of the experiment and collected and X-rayed at 20-21 weeks of age. Mice were housed individually in rat cages equipped with or without running wheels and maintained in light-tight, ventilated closets within a temperature- and humidity-controlled facility. Food and water were available *ad libitum*. The animals were maintained on a 12 hour light:12 hour dark (LD) lighting cycle before and during the study. White light was emitted from fluorescent bulbs controlled by a timer and dim red light (~200 lux) was present continuously. Running wheels were equipped with magnets on opposing sides and activity was detected as switch closures using a magnetic reed switch mounted on top of each cage. ClockLab Data Collection (Actimetrics) software monitored and stored activity in 1-minute bins. ClockLab Data Analysis software was used to produce the double-plotted acrograms. Two *Clock*$^{-/-}$*;Npas2*$^{m/m}$ double mutant mice (one male, one female) were placed in cages with running wheels, three *Clock*$^{-/-}$*;Npas2*$^{m/m}$ double mutant mice (all female) were in cages without running wheels, three wild-type mice (one male, two female) were in cages with running wheels, and three wild-type mice (two male, one female) were in cages without running wheels.

X-rays

Skeletal tissues were X-rayed with a high resolution MX-20 Faxitron on mammography film. Please see “Chapter II: Experimental procedures” for details.

Serology

Ten male 37-49 week-old (five wild-type, mean age 40.5 ± 3.6 weeks; five *Clock*$^{-/-}$;*Npas2*$^{m/m}$ double mutants, mean age 40.0 ± 5.0 weeks) mice were decapitated and trunk blood was collected in anti-coagulant-free tubes at room temperature between 12-1pm. Within two hours, samples were processed by Michelle Bombard et al. as follows: samples were centrifuged at 5500 rpm for 10 minutes at room temperature to isolate serum, and then 100 ul of serum were dispensed into Abaxis Comprehensive Diagnostic Profile rotors and the rotors were analyzed by an Abaxis VetScan Chemistry Analyzer (Abaxis, Union City, CA). Of the ten mice collected in this study, one wild-type mouse was excluded from statistical analyses because it exhibited elevated markers of kidney function beyond the reference range, indicating that the mouse was undergoing kidney failure. One *Clock*$^{-/-}$;*Npas2*$^{m/m}$ mouse was also excluded because its blood sample was grossly hemolytic.

Statistical analysis

Serology results were normalized to the average wild-type value for a given serum marker. Normalized serology results were analyzed using unpaired t-tests (Prism 5 for Mac OS X software). P-values less than 0.05 were considered statistically significant.

Results and discussion

Assessing effect of mechanical stress on arthropathy

The hypothesis that mechanical stress contributes to the development of age-dependent arthropathy in *Clock*$^{-/-}$;*Npas2*$^{m/m}$ double mutant mice was tested by placing animals in cages with and without running wheels. Mice were 4-5 weeks old at the beginning of the experiment and 20-21 weeks old at the end, meaning they spent 16 weeks singly housed in cages with or without running wheels. On X-ray, ectopic calcification is detectable at 11-12 weeks in both costosternal junction and calcaneal tendon (Figure 2.4) so it was expected that by 20-21 weeks of age calcification would be visible.

Gross visual analysis of X-ray images revealed that *Clock*$^{-/-}$;*Npas2*$^{m/m}$ double mutant mice with access to running wheels do not develop noticeably more calcification than *Clock*$^{-/-}$;*Npas2*$^{m/m}$ double mutant mice without access to running wheels (Figure 3.1). The vertebrae, pelvis, sternum, forepaws, hindlimbs, and forelimbs were examined (Figure 3.1, data not shown). This result suggests that mechanical stress does not play a significant role in arthropathy development in *Clock*$^{-/-}$;*Npas2*$^{m/m}$ double mutant mice. Closer evaluation of *Clock*$^{-/-}$;*Npas2*$^{m/m}$ double mutant mice using micro-CT would more meticulously evaluate running wheel effects, but these X-ray results suggest that there is not a significant effect of running wheel access to the progression of arthropathy.

However, an important assumption of this experimental design is that access to a running wheel leads to more mechanical stress on weight-bearing joints. It has been

observed that *Clock*$^{-/-}$*;Npas2*$^{m/m}$ double mutant mice are less active than their wild-type counterparts when both are given access to running wheels (our unpublished data). Control mice in cages without running wheels were not evaluated for overall activity, so it is unclear if *Clock*$^{-/-}$*;Npas2*$^{m/m}$ double mutant mice with access to running wheels were actually more active than *Clock*$^{-/-}$*;Npas2*$^{m/m}$ double mutant mice without access to running wheels. It is possible that *Clock*$^{-/-}$*;Npas2*$^{m/m}$ double mutant mice with running wheels did not, in fact, exert more mechanical stress on their weight-bearing joints compared to control mice.

Also, the anatomical distribution of early onset arthropathy, namely the costosternal junction and calcaneal tendon, suggests that weight-bearing joints are not necessarily specific targets of age-dependent arthropathy in *Clock*$^{-/-}$*;Npas2*$^{m/m}$ double mutant mice. Granted, costosternal junction and calcaneal tendon undergo mechanical stress in quadrupeds, but joints such as the carpus, tarsus, elbows, and stifles undergo much more. If this arthropathy is truly specific to weight-bearing joints, then one would expect the joints that undergo the most weight and mechanical stress to develop ectopic calcifications first. Clearly this is not the case, as ectopic calcification of the carpus, tarsus, elbows, and stifles appear later than calcification of costosternal junction and calcaneal tendon. So while it cannot be concluded with certainty from this running wheel experiment if mechanical stress has *no* effect on arthropathy development, the lack of intensified ectopic calcifications in *Clock*$^{-/-}$*;Npas2*$^{m/m}$ double mutant mice with access to running wheels coupled with the site-specificity of arthropathy together suggest that

mechanical stress does not significantly contribute to the development of age-dependent ectopic calcification in *Clock*$^{-/-}$;*Npas2*$^{m/m}$ double mutant mice.

Assessing effect of brain-specific gene disruption on arthropathy

The role of *Clock*, *Npas2*, and *Bmal1* in the circadian feedback loop suggests that disruption of behavioral circadian rhythms in *Clock*$^{-/-}$;*Npas2*$^{m/m}$ double mutant mice may contribute to the development of arthropathy. However, CLOCK/NPAS2:BMAL1 transcriptionally regulate both core clock and clock output genes, making it difficult to discern between their regulation of core clock versus clock output genes. In an attempt to tease apart the role of *Clock* and *Npas2* in the circadian oscillator and their role in regulating clock output gene expression, an experiment targeting *Clock* and *Npas2* disruption in the brain, including the SCN, was conducted. In this experiment, *Clock*$^{fl/fl}$;*Npas2*$^{m/m}$ mice were crossed with *Vgat-Cre+* mice to generate brain-specific disruption of *Clock* and *Npas2*. The rest of the transgenic animal still expresses functional CLOCK, but dysfunctional NPAS2 (Figure 3.2A, right). It has been shown previously that *Npas2*$^{m/m}$ mice do not develop arthropathy or disrupted circadian rhythms (our unpublished results) [39]. Animals were placed in running wheel cages to assess behavioral rhythmicity and then sacrificed and X-rayed to assess ectopic calcification.

Vgat-Cre+;Clock$^{fl/fl}$;*Npas2*$^{m/m}$ mice are behaviorally arrhythmic in constant darkness and do not develop arthropathy by 20-21 weeks of age (Figure 3.2A&B), whereas *Clock*$^{-/-}$;*Npas2*$^{m/m}$ double mutant mice exhibit arthropathy by this age (Figure 2.4 & 2.5). *Vgat-Cre-;Clock*$^{fl/fl}$;*Npas2*$^{m/m}$ control mice, which express *Clock* in every tissue

and are equivalent to *Npas2*$^{m/m}$ mice, are behaviorally rhythmic in constant darkness and also do not develop ectopic calcification (Figure 3.2A&B). This finding shows that disruption of centrally regulated circadian rhythms, as evidenced by behavioral arrhythmicity in constant darkness, is **not** sufficient to cause age-dependent arthropathy. Any rhythmic output from the SCN to peripheral tissues has been disrupted in this transgenic mouse model. However, peripheral tissues still contain functional oscillators, so it is possible that intact peripheral tissue oscillator function is sufficient to *prevent* arthropathy development. Unfortunately, it is nearly impossible to differentiate between the role of *Clock* and *Npas2* in regulating circadian oscillator function and their role in regulating non-oscillator output genes. When *Clock* and *Npas2* expression is disrupted, so are all of their target genes, both oscillator-related and not. However, the lack of arthropathy in other arrhythmic circadian mutant mice supports the conclusion that disruption of centrally-regulated rhythms is insufficient to cause arthropathy. *Per1*$^{-/-}$*;Per2*$^{-/-}$ and *Cry1*$^{-/-}$*;Cry2*$^{-/-}$ double knockout mice are arrhythmic but have not been shown to develop age-dependent arthropathy (Figure 2.6) [37]. The results of this experiment show that disruption of centrally regulated circadian rhythms is insufficient to cause arthropathy, suggesting that these *Clock* and *Npas2* influence arthropathy through local mechanisms, rather than through central circadian function.

Serology of *Clock*$^{-/-}$*;Npas2*$^{m/m}$ double mutant mice

In the study first describing age-dependent arthropathy in *Bmal1*$^{-/-}$ mice, the authors measured serum calcium and phosphorus levels to investigate a systemic cause of

arthropathy [64]. The authors found no significant difference in serum calcium or phosphorus levels in *Bmal1*$^{-/-}$ mice as compared to wild-type mice, fueling their conclusion that systemic mineral imbalances are not responsible for age-dependent arthropathy in *Bmal1*$^{-/-}$ mice.

To investigate this same possibility in *Clock*$^{-/-}$*;Npas2*$^{m/m}$ double mutant mice, serum chemistry analysis was performed. Serum from 37-49 week-old *Clock*$^{-/-}$*;Npas2*$^{m/m}$ double mutant and wild-type mice were analyzed for a number of markers, including calcium, phosphorus, alkaline phosphatase (ALP), and alanine transferase (ALT). ALP and ALT together are considered indicators of liver function, but ALP is also a critical enzyme involved in calcification. ALP is produced by hypertrophic chondrocytes and osteoblasts, and is responsible for calcifying extracellular matrix [14, 15].

In *Clock*$^{-/-}$*;Npas2*$^{m/m}$ double mutant mice, serum calcium and phosphorus levels are not significantly different from wild-type levels (Figure 3.3). ALP and ALT levels, on the other hand, are significantly higher in *Clock*$^{-/-}$*;Npas2*$^{m/m}$ double mutant mice (Figure 3.3). The presence of ectopic calcification in *Clock*$^{-/-}$*;Npas2*$^{m/m}$ double mutant mice at this age is consistent with elevated ALP levels, but parallel increases in ALT levels suggest liver dysfunction, rather than increased osteoblast activity. Elevated ALT and aspartate aminotransferase, another liver function marker, levels were also found in *Bmal1*$^{-/-}$ mice, but upon histological inspection there did not appear to be any liver pathology [95].The normal serum levels of calcium and phosphorus in *Clock*$^{-/-}$*;Npas2*$^{m/m}$ double mutant mice strongly suggests that systemic mineral imbalances are not at play here. Systemic mineral imbalance is the cardinal sign of metastatic calcification. A classic example of metastatic

calcification is hyperparathyroidism, in which elevated parathyroid hormone levels cause systemic increases in serum calcium and phosphate, leading to diffuse ectopic calcification in soft tissues [97]. Thus, the unremarkable serum calcium and phosphorus levels in *Clock*$^{-/-}$*;Npas2*$^{m/m}$ double mutant mice suggest that metastatic calcification is not the cause of age-dependent arthropathy in this mutant mouse model.

Systemic influences on arthropathy

While these experiments do not identify of a specific mechanism responsible for age-dependent arthropathy in *Clock*$^{-/-}$*;Npas2*$^{m/m}$ double mutant mice, the findings presented here bring us a step closer to that goal. These results show that mechanical stress, disruption of centrally-regulated circadian rhythms, and systemic effects leading to metastatic calcification are unlikely to play a role in this pathogenesis, which leaves specific, local mechanisms open to investigation. However, the results presented in this chapter do not completely rule out the involvement of systemic factors. Systemic factors may interact with local mechanisms to induce site-specific ectopic calcification. Local mechanisms could include cell-autonomous pathways and tissue-specific changes in gene expression, and the next chapter discusses a potential *in vitro* model system in which to study cell-autonomy as well as local changes in gene expression.

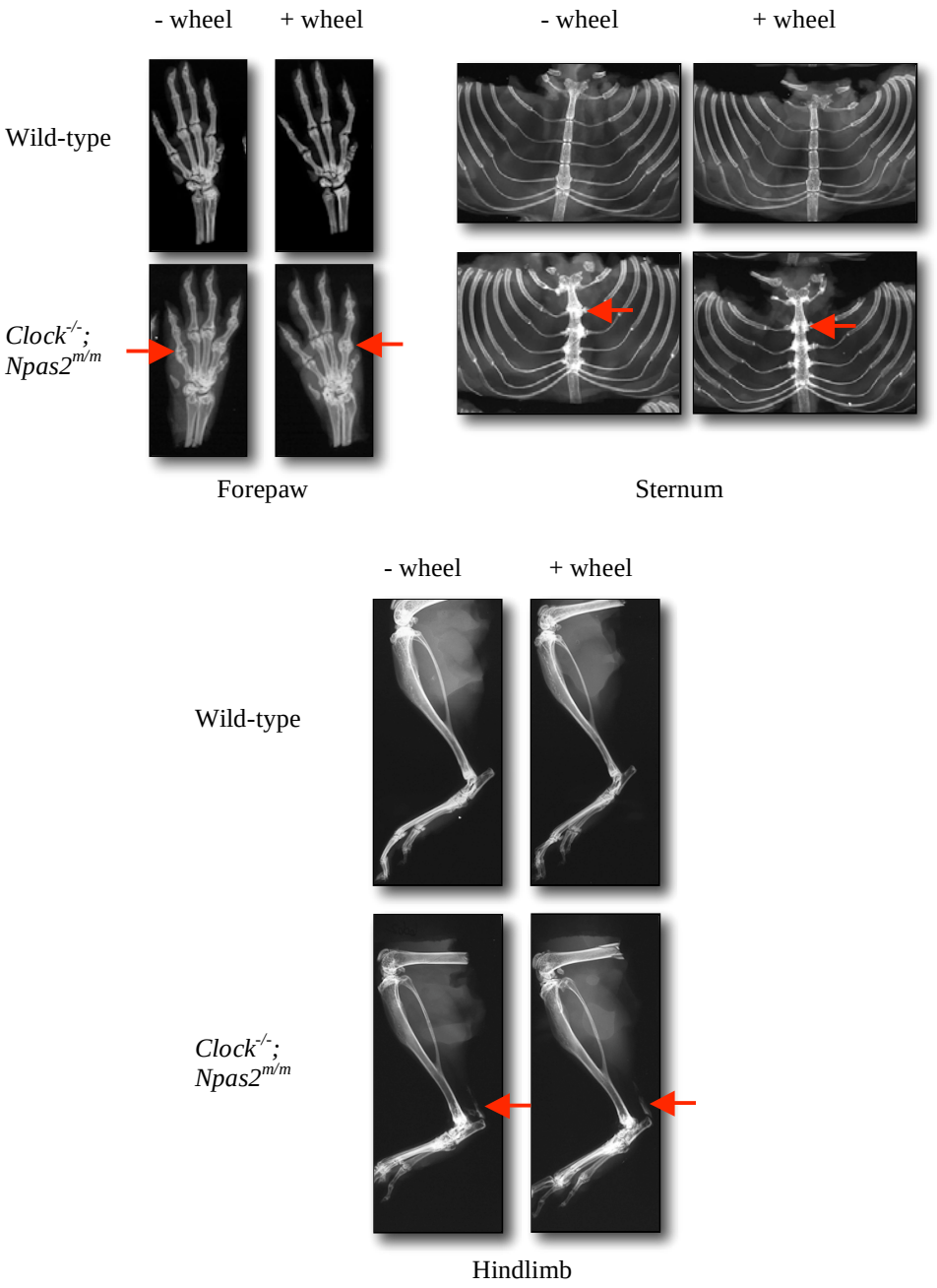

Figure 3.1. Mechanical stress does not seem to contribute to arthropathy development in *Clock*$^{-/-}$;*Npas2*$^{m/m}$ double mutant mice. Representative X-ray images of various joints from animals used in the study. Ectopic calcification of 20-21 week-old *Clock*$^{-/-}$;*Npas2*$^{m/m}$ double mutant mice with running wheels is indistinguishable from age-matched *Clock*$^{-/-}$;*Npas2*$^{m/m}$ double mutant mice without running wheels. Red arrows highlight ectopic calcification.

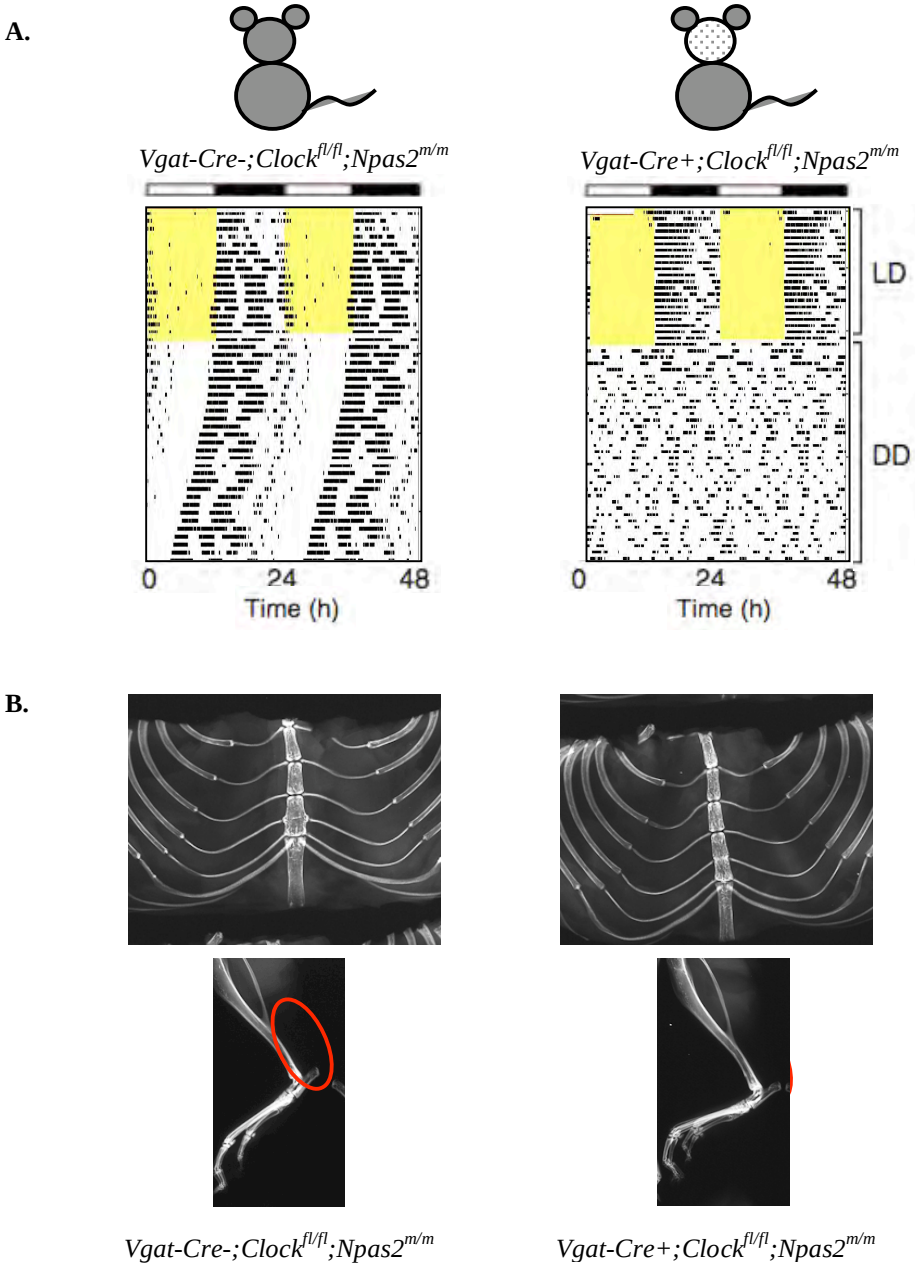

Figure 3.2. Disruption of centrally regulated circadian rhythms is not sufficient to cause age-dependent arthropathy. (A) (Top) Cartoon depicting *Clock* and *Npas2* expression in transgenic mice. Grey: *Clock*$^{fl/fl}$;*Npas2*$^{m/m}$ tissue; white with grey spots: *Clock*$^{-/-}$;*Npas2*$^{m/m}$ tissue (white) mixed with *Clock*$^{fl/fl}$;*Npas2*$^{m/m}$ tissue (grey spots). (Bottom) Double-plotted actograms of representative mice of the indicated genotypes. Note that *Vgat-Cre+;Clock*$^{fl/fl}$;*Npas2*$^{m/m}$ mice are behaviorally arrhythmic in DD. Yellow: lights on; LD: light:dark; DD: constant darkness. (B) Sterna and hindlimb X-ray images of 25 week-old mice. Note that *Vgat-Cre+;Clock*$^{fl/fl}$;*Npas2*$^{m/m}$ mice do **not** develop ectopic calcification (red circles).

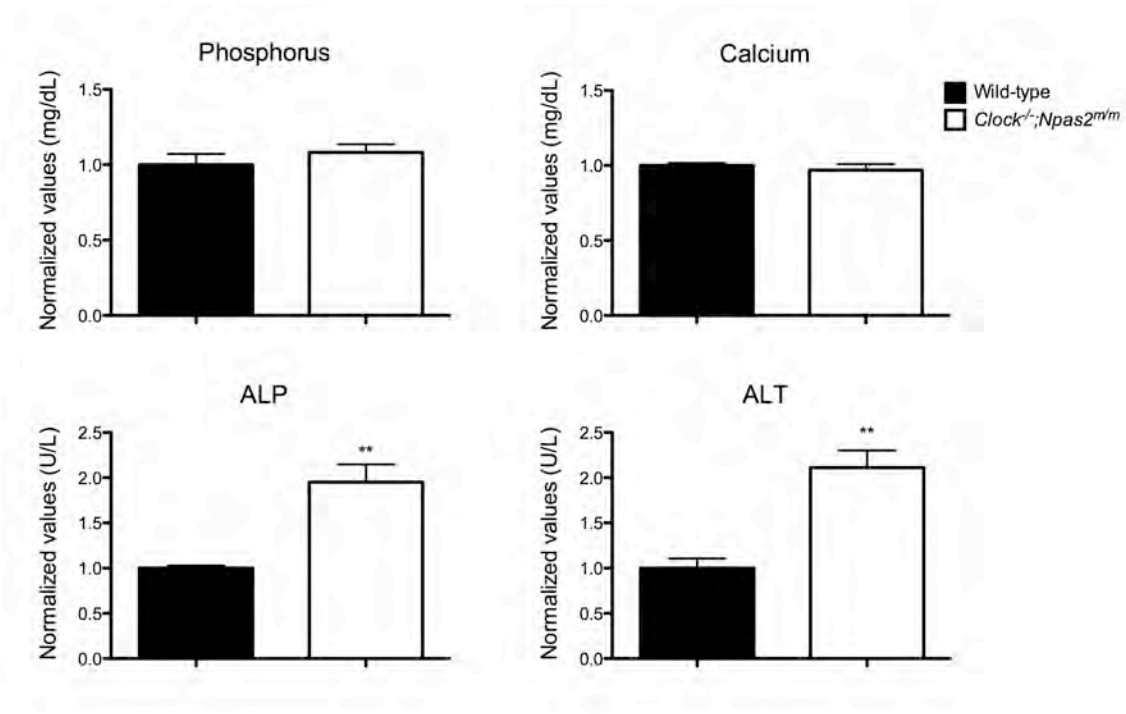

Figure 3.3. Normal serum calcium and phosphorus levels in *Clock*$^{-/-}$;*Npas2*$^{m/m}$ double mutant mice. Serum chemistry analysis of male, 37-49 week-old *Clock*$^{-/-}$;*Npas2*$^{m/m}$ double mutant and wild-type mice. N = 4 for each genotype. **p<0.01.

Chapter IV

Gene dysregulation in *Clock*$^{-/-}$;*Npas2*$^{m/m}$ double mutant mice

Summary

Clock, *Npas2*, and *Bmal1* are transcription factors integral to the circadian oscillator loop, but they are also capable of regulating clock output gene expression that does not feed back into the oscillator loop. CLOCK/NPAS2:BMAL1 could regulate the expression of a gene(s) involved in ectopic calcification. The studies described in this chapter aim to elucidate changes in gene expression in *Clock*$^{-/-}$;*Npas2*$^{m/m}$ double mutant mice. The first strategy employs *in vitro* micromass cultures and the second targets *in vivo* intersternebral tissue. Quantitative real-time polymerase chain reaction (RT-PCR) analyses were conducted using RNA extracted from micromass cultures and intersternebral tissue. Genes examined were markers of chondrocyte maturation and genes involved in calcification and apoptosis. No changes in gene expression were identified. Consistent with this finding, micromass cultures generated from *Clock*$^{-/-}$;*Npas2*$^{m/m}$ double mutant embryos did not differentially stain for cartilage or calcification markers as compared to wild-type micromass cultures. The findings of this chapter show that generalized chondrocyte maturation dysfunction is likely not involved in mediating age-dependent arthropathy of the costosternal junction in *Clock*$^{-/-}$;*Npas2*$^{m/m}$ double mutant mice, and that intersternebral tissue is possibly too general of an area in which to detect changes in gene expression associated with site-specific arthropathy.

Acknowledgments

This chapter is a result of collaboration between our laboratory and the laboratory of Jane Lian in the Department of Cell Biology at the University of Massachusetts Medical School (UMMS). As such, I would like to acknowledge the appropriate people for their contribution to the work presented here.

Tripti Gaur and Kimberly LeBlanc taught me how to micromass culture MEFs and assisted with initial cell culture troubleshooting. Christopher Lambert taught me how to design and validate primers and use the RT-PCR machine, and also assisted with primer validation data interpretation. Keith Reddig showed me how to use the camera and software for imaging stained micromass cultures.

Figure 4.1. Representative primer validation data.
Elizabeth Yu – Department of Neurobiology, UMMS

Figure 4.2. Micromass culture stains reveal no difference in chondrogenic differentiation between *Clock*$^{-/-}$*;Npas2*$^{m/m}$ double mutant and wild-type MEFs.
Elizabeth Yu – Department of Neurobiology, UMMS

Figure 4.3. Gene expression profiles of chondrogenesis markers do not significantly differ between *Clock*$^{-/-}$*;Npas2*$^{m/m}$ double mutant and wild-type micromass cultures.
Elizabeth Yu – Department of Neurobiology, UMMS

Figure 4.4. Diagram of instersternebral tissue dissection.
Elizabeth Yu – Department of Neurobiology, UMMS

Figure 4.5. Chondrocyte marker gene expression in *Clock*$^{-/-}$*;Npas2*$^{m/m}$ intersternebral tissue does not significantly differ from wild-type.
Elizabeth Yu – Department of Neurobiology, UMMS

Figure 4.6. Candidate gene expression in *Clock*$^{-/-}$*;Npas2*$^{m/m}$ intersternebral tissue does not significantly differ from wild-type.
Elizabeth Yu – Department of Neurobiology, UMMS

Introduction

Bmal1, Clock, and *Npas2* are core components of the circadian oscillator feedback loop. BMAL1 binds to CLOCK or NPAS2 to form a transcriptional activator complex that drives rhythmic expression of core clock and clock output genes. Approximately 10% of the genome is rhythmically expressed, showing that BMAL1, CLOCK, and NPAS2 drive the expression of many clock output genes [102, 103]. The specific genes rhythmically expressed depend on the type of tissue, but generally rate-limiting steps are rhythmic [104]. One or more of those genes could play a role in regulating downstream genes that affect ectopic calcification. *Bmal1*$^{-/-}$ mice display age-dependent, non-inflammatory arthropathy, prominent in the costosternal junction, calcaneal tendon, stifles, and posterior longitudinal ligament of the spine [64]. *Clock*$^{-/-}$*;Npas2*$^{m/m}$ double mutant mice display a similar age-dependent, non-inflammatory arthropathy, which is also prominent in the costosternal junction, calcaneal tendon, and stifles. The similarity in arthropic phenotypes suggests that CLOCK:BMAL1 or NPAS2:BMAL1 drives the expression of a clock output gene that directly or indirectly regulates ectopic calcification. Identification of the gene(s) could provide novel insight into a calcification pathway regulated by circadian oscillator genes.

The costosternal junction and calcaneal tendon, the two sites with the most prominent arthropathy, are very different tissues. Costosternal tissue is comprised mainly of hyaline cartilage and chondrocytes, and connects cartilage to bone [105]. Calcaneal tendon is comprised mainly of fibrous connective tissue, fibroblasts and tenocytes, and

connects muscle to bone [106]. How do two different tissues develop the same type of age-dependent ectopic calcification? It seems that separate mechanisms could be at play in these two different tissues since they have so little in common. To focus the molecular studies, we decided to concentrate on one of the two tissues: the costosternal junction. The histology at the costosternal junction shows the presence of chondrocytes in these areas, as identified morphologically (Figure 2.8). Physiologically, chondrocytes undergo maturation during development and in the growth plate that culminate in the calcification of the surrounding cartilage matrix. The presence of chondrocytes in a site that develops ectopic calcification raises the possibility that chondrocytes are involved in age-dependent arthropathy of the costosternal junction.

One of the difficulties associated with using a mouse model is the large amount of time and money required to maintain animals for *in vivo* studies. In an attempt to circumvent those obstacles, efforts were made to use an established *in vitro* cell culture system in which mouse embryonic fibroblasts (MEFs) are differentiated into chondrocytes [107, 108]. In this system, referred to as micromass culture, MEFs are harvested from embryonic day 12.5-13.5 fetuses and plated in high-density cultures. Treatment of these cultures with bone morphogenic protein 2 (BMP2) stimulates MEF chondrogenic differentiation. BMP2 is a potent chondrogenic factor for mesenchymal cells *in vitro* and plays a role in the chondrogenesis of condensed mesenchyme *in vivo* [109-111]. The beauty of this *in vitro* micromass system is that MEFs undergo normal chondrogenic differentiation under these conditions, enabling the assessment of chondrocyte differentiation and calcification. Micromass cultures can be stained for alcian blue and

safranin-O to assess cartilage formation, alkaline phosphatase (ALP) to assess enzyme activity, and von Kossa to assess phosphate as an index of calcium phosphate deposition. RNA from cultures can also be collected at various time points to assess temporal changes in gene expression.

Establishing an *in vitro* assay has additional benefits. Should the *Clock*$^{-/-}$*;Npas2*$^{m/m}$ double mutant MEFs in micromass culture exhibit an accelerated differentiation and calcification phenotype compared to wild-type, this result would show that chondrocytes are cell-autonomous in their ability to mediate ectopic calcification. Micromass cultures would also provide a system in which genes could be manipulated to study the molecular pathway of arthropathy. We could knockdown gene expression using RNA interference (RNAi) and restore gene expression using viral vectors to test the functional importance of genes in this phenotype. Clearly, establishing an *in vitro* assay has great potential to enhance the investigation of arthropathy in *Clock*$^{-/-}$*;Npas2*$^{m/m}$ double mutant mice.

While *in vitro* systems can be an invaluable source of information, especially in terms of their ability to facilitate genetic manipulation, nothing can replace the value of studying an *in vivo* system. There are infinite complexities of the *in vivo* environment that may not be reliably replicated *in vitro*. Keeping in line with the focus on the costosternal junction, intersternebral tissue was collected from 6-7 week-old *Clock*$^{-/-}$*;Npas2*$^{m/m}$ double mutant, *Clock*$^{-/-}$ single knockout, *Bmal1*$^{-/-}$, and wild-type mice to study differences in gene expression. Mice of 6-7 weeks of age were used in this study because costosternal junction calcification is first beginning to consistently appear in *Clock*$^{-/-}$*;Npas2*$^{m/m}$ double

mutant mice at this age. In 4-5 week-old *Clock*$^{-/-}$;*Npas2*$^{m/m}$ double mutant mice, costosternal junction lesions appear inconsistently, making it difficult to be sure if calcification has begun in all mutants. By selecting 6-7 week-old *Clock*$^{-/-}$;*Npas2*$^{m/m}$ double mutant, we can be confident that calcification has begun in all *Clock*$^{-/-}$;*Npas2*$^{m/m}$ double mutants and that the pathology is still relatively in its infancy.

Clock$^{-/-}$ single knockout tissues were also included in this analysis to further screen genes of interest. *Clock*$^{-/-}$ mice do not develop ectopic costosternal junction calcification (Figure 2.6), so genes dysregulated in both *Clock*$^{-/-}$ single knockout and *Clock*$^{-/-}$;*Npas2*$^{m/m}$ double mutant costosternal junction tissue probably do not contribute to costosternal junction arthropathy in *Clock*$^{-/-}$;*Npas2*$^{m/m}$ double mutant mice. In other words, genes dysregulated in *Clock*$^{-/-}$ single knockout tissue are not involved in costosternal junction arthropathy because *Clock*$^{-/-}$ mice do not develop costosternal junction arthropathy. *Bmal1*$^{-/-}$ tissues were also analyzed to determine if *Clock*$^{-/-}$;*Npas2*$^{m/m}$ double mutant and *Bmal1*$^{-/-}$ costosternal junction tissues exhibit the same changes in gene expression. Because we hypothesize that disruption of the CLOCK/NPAS2:BMAL1 transactivator complex leads to the same age-dependent arthropathy in *Clock*$^{-/-}$;*Npas2*$^{m/m}$ double mutant and *Bmal1*$^{-/-}$ mice, we expect to see similar changes in calcification-related gene expression in both mutants.

Chondrocyte maturation marker gene and candidate gene expression in intersternebral tissue were evaluated. Some of these genes were chosen based on the phenotypes of mutant mice in which these genes are disrupted and all were chosen based on their potential to be involved in ectopic calcification pathology. *Ank*$^{-/-}$ and *ank/ank*

mutant mice develop age-progressive calcification of joints and spine [73]. *Enpp1*$^{-/-}$ mice develop progressive ankylosing intervertebral and peripheral joint hyperostosis [26, 69-72]. ANK and ENPP1 both generate extracellular PP_i [25-27]. ANK transports PP_i from the intracellular space to the extracellular space while ENPP1 hydrolyzes ATP to form PP_i. TNAP decreases extracellular PP_i by hydrolyzing it to form P_i, which can crystallize with calcium to form HA. PP_i inhibits HA formation, such that too little PP_i leads to HA deposition. However, too much PP_i leads to CPPD deposition [25-27]. The finding that ectopic calcification in *Bmal1*$^{-/-}$ sternum consists of CPPD crystals suggests that *Ank*, *Enpp1*, and/or *TNAP* dysregulation could lead to extracellular PP_i dysregulation that could cause arthropathy.

HDAC4$^{-/-}$ mice display premature ossification of developing bones secondary to ectopic and precocious chondrocyte hypertrophy [80]. Because HDAC4 regulates chondrocyte hypertrophy, its down regulation could lead to inappropriate chondrocyte hypertrophy and calcification. *Mglap*$^{-/-}$ mice exhibit spontaneous calcification of arteries and cartilage, including the growth plate [84]. MGP inhibits ectopic calcification, so it is possible that down regulation of *Mglap* leads to arthropathy. *Prrx1* and *Sox7* were found to be directly regulated by *Bmal1* in mouse liver [112]. *Prrx1* encodes paired related homeobox 1, a transcription factor that mediates inhibition of osteoblast progenitors [113]. *Prrx1*$^{-/-}$ mice have defects of skeletogenesis, such as loss of craniofacial, limb, and vertebral structures [114]. *Sox7* is a transcription factor that positively regulates caspases and thus induces apoptosis [115]. Apoptosis is the last step in chondrocyte maturation, so assessing apoptosis markers, such as *Sox7* and *Bax*, in addition to chondrocyte marker

genes could prove to be complementary. Bax, or Bcl-2 associated protein X, promotes apoptosis by competing with Bcl-2 [116].

To establish an *in vitro* system in which to study arthropathy, micromass cultures were generated from *Clock*$^{-/-}$;*Npas2*$^{m/m}$ double mutant and wild-type MEFs. Micromass cultures were stained to assess cartilage deposition and calcification, and RNA was collected and analyzed by RT-PCR to assess changes in chondrogenic maturation gene expression profiles. To study *in vivo* changes in gene expression, intersternebral tissue was collected from *Clock*$^{-/-}$;*Npas2*$^{m/m}$ double mutant and wild-type mice and expression levels of chondrogenic and candidate genes were measured by RT-PCR.

Experimental procedures

Generation, maintenance, and genotyping of study animals

Please see "Chapter II: Experimental procedures" for details.

MEF generation

To generate *Clock*$^{-/-}$;*Npas2*$^{m/m}$ double mutant fetuses for MEF collection, *Clock*$^{+/-}$;*Npas2*$^{m/m}$ three-allele mutants were intercrossed. Overnight, timed pairings of one male with three to four females per cage were performed, during which the male was removed the following morning before noon. Pregnant mice were identified and sacrificed when embryos were 13.5 days old (E13.5, where day 0.5 is the morning following the pairing with the male). E13.5 embryos were removed and each fetus was used to generate a separate line [107, 108], whose genotype was confirmed by PCR. Liver and heart were removed and the rest of the embryo was sheared in an 18-gauge syringe in the presence of 1 ml 0.25% trypsin-EDTA. After 15 minutes incubation at room temperature, Dulbecco's modified eagle medium (DMEM) with 15% fetal bovine serum (FBS) was added to inactivate trypsin. One hundred microliters of cell suspension was used to genotype each embryo. The rest of the cell suspension was plated one embryo per 100 mm plate and incubated at 37^{o}C with 5% CO_2. These cells will be referred to as passage-0 (P0) cells, as they have not yet been split. Cells were always grown in a 37^{o}C incubator with 5% CO_2. The next day, the cells were washed with 1X PBS and fed fresh DMEM supplemented with 15% FBS (DMEM+15%FBS). Media were changed every other day

until the cells reached 80-90% confluence, at which point they were split 1:5 (generating passage-1, or P1, cells). Once P1 cells reached ~90% confluence, they were frozen down and stored at -80^{o}C. It generally did not take longer than 3-4 days for cells to reach 80-90% confluence. To freeze down MEFs, cells were collected by trypsin digestion and cell suspensions were spun at 1500 rpm for 5 minutes to obtain cell pellets. Each pellet was resuspended in 1 ml media and cell suspensions were mixed 1:1 in freezing media (20% FBS, 20% dimethyl sulfoxide (DMSO), in DMEM). Cell suspensions were placed in cryogenic tubes and slowly frozen to -80^{o}C in a freezing container before being moved to -150^{o}C.

Micromass culture and RNA collection

The following micromass culture protocol has been described previously [107, 108]. To revive frozen P1 MEFs prior to initiating an experiment, quick-thawed MEFs were pelleted (1500 rpm x 5 minutes), plated in DMSO-free DMEM+15%FBS, and grown to ~90% confluence before being split 1:5, generating P2 cells. The day after splitting, cells were collected by 0.25% trypsin-EDTA digestion and counted using a hemacytometer. Cells were plated in 10 ul high-density droplets (1x10^{7} cells/ml): 12-15 droplets per 60 mm plate for RNA collection and 2-3 droplets per well of a 12-well plate for histochemical staining. Great care was taken to ensure droplets did not touch one another or smear. Micromass cultures were incubated for 2.5-3 hours in a 37^{o}C incubator with 5% CO_2 to allow adherence of the cells to the plates. Then, without disturbing the droplets, 1X Nutrient Mixture F12 Ham's (F12) media supplemented with 15% FBS

(F12+15%FBS) were slowly added to the cells. For +BMP2 treated micromass cultures, 100 ng/ml BMP2 was added to F12+15%FBS. 2.5 ml and 0.75 ml media were added to 60 mm and each well of a 12-well plate, respectively, so the 10 ul droplets did not significantly dilute the final BMP2 concentration in the media. Media were changed every other day and +BMP2 media were made fresh each time. Micromass cultures were harvested for RNA on culture days 1, 3, 6, 9, and 12 in 500 ul TRIzol reagent (Invitrogen) and cell suspensions were frozen at -80^{o}C until processing. Table 4.2 shows the number of cultures collected for each genotype and treatment across five time points.

Micromass histochemical staining

Alcian blue, safranin-O, and alkaline phosphatase stains were all performed on culture Day 9. Von Kossa stains were performed on culture Day 15.

Micromass cultures were fixed in 4% paraformaldehyde for 10 minutes prior to alcian blue and safranin-O histological analysis, while cultures for von Kossa and alkaline phosphatase (ALP) analysis were fixed in 2% paraformaldehyde for 10 minutes prior to staining. Alcian blue staining was performed using 1% alcian blue solution overnight at room temperature. Safranin-O staining was performed using 0.1% safranin-O solution for 10 minutes at room temperature. Von Kossa staining was performed using 3% silver nitrate solution for 15 minutes in sunlight (through windows in the lab). ALP enzymatic activity was detected by colorimetric reaction using a 0.1M Tris maleate buffer (pH 8.4) containing 0.05% Napthol AS MX phosphate disodium salt, 2.8% N,N dimethyl formamide, and 0.1% fast red salt for 30 minutes at 37^{o}C. Images were captured

using a Nikon SMZ 745t microscope, Pixelink PL-B681 microscopy camera, and Pixelink Capture OEM software. Table 4.3 shows the number of MEF lines stained for each genotype and treatment. For each stain, there were 3-11 replicate micromass cultures for each genotype and treatment of a given MEF line. For instance, there were 9 replicate micromass droplet/cultures of a wild-type MEF line treated with BMP2 that was stained for von Kossa, but this wild-type MEF line was only counted once toward the sample size.

Intersternebral RNA collection

13 *Clock*$^{-/-}$;*Npas2*$^{m/m}$ double mutant, 9 *Clock*$^{-/-}$, 8 *Bmal1*$^{-/-}$, and 9 wild-type mice, all 6-7 weeks of age, were used in this experiment. Mice were asphyxiated in a CO_2 chamber and decapitated. Sterna were removed, quick frozen in 2-methylbutane on dry ice, and stored at -80^{o}C until sectioned. For sectioning, unfixed tissue was embedded in O.C.T. mounting media and sectioned in a cryostat at 60 um. Sections were then dissected using scalpels under a dissecting microscope and intersternebral tissues from three animals were pooled together in 500 ul TRIzol reagent (Invitrogen) to form one sample. For each animal, intersternebral tissues adjacent to ribs 3-6 were collected. For each genotype, there were 3-4 samples. In other words, one of the wild-type samples consists of intersternebral tissues pooled together from 3 separate wild-type sterna, and from each wild-type sterna, intersternebral tissue from 4 rib junctions was collected. One *Bmal1*$^{-/-}$ sample only contained pooled tissue from 2 animals and one *Clock*$^{-/-}$;*Npas2*$^{m/m}$

double mutant sample contained pooled tissue from 4 animals. See Figure 4.4 for a diagram of the tissue area collected.

RNA isolation

Total RNA was extracted using Trizol (Invitrogen) according to the manufacturer's protocol and each sample was treated with 1 ul RQ1 DNase (Promega) for 2 hours at 37^{o}C before the DNase activity was stopped using 1 ul ethylene glycol tetraacetic acid (EGTA) for 10 minutes at 95^{o}C. Random hexamers (Promega) with 0.7ug RNA were used to prime reverse-transcription reactions with Superscript II (Invitrogen) using protocols from the manufacturers. cDNA was stored at -80^{o}C. PCR reactions were assembled by creating a master mix for each primer pair and combining 20ul of master mix and 5ul cDNA in each well of a 96-well optical reaction PCR plate (Applied Biosystems).

Real-time polymerase chain reaction (RT-PCR)

Quantitative RT-PCR was performed using SYBR green 2x master mix, a two-step cycling protocol (anneal and elongate at 60^{o}C, denature at 95^{o}C), and an ABI SDS 7000 instrument (Applied Biosystems, Foster City, CA). Each sample was assessed in duplicate. In some cases, micromass sample cDNA did not amplify accurately, as evidenced by the sample's amplification curve being indistinguishable from those of negative controls (no-transcriptase and premix only controls, which lack cDNA). These cDNA samples amplified with other primer sets in separate experiments, showing that the

cDNA quality was good; lack of amplification was most likely due to pipetting error. Samples that did not amplify were excluded, explaining any discrepancies in sample number shown in Table 4.2 and Figure 4.3. All intersternebral tissue sample cDNA amplified appropriately, so none were excluded from those statistical analyses. The data for each transcript were normalized to glyceraldehyde-3-phosphate dehydrogenase (GAPDH) using the $2^{-\Delta\Delta Ct}$ method. Primers used for RT-PCR reactions are listed in Table 4.1 and a representative primer validation data set is shown in Figure 4.1. All primers were validated prior to use and evaluated based on amplification plot, slope (~3.3), and dissociation peak.

Statistical analysis

Micromass culture RT-PCR Ct values were normalized to GAPDH values and then further normalized to the average wild-type BMP2 untreated value (over all sample days). $2^{-\Delta\Delta Ct}$ values were analyzed by two-way ANOVA (Prism 5 for Mac OS X software). Bonferroni post-tests were performed for comparisons among treatments and genotypes.

Intersternebral tissue RT-PCR $2^{-\Delta\Delta Ct}$ values were analyzed by one-way ANOVA. Dunnett post-tests were performed for comparisons of mutant tissue to wild-type tissue values. P-values less than 0.05 were considered statistically significant. P-values between 0.05 and 0.1 were considered to indicate a trend, and are noted.

Results and discussion

Assessing phenotype of micromass cultures

To assess changes in gene expression, an *in vitro* micromass culture system was employed. MEFs cultured from *Clock*$^{-/-}$*;Npas2*$^{m/m}$ double mutant and wild-type E13.5 embryos were plated in high density cultures and treated with or without BMP2 to stimulate chondrogenic differentiation and as a control, respectively. The cultures treated with BMP2 underwent chondrogenic differentiation, as evidenced by their stronger alcian blue, safranin-O, alkaline phosphatase (ALP), and von Kossa stains compared to cultures not treated with BMP2 (Figure 4.2A). In this experiment, it appeared that *Clock*$^{-/-}$ *;Npas2*$^{m/m}$ double mutant MEFs underwent accelerated chondrogenic differentiation, as evidenced by increased alcian blue, safranin-O, alkaline phosphatase, and von Kossa staining (Figure 4.2A). However upon replication, it was concluded that there is no consistent difference between the staining of *Clock*$^{-/-}$*;Npas2*$^{m/m}$ double mutant and wild-type micromass cultures treated with BMP2 (Figure 4.2B). Different wild-type MEF lines treated with BMP2 in separate experiments generated micromass cultures with highly variable staining intensity (Figure 4.2A&B). However, when the same MEF line was used in separate experiments, consistent staining results between experiments were obtained, showing that the variability is within the genotypes and not a complete result of experimental protocol variability. These data show that there appears to be significant variation in staining intensity within genotypes and that this variability nullifies any significance of the initially promising results.

The staining results that show a lack of altered chondrogenic differentiation in *Clock*$^{-/-}$*;Npas2*$^{m/m}$ double mutant MEFs are supported by micromass culture RNA analyses. In this experiment, multiple RNA samples of both genotypes and both treatments across five time points were collected, and chondrocyte maturation markers were measured and analyzed by RT-PCR and 2-way ANOVA, respectively (Table 4.2). Samples were analyzed as four groups (wild-type +BMP2, *Clock*$^{-/-}$*;Npas2*$^{m/m}$ +BMP2, wild-type –BMP2, *Clock*$^{-/-}$*;Npas2*$^{m/m}$ –BMP2) across time. Days in culture, and genotype and BMP2 treatment had significant effects on *Col2a1*, *Sox9*, *Ihh*, *Col10a1*, *ALP*, and *osteocalcin* (*Ocn*) gene expression, but there were only significant interactions in *Col2a1*, *Ocn*, and *Hist4h4* expression (Table 4.4). In other words, *Sox9*, *Ihh*, *Col10a1*, *ALP*, and *H3f3a* expression differences between groups did not change over time but *Col2a1*, *Ocn*, and *Hist4h4* expression differences between groups did change over time.

Bonferroni post-tests were performed to compare individual genotypes with and without BMP2 treatment over time. *Col2a1*, *Sox9*, *Ihh*, *Col10a1*, *ALP*, and *Ocn* expression levels are not significantly different between wild-type and *Clock*$^{-/-}$*;Npas2*$^{m/m}$ double mutant MEFs treated with BMP2 (Figure 4.3A). However, cells of both genotypes treated with BMP2 express statistically higher levels of these genes than cells not treated with BMP2, showing that BMP2 successfully stimulated chondrogenic differentiation regardless of cells' genotype. In fact, the rise of *Col2a1*, *Sox9*, and *Ihh* expression over time is consistent with an increase in proliferative and pre-hypertrophic chondrocytes. The rise of *ALP* and *Ocn* towards the end of the time course signifies the presence of mature hypertrophic chondrocytes and thus an increase in calcification markers. The

expression pattern of *Col10a1* is less clear. *Col10a1* expression rises over time, which is consistent with the patterns of *Ihh*, *ALP*, and *Ocn* gene expression. However, the peak of *Col10a1* expression around Day 6 is unexpected and could be due to a surge of hypertrophic chondrocyte production of Type X collagen that does not persist to later days. The reason for this surge is unclear, as other markers of hypertrophic chondrocytes do not exhibit the same mid-course peak, but primary cultures can behave differently depending on the experimental parameters and this could simply be an interesting characteristic of MEFs from these mice collected and cultured under these conditions.

H3f3a and *Hist4h4* are genes encoding histones 3 and 4, respectively, which are essential elements of the nucleosome core around which DNA is wound. Histone gene expression is an indirect measure of cell proliferation, as increased histone gene expression indicates increased cell proliferation. *H3f3a* and *Hist4h4* levels are not significantly different in cells of either genotype treated or untreated with BMP2, showing that neither BMP2 treatment nor genotype affects cell proliferation (Figure 4.3B). There is a significant interaction of genotype and BMP2 with days in culture for *Hist4h4* expression (Table 4.4), showing that over time, genotype and BMP2 treatment affect *Hist4h4* expression. Both *H3f3a* and *Hist4h4* expression increases over time, suggesting that cells are proliferating. The pattern of chondrocyte marker gene expression suggests that BMP2 treated cells are maturing, so they could be dying prematurely after proper maturation. The gradual increase in cell proliferation could reflect the surviving MEFs' attempt to fill the space left by the dead MEFs. To test the hypothesis that MEFs are dying over time, RT-PCR for an apoptotic marker, such as *Bax*, could be performed.

If *Bax* expression rises as *H3f3a* and *Hist4h4* levels rise, then that pattern of gene expression would be consistent with an increase in cell death followed by a compensatory rise in cell proliferation.

Those follow-up studies were not conducted because the main purpose of this particular experiment was to determine if micromass culture is an appropriate *in vitro* system in which to study ectopic calcification of *Clock*$^{-/-}$*;Npas2*$^{m/m}$ double mutant mice. The results presented here show that *Clock*$^{-/-}$*;Npas2*$^{m/m}$ double mutant MEFs are not phenotypically distinct from wild-type MEFs when stimulated to undergo chondrogenic differentiation. There are a number of conclusions that can be drawn from this finding. First, the lack of phenotypic differences *in vitro* could indicate that the process of ectopic calcification in *Clock*$^{-/-}$*;Npas2*$^{m/m}$ double mutant mice is not chondrocyte cell-autonomous. By creating an *in vitro* system, all systemic *in vivo* signals have been removed. Perhaps the development of ectopic calcification requires a combination of site-specific and systemic factors interacting with one another. Or ectopic calcification may require a combination of cell types interacting with one another. To test that hypothesis, chondrocytes and osteoblasts could be co-cultured. However, *in vitro* studies will always be limited by the parameters by which they are set. If multiple factors, such as different cell types or paracrine signals, that are not included in the *in vitro* system are required to instigate ectopic calcification, then phenotypic differences in the cell cultures will not be observed. Second, these findings could indicate that chondrocytes are not involved in this pathology at all. Perhaps the wrong cell type was chosen to study *in vitro*. Future studies could focus on using primary osteoblasts or mesenchymal stem cells isolated from bone

marrow of *Clock*$^{-/-}$;*Npas2*$^{m/m}$ double mutant mice. Third, it's possible that the chondrocytes in the micromass culture do not accurately represent the chondrocytes localized to sites of ectopic calcification in adult *Clock*$^{-/-}$;*Npas2*$^{m/m}$ double mutant mice. MEFs are fibroblasts isolated from whole embryos and include chondrocytes indigenous to other areas of the animal that are not affected by arthropathy, such as articular cartilage of the shoulder. In fact, most cartilage in *Clock*$^{-/-}$;*Npas2*$^{m/m}$ double mutant mice do not appear abnormal. *Clock*$^{-/-}$;*Npas2*$^{m/m}$ double mutant mice develop to young adulthood without any problems in endochondral bone ossification, which involves intermediate cartilage scaffolding structures. It is possible that the chondrocytes in micromass culture simply do not represent those chondrocytes of interest, or non-pathologic chondrocytes constitute the majority of the chondrocytes in micromass culture and dilute any potential pathologic phenotype of the chondrocytes that are actually involved in age-dependent arthropathy. In the end, micromass cultures did not recapitulate the ectopic calcification phenotype of *Clock*$^{-/-}$;*Npas2*$^{m/m}$ double mutant mice, and efforts to investigate *in vivo* tissue gene dysregulation were pursued instead.

Investigating changes in intersternebral tissue gene expression

Intersternebral tissue was collected from 6-7 week-old *Clock*$^{-/-}$;*Npas2*$^{m/m}$ double mutant, *Clock*$^{-/-}$, *Bmal1*$^{-/-}$, and wild-type mice to study differences in gene expression (Figure 4.4). Presumably, many genes in *Clock*$^{-/-}$;*Npas2*$^{m/m}$ double mutant tissue are disrupted. To exclude some of those genes, *Clock*$^{-/-}$ tissue was included in the analyses because a hallmark of the age-dependent arthropathy of *Clock*$^{-/-}$;*Npas2*$^{m/m}$ double mutant

mice is that single *Clock*$^{-/-}$ and *Npas2*$^{m/m}$ mice do not exhibit arthropathy in the costosternal junction (Figure 2.6). Detecting changes in gene expression in *Clock*$^{-/-}$*;Npas2*$^{m/m}$ double mutant tissue but not *Clock*$^{-/-}$ tissue would identify genes specifically affected by both *Clock* and *Npas2* disruption.

Unfortunately, chondrogenic gene expression levels are not significantly different among the four genotypes (Figure 4.5, one-way ANOVA, $p > 0.05$). To assess any changes in apoptosis, *Bax* and *Sox7* gene expression levels were evaluated. No differences are present in *Sox7* levels, but *Bax* is significantly less in *Clock*$^{-/-}$ tissue compared to wild-type tissue (Figure 4.6, one-way ANOVA, Dunnett's multiple comparisons test, $p < 0.05$). We then investigated a select group of candidate genes (*Ank*, *Enpp1*, *HDAC4*, *Mglap*, and *Prrx1*) based on the interesting, and potentially related, calcification phenotypes exhibited by their mutant mouse models. Unfortunately, there are no significant changes in expression of these genes in *Clock*$^{-/-}$*;Npas2*$^{m/m}$ double mutant or *Bmal1*$^{-/-}$ tissue compared to wild-type and *Clock*$^{-/-}$ tissue (Figure 4.6, one-way ANOVA, $p > 0.05$). A possible explanation for the lack of gene expression change in intersternebral tissue could be that too large a tissue area was analyzed compared to the smaller, localized areas that actually develop calcific lesions. Unaffected gene expression in the intersternebral space could be overpowering any detectable changes in gene expression related to the development of costosternal junction calcification.

Concluding remarks

Specific gene dysregulation was not identified in the studies outlined in this chapter. The most appealing hypothesis to explain age-dependent arthropathy of the costosternal junction is that chondrocyte differentiation is dysregulated, causing inappropriate chondrocyte maturation and eventual apoptosis and tissue calcification. However, *in vitro* culturing of chondrocytes was unable to duplicate the increased calcification phenotype observed *in vivo* and *in vivo* tissues failed to show signs of chondrogenic gene dysregulation. To address the possibility of localized, site-specific changes in gene regulation, other experimental strategies must be employed and these are discussed in the next chapter.

Table 4.1. RT-PCR primer sequences.

Gene	Forward primer (5' → 3')	Reverse primer (5' → 3')	Design*
Col2a1	ACTCAAGTCACTGAACAACCAGATT	ATCAATCCAGTAGTCTCCGCTCT	Primer3
Sox9	GACTACGCTGACCATCAGAACTC	GAGCTGTGTGTAGACTGGTTGTTC	Primer3
Ihh	CTCTTGCCTACAAGCAGTTCA	CCGTGTTCTCCTCGTCCTT	14149643a1
Col10a1	TTCTGCTGCTAATGTTCTTGACC	GGGATGAAGTATTGTGTCTTGGG	6753480a1
ALP	CCAACTCTTTTGTGCCAGAGA	GGCTACATTGGTGTTGAGCTTTT	6671533a1
Ocn	CTGACCTCACAGATGCCAAG	GGGTTAAGCTCACACTGCTC	Primer3
Hist4h4	GAAGCGCATCTCGGGTCTC	CATAGCCGTAACCGTCTTGC	28316746a1
H3f3a	TGTGGCCCTCCGTGAAATC	GGCATAATTGTTACACGTTTGGC	6680159a1
Gapdh	AGGTCGGTGTGAACGGATTTG	TGTAGACCATGTAGTTGAGGTCA	6679937a1
Ank	CAGTCAAGGAGGATGCAGTAGA	CACTGTAGGCTATCAGGGTGT	31560341a1
Enpp1	CTGGTTTTGTCAGTATGTGTGCT	CTCACCGCACCTGAATTTGTT	12597623a1
Prrx1	GAGCGTGTCTTTGAGCGGA	CATGTGGCAGAATAAGTAGCCAT	6755116a1
Sox7	ATGCTGGGAAAGTCATGGAAG	CGTGTTCTGGTCACGAGAGA	6755612a1
Bax	TGAAGACAGGGGCCTTTTTG	AATTCGCCGGAGACACTCG	6680770a1
HDAC4	ATTGAGAGTGAGGAGGAAGAAGC	GCCTCCATAGATGCCTGGTA	Primer3
Mglap	GGCAACCCTGTGCTACGAAT	CCTGGACTCTCTTTTGGGCTTTA	6678876a1

*"Primer3" refers to Primer3 (v. 0.4.0) online software [117]. Serial numbers refer to MGH PrimerBank number [118].

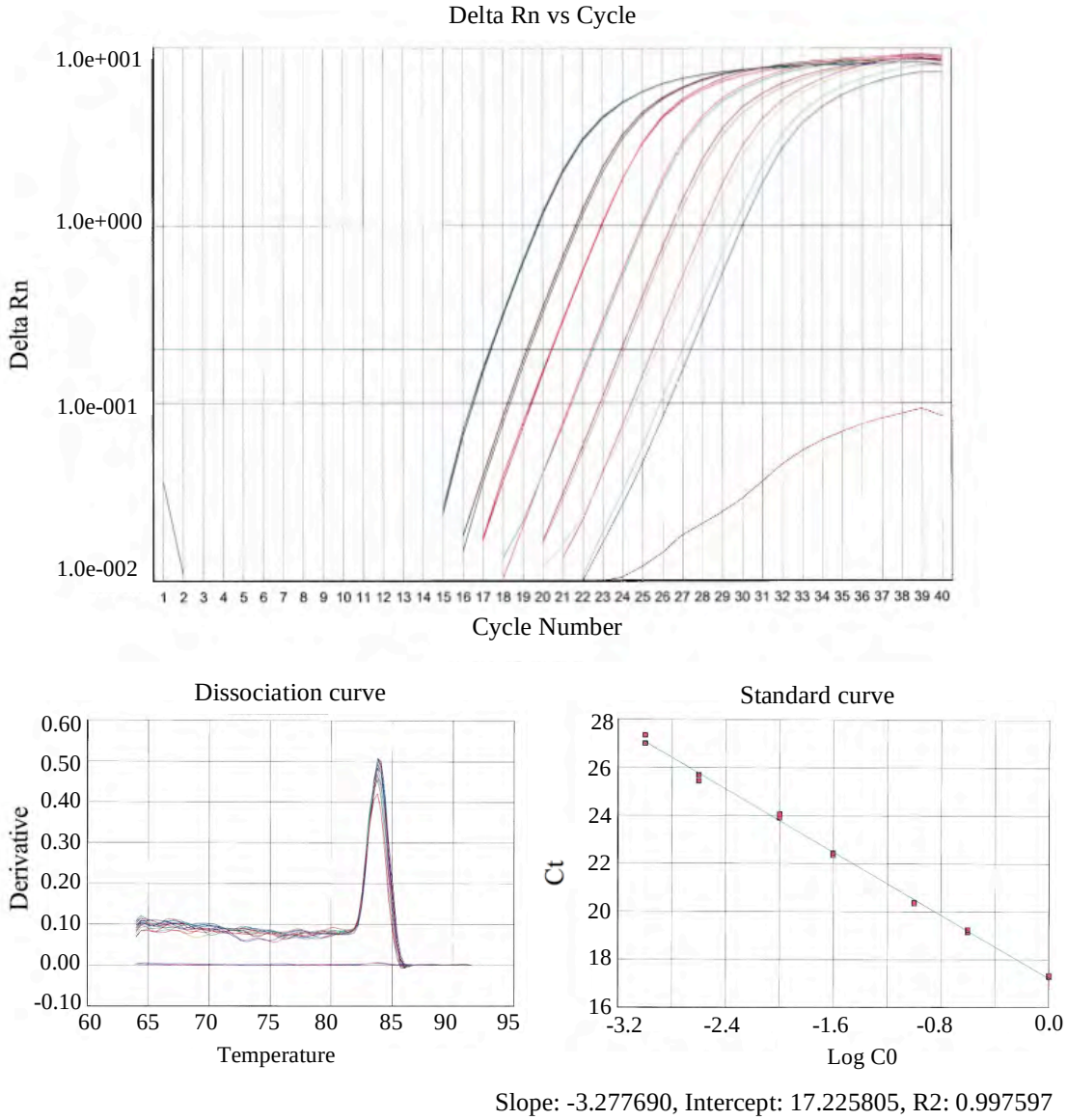

Figure 4.1. Representative primer validation data. Amplification plot (above), dissociation curve (bottom left), and standard curve (bottom right) for the *Col2a1* RT-PCR primer set. The bottom two samples of the amplification plot that did not amplify represent the no-transcriptase and premix controls, neither of which contain cDNA and are not expected to amplify. All standard cDNA samples were evaluated in duplicate.

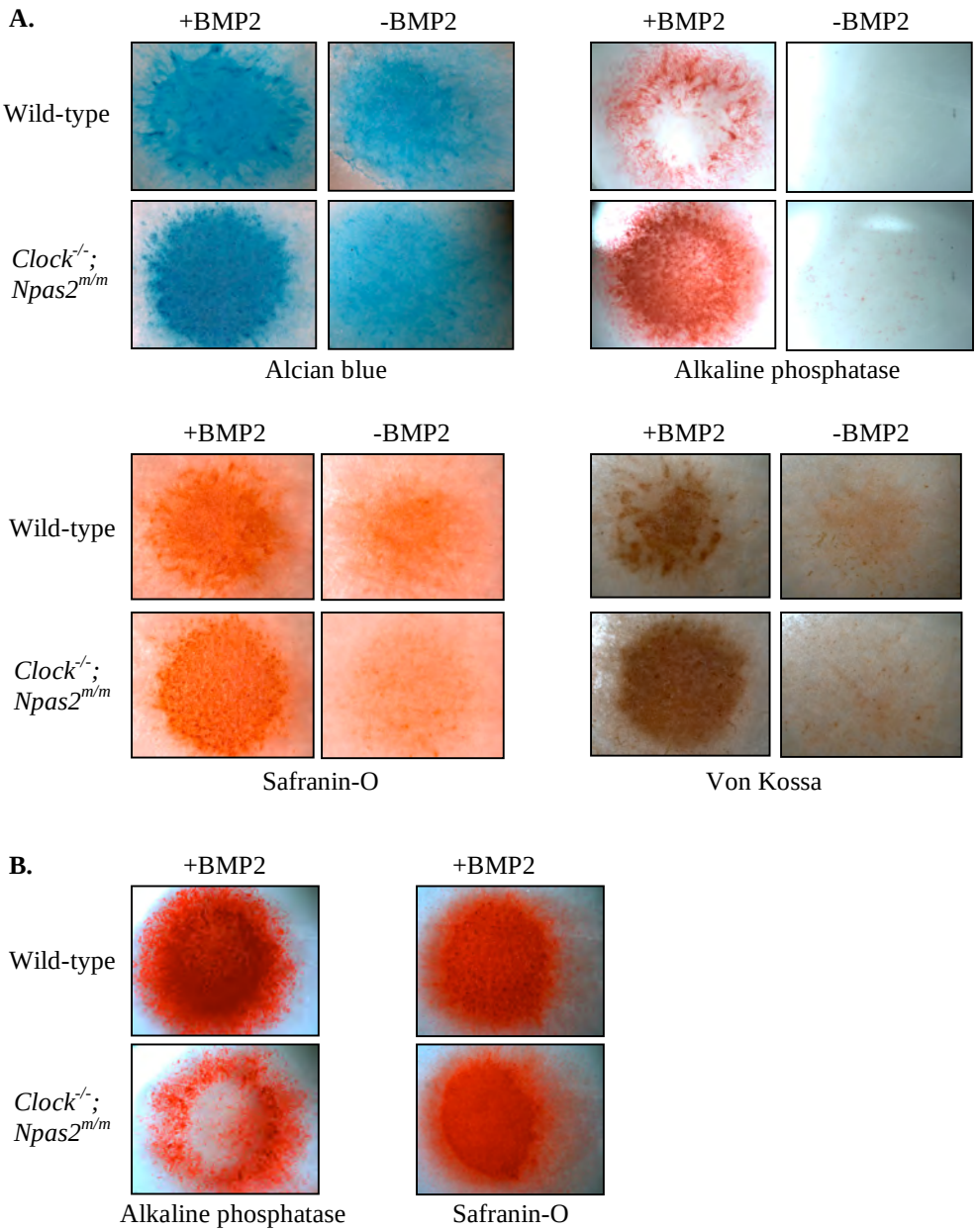

Figure 4.2. Micromass culture stains reveal no difference in chondrogenic differentiation between *Clock*$^{-/-}$;*Npas2*$^{m/m}$ double mutant and wild-type MEFs. (A) Initial staining results of micromass culture experiments show increased alcian blue, alkaline phosphatase, safranin-O, and von Kossa staining in *Clock*$^{-/-}$;*Npas2*$^{m/m}$ double mutant MEFs treated with BMP2 ("+BMP2"). BMP2 untreated cultures ("-BMP2") of both genotypes show much less staining intensity, indicating that BMP2 treatment stimulated chondrogenic differentiation. (B) Replicate micromass culture experiments showed high variability of staining intensity among MEFs of identical genotype, indicating that the degree of variation within genotypes nullifies any significance of the initial staining results in (A).

Table 4.2. Micromass culture RNA collection sample size.

	Wild-type +BMP2	***Clock*$^{-/-}$*;Npas2*$^{m/m}$ +BMP2**	**Wild-type -BMP2**	***Clock*$^{-/-}$*;Npas2*$^{m/m}$ -BMP2**
Day 1	2	2	2	2
Day 3	3	5	3	5
Day 6	3	3	3	3
Day 9	3	5	3	5
Day 12	4	5	4	5

Note that any discrepancies between the sample size listed here and the sample size shown in Figure 4.3 are due to samples excluded from statistical analysis (see Experimental Procedures).

Table 4.3. Micromass culture staining sample size.

	Wild-type +BMP2	***Clock*$^{-/-}$*;Npas2*$^{m/m}$ +BMP2**	**Wild-type -BMP2**	***Clock*$^{-/-}$*;Npas2*$^{m/m}$ -BMP2**
Alcian blue	3	2	3	2
Safranin-O	6	3	6	3
Alkaline phosphatase	6	3	5	3
Von Kossa	4	2	4	2

Table 4.4. Summary of 2-way ANOVA results for micromass culture RNA samples.

	Genotype&BMP2 treatment	**Days in culture**	**Interaction**
Sox9	$p < 0.01$	$p < 0.0001$	ns ($p = 0.100$)
Col2a1	$p < 0.0001$	$p < 0.0001$	$p < 0.0001$
Ihh	$p < 0.01$	$p < 0.01$	ns* ($p = 0.081$)
Col10a1	$p < 0.01$	$p < 0.0001$	ns ($p = 0.325$)
ALP	$p < 0.01$	$p < 0.0001$	ns* ($p = 0.056$)
Ocn	$p < 0.05$	$p < 0.0001$	$p < 0.05$
Hist4h4	ns* ($p = 0.066$)	$p < 0.01$	$p < 0.05$
H3f3a	ns ($p = 0.274$)	$p < 0.0001$	ns ($p = 0.270$)

ns: not significant; *indicates a trend towards significance ($0.05 < p < 0.10$).

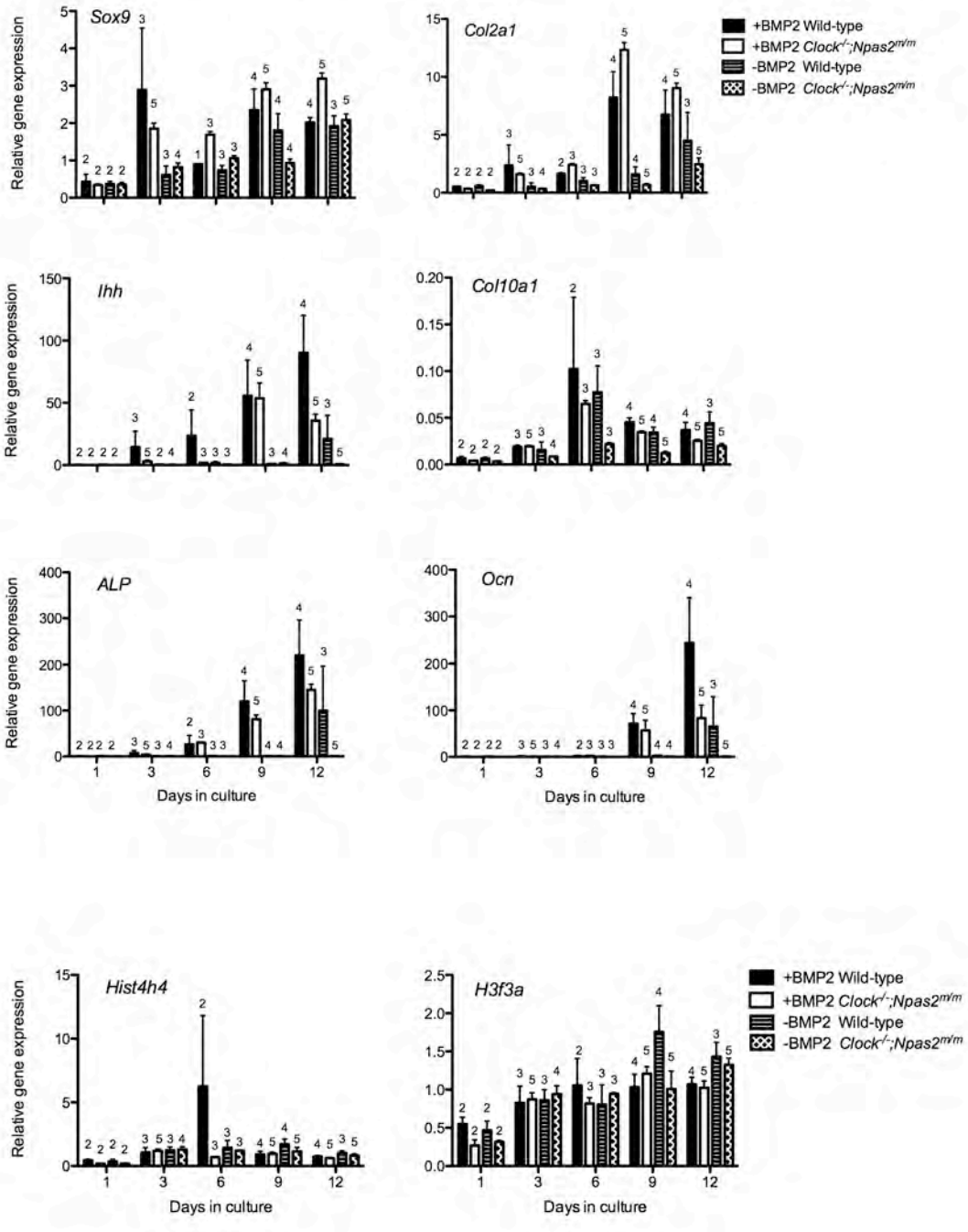

Figure 4.3. Gene expression profiles of chondrogenesis markers do not significantly differ between *Clock*$^{-/-}$*;Npas2*$^{m/m}$ double mutant and wild-type micromass cultures. Quantitative RT-PCR analysis of chondrogenesis markers (A) and histone genes (B) in *Clock*$^{-/-}$*;Npas2*$^{m/m}$ double mutant and wild-type MEFs, treated ("+BMP2") and untreated ("-BMP2") with BMP2. Numbers above error bars indicate sample size.

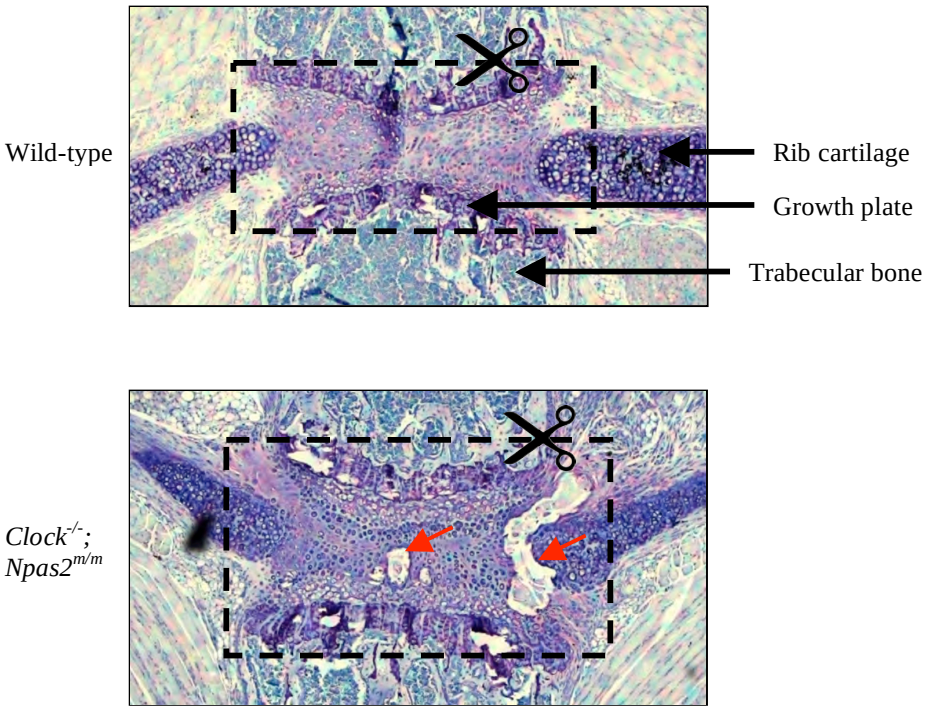

Figure 4.4. Diagram of intersternebral tissue dissection. Dotted black lines circumscribe intersternebral tissue isolated for RNA collection. Note that growth plate and parts of articulating rib cartilage were included in the dissection to ensure complete inclusion of ectopic calcification, when present. Trabecular bone was minimized in the collection as much as possible. Red arrows highlight ectopic calcification.

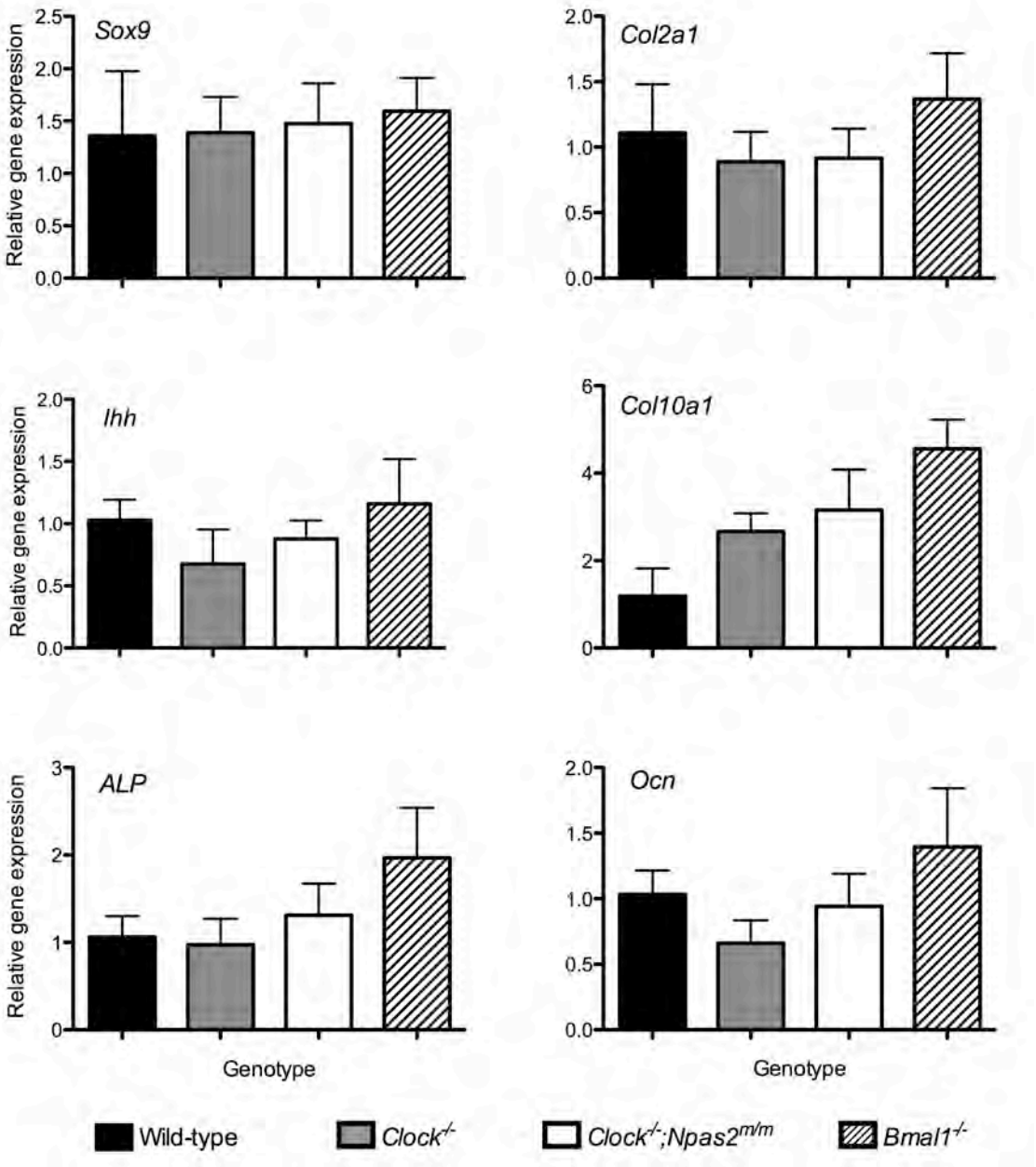

Figure 4.5. Chondrocyte marker gene expression in *Clock*$^{-/-}$;*Npas2*$^{m/m}$ intersternebral tissue does not significantly differ from wild-type. Quantitative RT-PCR analysis of chondrocyte maturation marker genes in 6-7 week-old wild-type (n=3), *Clock*$^{-/-}$ (n=3), *Clock*$^{-/-}$;*Npas2*$^{m/m}$ (n=4), and *Bmal1*$^{-/-}$ (n=3) intersternebral tissue. One-way ANOVA did not reveal significant differences in gene expression, although there is a trend toward higher *Col10a1* expression in *Clock*$^{-/-}$;*Npas2*$^{m/m}$ and *Bmal1*$^{-/-}$ tissue compared to wild-type tissue.

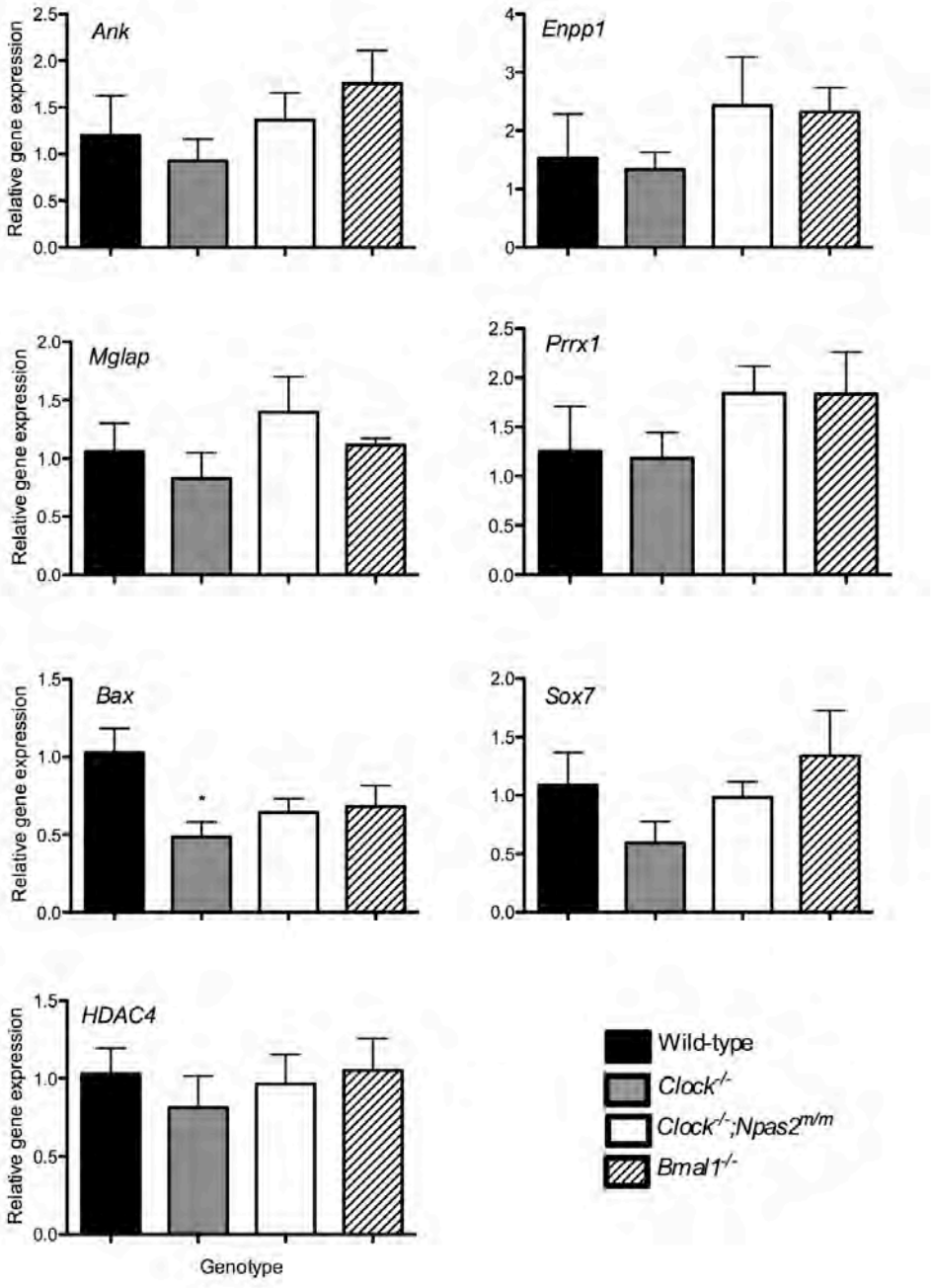

Figure 4.6. Candidate gene expression in *Clock*$^{-/-}$;*Npas2*$^{m/m}$ intersternebral tissue does not significantly differ from wild-type. Quantitative RT-PCR analysis of candidate genes in 6-7 week-old wild-type (n=3), *Clock*$^{-/-}$ (n=3), *Clock*$^{-/-}$;*Npas2*$^{m/m}$ (n=4), and *Bmal1*$^{-/-}$ (n=3) intersternebral tissue. One-way ANOVA did not reveal significant differences in gene expression, with the exception of *Clock*$^{-/-}$ tissue that exhibited significantly less *Bax* expression compared to wild-type when analyzed by Dunnett post-test. *$p<0.05$

Chapter V

Investigating protein expression in the costosternal junction of *Clock*$^{-/-}$;*Npas2*$^{m/m}$ double mutant mice

Summary

The lack of changes in gene expression profiles in micromass culture and grossly dissected intersternebral tissue suggests that the mechanism of arthropathy in *Clock*$^{-/-}$;*Npas2*$^{m/m}$ double mutant mice may be much more localized and complicated. Specific chondrocytes and/or additional cells most likely interact with systemic factors to initiate ectopic calcification at the costosternal junction. To establish the distribution of osteoclasts, osteoblasts, and chondrocytes, a series of histological stains and immunohistochemistry (IHC) was performed. Site-specific changes in chondrocyte maturation marker protein expression in costosternal junction tissue were also assessed by IHC. The anatomical distribution of osteoclasts, osteoblasts, and chondrocytic proteins does not differ between *Clock*$^{-/-}$;*Npas2*$^{m/m}$ double mutant and wild-type mice, suggesting that the distribution of cells does not contribute to arthropathy in *Clock*$^{-/-}$;*Npas2*$^{m/m}$ double mutant mice, or that the markers used do not adequately distinguish the subpopulations of affected cells. Instead, varying levels of gene or protein expression could be involved, in which case more quantitative methods must be employed.

Acknowledgments

This chapter is a result of collaboration between our laboratory and the laboratories of Jane Lian and Paul Fanning in the Department of Cell Biology at the University of Massachusetts Medical School (UMMS). As such, I would like to acknowledge the appropriate people for their contribution to the work presented here.

Dr. Paul Fanning provided the TUNEL IHC protocol and assisted in data interpretation. Sadiq Hussain taught me how to TRAP and ALP stain slides, and April Mason-Savas performed TRAP/ALP co-staining and type II collagen IHC. Kimberly LeBlanc and Melissa Matzelle shared their SOX9 IHC protocols and assisted with SOX9 IHC troubleshooting. Lastly, Dr. Jane Lian shared her lab's SOX9, RUNX2, and type X collagen primary antibodies.

Figure 5.1. Sample image of TUNEL IHC quantitative analysis.
Elizabeth Yu – Department of Neurobiology, UMMS

Figure 5.2. TRAP and ALP stains of 6-7 week-old *Clock*$^{-/-}$*;Npas2*$^{m/m}$ costosternal junction.
Elizabeth Yu – Department of Neurobiology, UMMS
Sadiq Hussain – Department of Cell Biology, UMMS
April Mason-Savas – Department of Cell Biology, UMMS

Figure 5.3. SOX9 IHC of 6-7 week-old *Clock*$^{-/-}$*;Npas2*$^{m/m}$ and wild-type sterna.
Elizabeth Yu – Department of Neurobiology, UMMS

Figure 5.4. RUNX2 IHC of 6-7 week-old *Clock*$^{-/-}$*;Npas2*$^{m/m}$ and wild-type sterna.
Elizabeth Yu – Department of Neurobiology, UMMS

Figure 5.5. TUNEL IHC of *Clock*$^{-/-}$*;Npas2*$^{m/m}$ and wild-type sterna.
Elizabeth Yu – Department of Neurobiology, UMMS

Figure 5.6. Type II collagen IHC of 6-7 week-old *Clock*$^{-/-}$*;Npas2*$^{m/m}$ and wild-type sterna.
April Mason-Savas – Department of Cell Biology, UMMS

Figure 5.7. Type X collagen IHC of 6-7 week-old *Clock*$^{-/-}$;*Npas2*$^{m/m}$ and wild-type sterna.
Elizabeth Yu – Department of Neurobiology, UMMS

Figure 5.8. Quantitative analysis of SOX9- and TUNEL-positive cells around costosternal junction lesions.
Elizabeth Yu – Department of Neurobiology, UMMS

Introduction

Attempts to reveal genotype-related changes in gene expression during chondrogenic differentiation *in vitro* and in intersternebral tissue proved to be unfruitful (see Chapter IV). While positive results from those experiments could have been informative, the negative results show us that the mechanism of age-dependent arthropathy in the costosternal junction is more complicated than originally anticipated. Chondrocytes may or may not be involved in this pathology and any changes in gene expression are probably localized to the small areas that develop calcification. These local changes could be interacting with systemic factors to ultimately generate ectopic calcification. Thus, studies to investigate *in vivo* protein expression changes were conducted. Histological stains and immunohistochemistry (IHC) were used to study the distribution of calcification-related cell types in the costosternal junction and assess varying levels of protein expression. TUNEL analyses were also conducted to assess apoptosis.

To identify the distribution of the three main cell types involved in bone homeostasis, stains and IHC were performed to locate osteoblasts, osteoclasts, and chondrocytes. Alkaline phosphatase (ALP) is specific to osteoblasts and mature chondrocytes, as these cells types calcify their surrounding extracellular matrix to form bone and cartilage, respectively. Tartrate-resistant acid phosphatase (TRAP) is secreted exclusively by osteoclasts to resorb bone, so staining for TRAP activity is a useful method to localize osteoclasts. Chondrocytes express a number of markers, but type X

collagen is a protein specifically produced and secreted by hypertrophic chondrocytes. IHC for type X collagen thus evaluates hypertrophic chondrocyte presence.

Identifying the type of tissue present in costosternal junctions is also important. The articulating rib cartilage, also known as costal cartilage, consists of hyaline cartilage [105]. Hyaline cartilage is one of three types of cartilage, the other two types being elastic cartilage and fibrocartilage. Hyaline cartilage is the most common of the three forms and consisted mainly of type II collagen. Elastic cartilage is more pliable and distensible and contains elastic fibers as well as type II collagen in its matrix. Fibrocartilage is characterized by a matrix containing type I and type II collagen fibers.

The RNA analyses of micromass culture and intersternebral tissue did not provide evidence for abnormal chondrogenic differentiation in *Clock*$^{-/-}$*;Npas2*$^{m/m}$ double mutant samples. However, the limitations of those experiments prevent us from concluding that chondrocyte differentiation is not involved. To further explore this hypothesis, IHC for chondrocyte-related proteins was performed. IHC is particularly useful in this regard because we can observe anatomical distribution of protein expression, including relative protein expression levels, and which cells are producing which proteins. Proteins of interest studied here include SOX9, RUNX2, type II collagen, and type X collagen. TUNEL IHC was also performed to assess apoptosis, as apoptosis is the last stage of chondrocyte maturation.

Experimental procedures

Generation, maintenance, and genotyping of study animals

Please see "Chapter II: Experimental procedures" for details.

Specimen collection, fixation, embedding, and sectioning

Please see "Chapter II: Experimental procedures" for details. Briefly, tissue sections were immersed in PLP fixative and then decalcified, paraffin-embedded, and sectioned at 6 um. Histology and IHC described in this chapter were performed on slide-mounted sections prepared in this fashion.

TRAP and ALP histology stains

Two tartrate-resistant acid phosphatase (TRAP) stains were conducted. In one, slides were stained for TRAP and counterstained with toluidine blue made in isopropanol. In the other, TRAP was co-stained with alkaline phosphatase (ALP). Sterna of 2 *Clock*$^{-/-}$*;Npas2*$^{m/m}$ double mutant and 2 wild-type mice, 6-7 weeks of age, were stained for TRAP alone. Sterna of 6 *Clock*$^{-/-}$*;Npas2*$^{m/m}$ double mutant and 4 wild-type mice, 6-7 weeks of age, were stained for TRAP and ALP. Three sections per mouse were analyzed. In both TRAP stains, TRAP stains osteoclasts red. ALP stains osteoblasts and hypertrophic chondrocytes blue. In the single TRAP stain, 6 um thick slide-mounted sections were incubated in TRAP staining solution "A" (0.5mg/ml Naphthol AS MX Phosphate, 2.8% N,N-dimethylformamide, 1 mg/ml fast red AS TR salt, 9.7 mg/ml

sodium tartrate, 50% Tris HCl buffer) at 37^{o}C for 30-45 minutes. Slides were then washed with distilled water and dried on a hot plate for 5 minutes prior to counterstaining with 0.5% methyl green for 2 minutes. After slides were washed thoroughly with tap water, they were dried on the hot plate again and coverslipped.

For the TRAP/ALP co-stain, slides were first stained for ALP. Six um thick slide-mounted sections were incubated overnight in 1% magnesium chloride in 100 mM Tris-maleate buffer, pH 9.2 and then incubated for 2 hours at room temperature in ALP substrate solution (0.2mg/ml Naphthol AS-MX phosphate, 0.4mg/ml fast blue BB salt, made in 100 mM Tris-maleate buffer, pH 9.2). After washing slides for 10 minutes with tap water, slides were incubated at 37^{o}C in the dark for 45 minutes in filtered TRAP staining solution "B" (0.016 mg/ml Naphthol AS-BI Phosphate, 1% N,N-dimethylformamide, 0.14 mg/ml fast red-violet LB diazonium salt, 0.004% magnesium chloride, 9.7 g/ml L(+) tartaric acid, made in 0.2 M acetate buffer, pH 6.0). Slides were washed with tap water and coverslipped.

Images were captured using a Zeiss Axioskop 40 microscope, Zeiss AxioCam HRc camera, and Zeiss AxioVision 4 (version 4.7.2.0) software.

Immunohistochemistry (IHC)

Sterna of 7 *Clock*$^{-/-}$*;Npas2*$^{m/m}$ double mutant and 3 wild-type mice, 6-7 weeks of age, were used for SOX9 and RUNX2 IHC. Six-micron thick slide-mounted sections were deparaffinized, rehydrated, and endogenous peroxidase was blocked using 10% hydrogen peroxide in methanol solution. Antigen heat retrieval was performed using the

Retriever 2100 (PickCell Laboratories) and then slides were placed in 50 mM ammonium chloride for 30 minutes at room temperature before incubating in blocking solution (1% bovine serum albumin (BSA), 0.2% gelatin, 0.05% saponin, made in 1X PBS) for 30 minutes at room temperature. Slides were incubated overnight at 4^{o}C in primary antibody diluted in antibody dilution buffer (0.1% BSA, Triton X-100, made in 1X PBS). SOX9 primary antibody (rabbit, anti-human, Santa Cruz sc-20095) was diluted 1:50. RUNX2 primary antibody (rabbit, anti-mouse, Covance 572) was diluted 1:1000. Negative control slides were not treated with primary antibody; they were treated with antibody dilution buffer only. The next day, slides were acclimated to room temperature and washed in wash buffer (0.1% BSA, 0.2% gelatin, 0.05% saponin, made in 1X PBS) three times for 10 minutes at room temperature and then incubated for 60-90 minutes at room temperature in secondary antibody (goat, anti-rabbit HRP, DakoCytomation) that was diluted 1:600 in antibody dilution buffer. The slides were then washed three times in wash buffer for 10 minutes each and incubated in DAB reagent (DakoCytomation) for 10 minutes for color development. After color development, slides were washed with 1X PBS and distilled water before counterstaining with 0.025% toluidine blue made in distilled water for five seconds. Lastly, slides were washed in running tap water, dehydrated through ascending concentrations of ethanol to xylene, and coverslipped.

Sterna of 4 *Clock*$^{-/-}$*;Npas2*$^{m/m}$ double mutant and 2 wild-type mice, 6-7 weeks of age, were used for type II collagen IHC. Slides were deparaffinized, rehydrated, and treated with preheated 1 mg/ml pepsin in Tris HCl for 15 minutes. After rinsing with distilled water, endogenous peroxidase activity was blocked by incubating slides in 3%

hydrogen peroxide for 10 minutes. Slides were washed with Tris HCl buffer and then blocked with 1% BSA in Tris HCl for 20 minutes at room temperature. Primary type II collagen antibody was diluted 1:200 and slides incubated overnight at 4^{o}C (anti-mouse, Chemicon International MAB8887), while negative control slides were not treated with primary antibody. The next morning, slides were washed with Tris HCl and then incubated in secondary biotinylated antibody (Dako K0690) for 30 minutes at room temperature, rinsed with Tris HCl again, and stained with DAB+ (Dako K3468) for 5 minutes. Slides were rinsed several times with water and then counterstained with 0.025% toluidine blue made in distilled water before being thoroughly rinsed and coverslipped.

Sterna of 4 *Clock*$^{-/-}$*;Npas2*$^{m/m}$ double mutant and 2 wild-type mice, 6-7 weeks of age, and two 4-5 week-old wild-type mice, were used for terminal deoxynucleotidyl transferase dUTP nick end labeling (TUNEL) staining. Slides from 4-5 week-old wild-type mice were used as positive and negative controls. Slides were deparaffinized, rehydrated, and treated with 20 ug/ml proteinase K at room temperature for 15 minutes prior to incubation in 10% hydrogen peroxide in methanol at room temperature for 15 minutes. Slides were washed with 1X PBS at room temperature three times for 2 minutes. The positive control slide was washed with 1X RQ1 RNAse-free buffer (Promega), treated with 5-10 units of DNAse 1 (Promega) in 1X RQ1 buffer at room temperature for 10 minutes, washed with distilled water, then washed with 1X PBS for 5 minutes. Slides (positive and experimental) were then incubated in mastermix solution (0.3 nmol/ul biotin-dUTP, 25 mM cobalt chloride, 5X TdT buffer (Promega), 25 U/ul TdT enzyme

(Promega), made in distilled water) and the negative control slide was incubated in mix solution without enzyme for 1 hour in a humidity chamber at 37^{o}C. After washing the slides with 1X PBS three times for 2 minutes at room temperature, they were blocked with 2% FBS in 1X PBS at room temperature for 10 minutes. Slides were then incubated in ABC Reagent (Vectastain Elite) at room temperature for 10 minutes, washed with 1X PBS, and then distilled water. For color development, slides were incubated with DAB mix (0.05% DAB, 0.015% hydrogen peroxide, made in 1X PBS) at room temperature for 10-30 minutes. Finally, slides were washed with tap water, counterstained with 0.025% toludine blue made in water for 5 seconds, washed in running tap water, dehydrated, and coverslipped.

Three sections per mouse were analyzed for all IHC. Images were captured using a Zeiss Axioskop 40 microscope, Zeiss AxioCam HRc camera, and Zeiss AxioVision 4 (version 4.7.2.0) software.

Quantitative analysis

To quantitatively analyze SOX9 and TUNEL IHC slides, concentric 1 cm rings were drawn around equal sized, 20X-magnified printed images of *Clock*$^{-/-}$*;Npas2*$^{m/m}$ double mutant costosternal junction lesions (Figure 5.1). The area of interest was intersternebral tissue medial to the lesion. Calcified tissue on the surface of sternebrae (as identified by von Kossa and alizarin red staining, Figure 2.8A&B) and rib cartilage were excluded from the areas quantified, as there was excessive, consistent staining in those regions on all slides (both wild-type and *Clock*$^{-/-}$*;Npas2*$^{m/m}$ double mutant mice). Positive

and total cells were counted manually. There were a total of 7 *Clock*$^{-/-}$;*Npas2*$^{m/m}$ double mutant sterna that were labeled with SOX9, and 4 *Clock*$^{-/-}$;*Npas2*$^{m/m}$ double mutant sterna that were labeled with TUNEL, with 3 serial sections per sterna. In the majority of sections, multiple costosternal junctions in each section contained lesions. For each mouse, the ratios calculated from all of its lesions were averaged, so that each mouse is an n = 1 (i.e. n = 7 for SOX9 and n = 4 for TUNEL statistical analysis). A total of 47 SOX9 images and 54 TUNEL images were analyzed. For SOX9 images, there were 304/886 positive/total cells in the first ring, 360/872 in the second ring, and 393/938 in the third ring. For TUNEL images, there were 247/915 positive/total cells in the first ring, 258/885 in the second ring, and 283/917 in the third ring. Statistical analysis of data is graphically represented in Figure 5.8.

Statistical analysis

SOX9 and TUNEL positive:total cell proportions were analyzed by one-way ANOVA (Prism 5 for Mac OS X software). P-values less than 0.05 were considered statistically significant.

Results and discussion

Assessing distribution of cell types in costosternal junction

To elucidate the mechanism of age-dependent arthropathy, identifying the cell type(s) involved is an important first step. Based on the histology of the costosternal junction, we presumed chondrocytes were involved, but the micromass culture results suggest that chondrocytes alone are probably not the cause of ectopic calcification. To identify cells present in costosternal junction around calcific lesions, then, histological and immunohistochemical stains were performed. TRAP and ALP stains were performed on 6-7 week-old sterna of *Clock*$^{-/-}$*;Npas2*$^{m/m}$ double mutant and wild-type mice. Because co-staining TRAP with ALP on this tissue leads to significant ALP-related background staining (Figure 5.2B), TRAP stains were also performed separately on other slides (Figure 5.2A).

In the TRAP stained slides, osteoclasts are present in the sternebral trabecular bone but there is no red staining in the intersternebral cartilage of either *Clock*$^{-/-}$*;Npas2*$^{m/m}$ double mutant or wild-type mice. This distribution of osteoclasts suggests that they are not actively involved in the pathogenesis of arthropathy. However, the absence of osteoclasts around costosternal junction lesions could reflect a defect in osteoclast function in *Clock*$^{-/-}$*;Npas2*$^{m/m}$ double mutant mice. Perhaps osteoclasts normally remove ectopic calcification in wild-type mice but are unable to perform this function in *Clock*$^{-/-}$*;Npas2*$^{m/m}$ double mutant mice. This defect could be due to dysfunctional osteoclast migration, secondary to impaired signaling pathways. To argue against this possibility is

the absence of osteoclasts in wild-type intersternebral cartilage. If pathological ectopic calcification were being actively prevented by osteoclasts in wild-type mice, one would expect to see residual osteoclasts in the area. Since osteoclasts are not detectable by TRAP staining in wild-type intersternebral tissue, it is unlikely that osteoclasts are normally there and thus they are probably not involved in ectopic calcification development in *Clock*$^{-/-}$*;Npas2*$^{m/m}$ double mutant mice.

In TRAP/ALP co-stained slides, TRAP is still localized to sternebral trabeculae, although the distinction between red-orange background staining and pure red TRAP staining is difficult to appreciate (Figure 5.2B). ALP, which stains blue and is specific to osteoblasts and mature chondrocytes, is localized to costal cartilage, the calcified tissue on the sternebral surfaces that face the intersternebral cartilage, and the growth plate (Figure 5.2B). ALP-positive cells juxtapose costosternal junction lesions such that it is possible that these ALP-positive cells contribute to the development of ectopic calcification. The ALP-positive cells of the costal cartilage and sternebral surface form a pocket of sorts in which the calcific lesion seems to grow.

Investigating changes in chondrocytic protein levels in costosternal junction

The presence of chondrocytes in the costosternal junction led to the hypothesis that inappropriate chondrocyte differentiation could contribute to the development of ectopic calcification. RNA analyses of chondrocyte maturation marker genes in the intersternebral cartilage did not yield results to clearly support or refute this hypothesis, so to assess site-specific changes in chondrocyte maturation, IHC was conducted. To

investigate the distribution of maturing chondrocytes, IHC for SOX9, type II collagen, type X collagen, and RUNX2 was performed. SOX9 and RUNX2 are transcription factors and thus are nuclear stains. Type II and X collagen are extracellular proteins so the majority of type II and X collgen staining is extracellular, although in some cases type II and X collagen is visible in the cytoplasm of chondrocytes.

SOX9 is present in nearly every cell of the costosternal junction, including costal cartilage and intersternebral cartilage, indicating that all of these cells are resting or proliferating chondrocytes (Figure 5.3). RUNX2, on the other hand, is more selectively expressed and only present in medial costal cartilage chondrocytes and cells on sternebral surfaces that face the intersternebral cartilage (Figure 5.4). TUNEL labeling is present in the same distribution as SOX9 (Figure 5.5). SOX9-, RUNX2-, and TUNEL-positive cells are similarly distributed in *Clock*$^{-/-}$*;Npas2*$^{m/m}$ double mutant and wild-type costosternal tissue. A common criticism of IHC provides a possible explanation for this lack of detectable difference. IHC relies on signal amplification and so while cells that express a given protein will be labeled, it is not possible to detect changes in protein expression levels between labeled cells. Thus, it is possible that there are changes in the expression levels of these proteins in *Clock*$^{-/-}$*;Npas2*$^{m/m}$ double mutant costosternal junction tissue compared to wild-type, but the IHC methods used were unable to detect those changes.

Type II and X collagen are present throughout the costosternal junction (Figure 5.6 & 5.7). Both types of collagen are in the intersternebral cartilage, costal cartilage, and growth plates. Type X collagen IHC was performed with two types of counterstain: in the first experiment, methyl green was the counterstain (Figure 5.7A) but due to inconsistent

counterstaining, another experiment using toluidine blue as a counterstain was performed (Figure 5.7B). In both experiments, type X collagen stains the same areas in *Clock*$^{-/-}$*;Npas2*$^{m/m}$ double mutant and wild-type tissue, although the intensity of staining seems less prominent in the toluidine blue counterstained slides. This variability is most likely due to repeat freeze-thaw cycles of the primary type X collagen antibody, which was used first on the methyl green counterstained slides and then subjected to a freeze-thaw cycle prior to usage on the toluidine blue counterstained slides. Type II collagen is the main component of hyaline cartilage and is present, as expected, throughout the intersternebral space and in the costal cartilage (Figure 5.6).

Quantitative analysis of chondrocyte proteins around costosternal junction lesions

Preliminary inspection of the SOX9 and type II collagen IHC suggested that there is a sparsity of SOX9 and type II collagen expression around the immediate periphery of calcific lesions. This down-regulation of SOX9 expression could lead to decreased expression of type II collagen, because SOX9 has been shown to increase transcription of *Col2a1* [4, 10]. Decreasing type II collagen, which is an unelastic fiber, could promote flexibility allowing calcific lesions to expand and enlarge with age. TUNEL-positive cells appeared more prevalently in areas immediately surrounding the calcific lesions – the same areas in which SOX9 and type II collagen seem reduced. These findings led to the hypothesis that chondrocytes around lesions could have dysregulated chondrocyte differentiation programs. More specifically, instead of remaining as resting chondrocytes, dysregulated chondrocytes may differentiate to hypertrophic chondrocytes and apoptose,

leading to the calcification of cartilage matrix and the formation of ectopic calcification. The down-regulation of SOX9 and type II collagen could be indicative of chondrocytes maturing into hypertrophic chondrocytes, which do not express SOX9 or make type II collagen. An increase in TUNEL-positive cells could indicate apoptosis of cells at the periphery of the lesions, which is the last step of chondrocyte differentiation.

To critically examine the possibility of differences in SOX9 and TUNEL expression in cells adjacent to calcific lesions, 47 images of costosternal junctions immunohistochemically stained for SOX9 and 54 images of costosternal junctions immunohistochemically stained for TUNEL were analyzed. Images came from four to six 6-7 week-old *Clock*$^{-/-}$*;Npas2*$^{m/m}$ double mutant mice. Type II and X collagen were not examined because quantifying an extracellular stain is not compatible with this quantitative analysis. In this quantitative analysis, individual cells were counted as either positively or negatively stained. Type II and X collagen are occasionally labeled within cells, but the majority of the stains are extracellular, making it difficult to differentiate positively labeled cells from negative ones. For SOX9 and TUNEL quantitative analysis, concentric 1 cm rings were manually drawn around equal sized, 20X-magnified printed images of the lesions (Figure 5.1) and the proportion of positively labeled cells was counted. Statistically, there is no difference in the proportion of SOX9- or TUNEL-labeled cells distributed around calcific lesions (Figure 5.8), refuting the initial observation that there may have been a difference in SOX9- and TUNEL-labeled cell distribution.

Concluding remarks

While these histology results do not show us definitively whether or not abnormal chondrocyte maturation is involved in the pathology of costosternal junction calcification, conclusions can still be drawn from these results. The absence of drastic differences in the distribution of osteoclasts, osteoblasts, and cells expressing chondrocyte markers in *Clock*$^{-/-}$*;Npas2*$^{m/m}$ double mutant and wild-type mice suggest that gross alterations in the distribution of cell types in costosternal junction may not contribute to the pathology of arthropathy. It is also possible that the chondrocyte markers used are unable to distinguish the subpopulation of cells involved in age-dependent arthropathy. It is likely that the cause of this site-specific arthropathy is much more discrete and could involve interactions with systemic factors, and future studies must be equally focused in order to elucidate changes in gene and protein expression patterns.

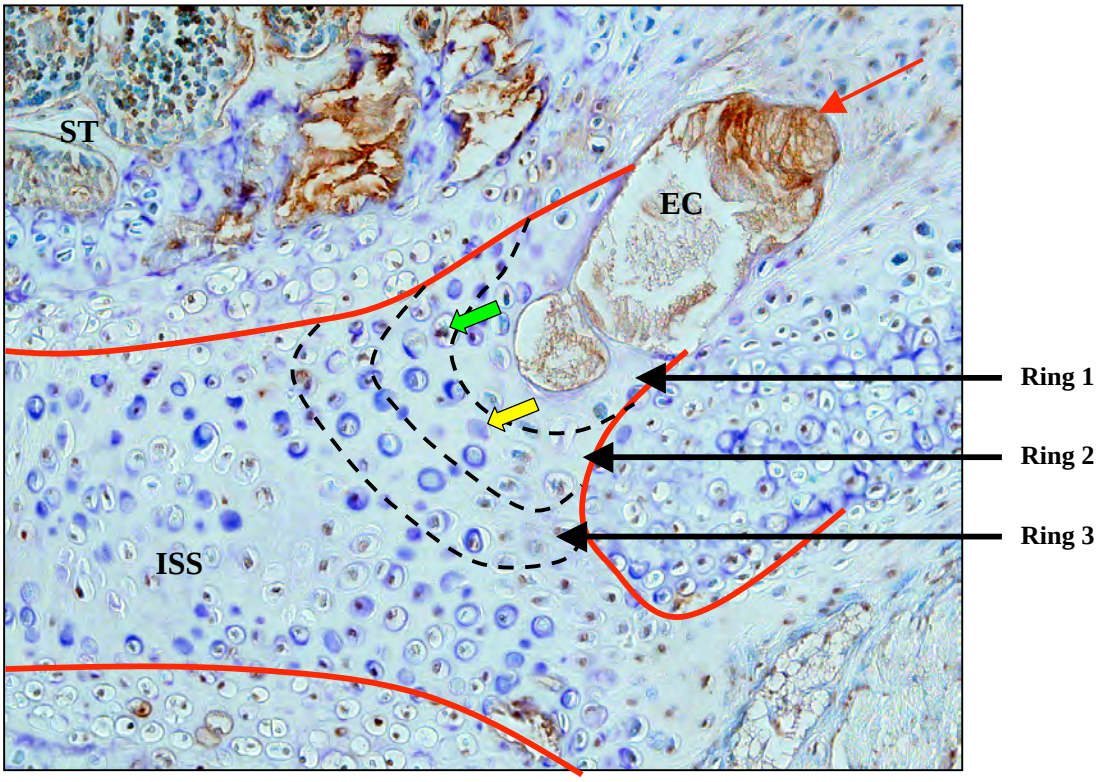

Figure 5.1. Sample image of TUNEL IHC quantitative analysis. Chondrocytes on sternebral surfaces facing the intersternebral space (ISS) and rib cartilage were excluded from the analysis. Only cells in the intersternebral space were included. The purpose of this quantitative analysis is to determine if the distribution of cells around the lesions differs as one moves further away from the lesions. This same technique was applied to SOX9 IHC quantitative analysis. In decalcified tissues, ectopic calcification (EC) appears as holes with acellular debris in them. Red lines border the excluded areas. Dotted black lines delineate concentric areas. Yellow arrow identifies a negative TUNEL-stained cell. Green arrow identifies a positive TUNEL-stained cell. Red arrow highlights ectopic calcification. 20X magnification. ST: sternebral trabeculae.

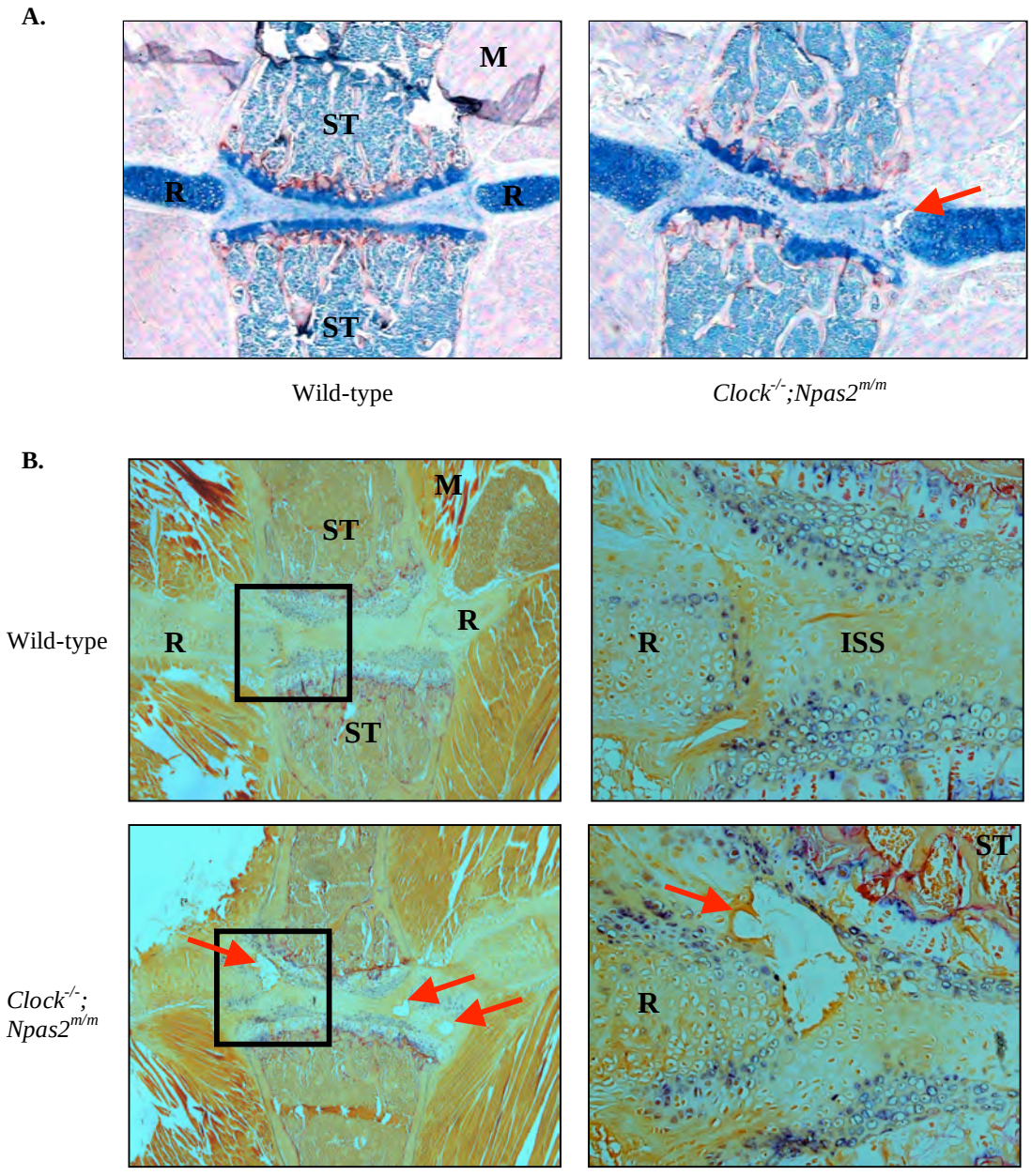

Figure 5.2. TRAP and ALP stains of 6-7 week-old *Clock*$^{-/-}$;*Npas2*$^{m/m}$ costosternal junction. (A) Single TRAP staining (red) of 6-7 week-old costosternal junction reveals normal osteoclast distribution in trabecular bone but none around costosternal junction calcific lesions. 5X magnification. (B) Double TRAP (red) and ALP (blue) staining reveals ALP-positive cells in costal cartilage and growth plate and on the surface of sternebrae. Orange staining is from the ALP staining process. Images on the right are 20X magnifications of the boxed sections indicated on the 5X images on the left. Red arrows highlight ectopic calcification. ST: sternebral trabeculae; R: rib cartilage; ISS: intersternebral space; M: muscle.

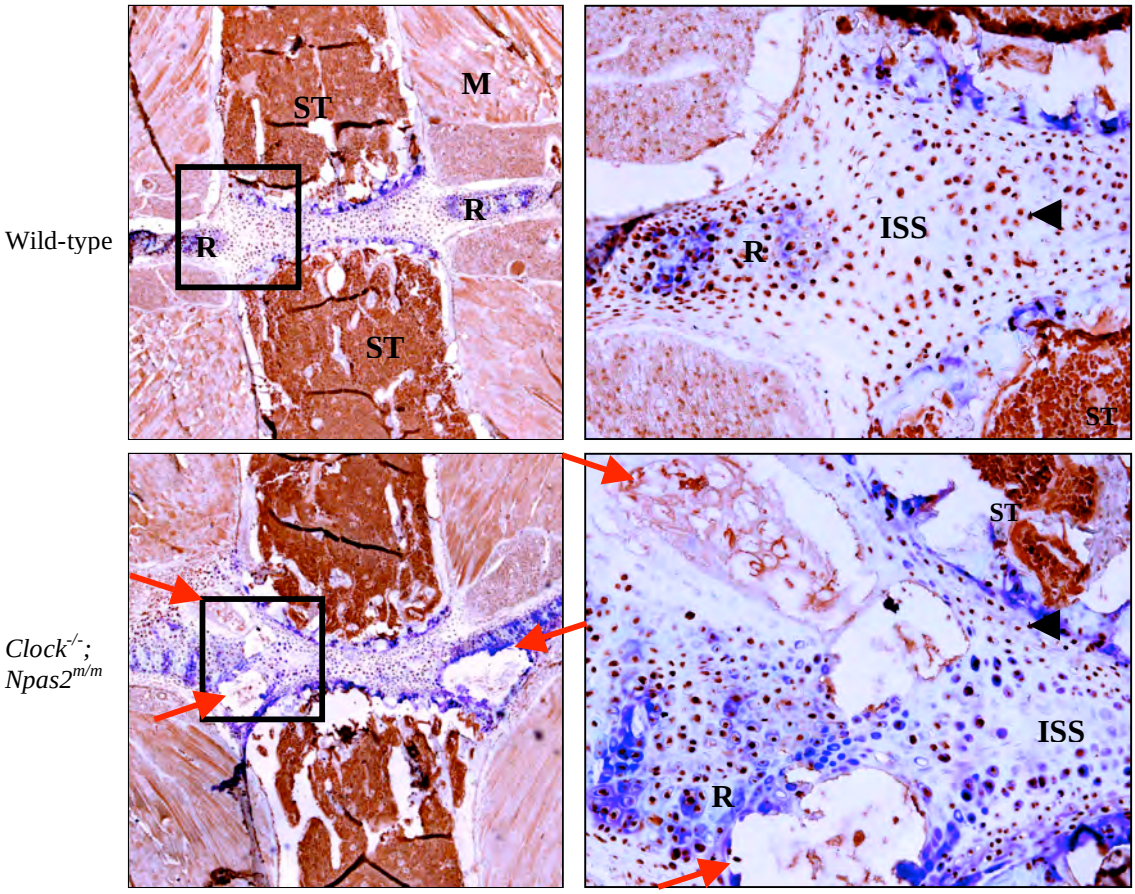

Figure 5.3. SOX9 IHC of 6-7 week-old *Clock*$^{-/-}$;*Npas2*$^{m/m}$ and wild-type sterna. Wild-type and *Clock*$^{-/-}$;*Npas2*$^{m/m}$ costal cartilage, intersternebral cartilage, and sternebral surface cartilage all stain strongly for SOX9 (brown). Images on the right are 20X magnifications of the boxed sections indicated on the 5X images on the left. Black arrowhead identifies a positively labeled cell. Red arrows highlight ectopic calcification. Slides are counterstained with toluidine blue made in water. ST: sternebral trabeculae; R: rib cartilage; ISS: intersternebral space; M: muscle.

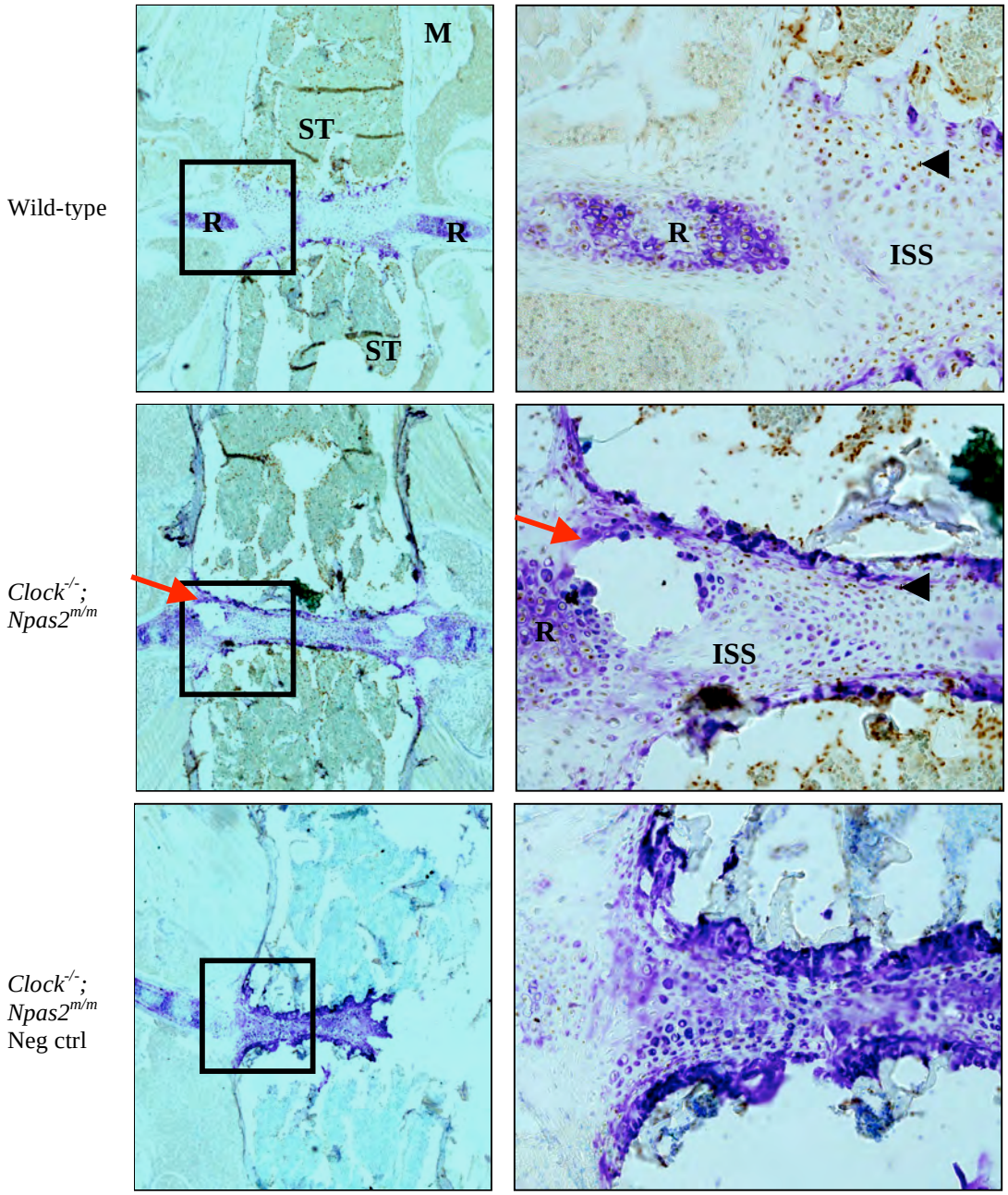

Figure 5.4. RUNX2 IHC of 6-7 week-old *Clock*$^{-/-}$;*Npas2*$^{m/m}$ and wild-type sterna. Wild-type and *Clock*$^{-/-}$;*Npas2*$^{m/m}$ costal cartilage and sternebral surface cartilage stain strongly for RUNX2 (brown). The negative control (bottom) shows nonspecific background staining. Images on the right are 20X magnifications of the boxed sections indicated on the 5X images on the left. Black arrowhead identifies a positively labeled cell. Red arrows highlight ectopic calcification. Slides are counterstained with toluidine blue made in water. ST: sternebral trabeculae; R: rib cartilage; ISS: intersternebral space; M: muscle.

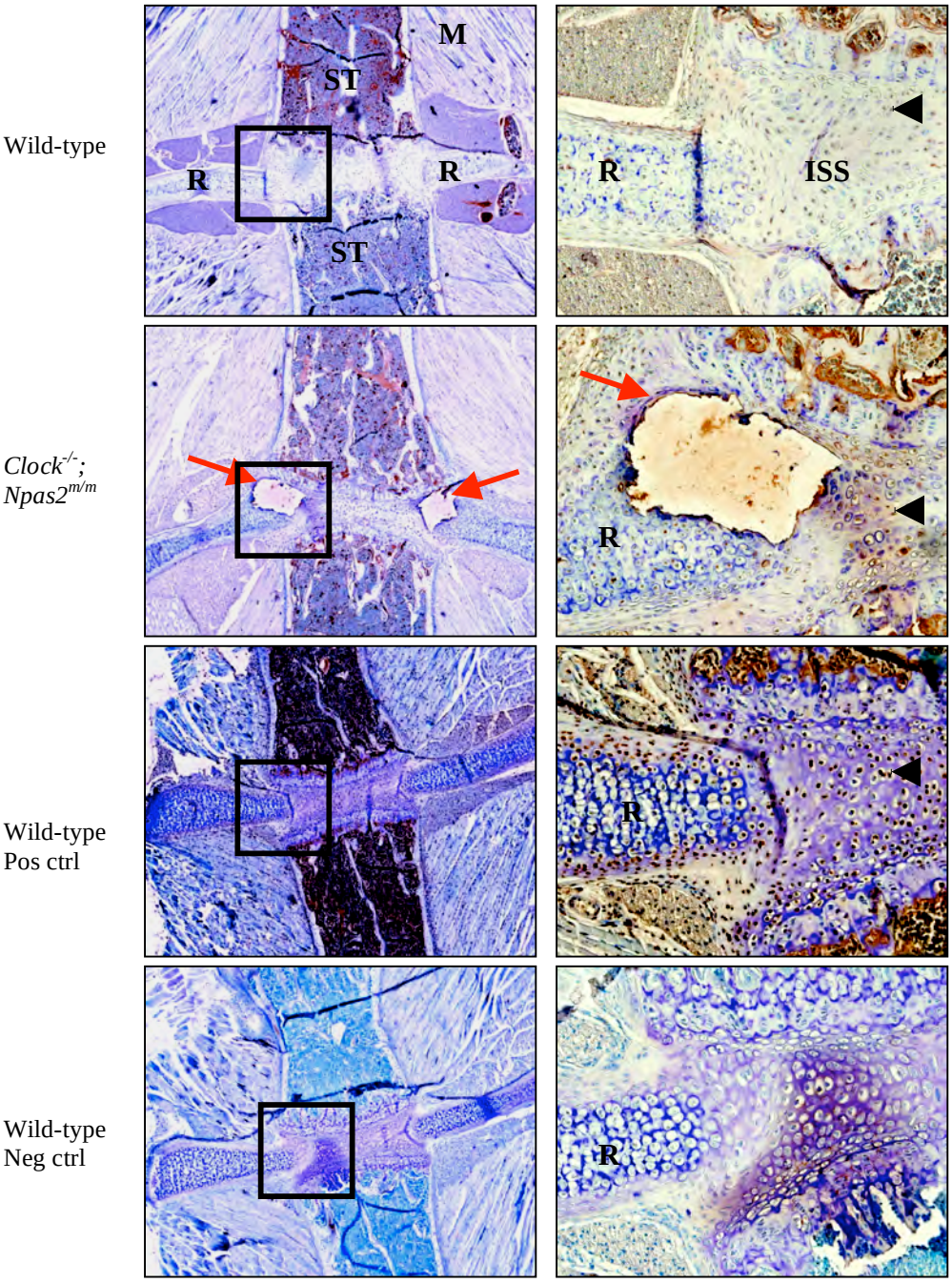

Figure 5.5. TUNEL IHC of *Clock*$^{-/-}$;*Npas2*$^{m/m}$ and wild-type sterna. 6-7 week-old wild-type and *Clock*$^{-/-}$;*Npas2*$^{m/m}$ costal cartilage, intersternebral cartilage, sternebral surface cartilage, and growth plate stain with TUNEL (brown). Positive and negative controls are of 4-5 week-old wild-type mice. Images on the right are 20X magnifications of the boxed sections indicated on the 5X images on the left. Black arrowhead identifies a positively labeled cell. Red arrows highlight ectopic calcification. Slides are counterstained with toluidine blue made in water. ST: sternebral trabeculae; R: rib cartilage; ISS: intersternebral space; M: muscle.

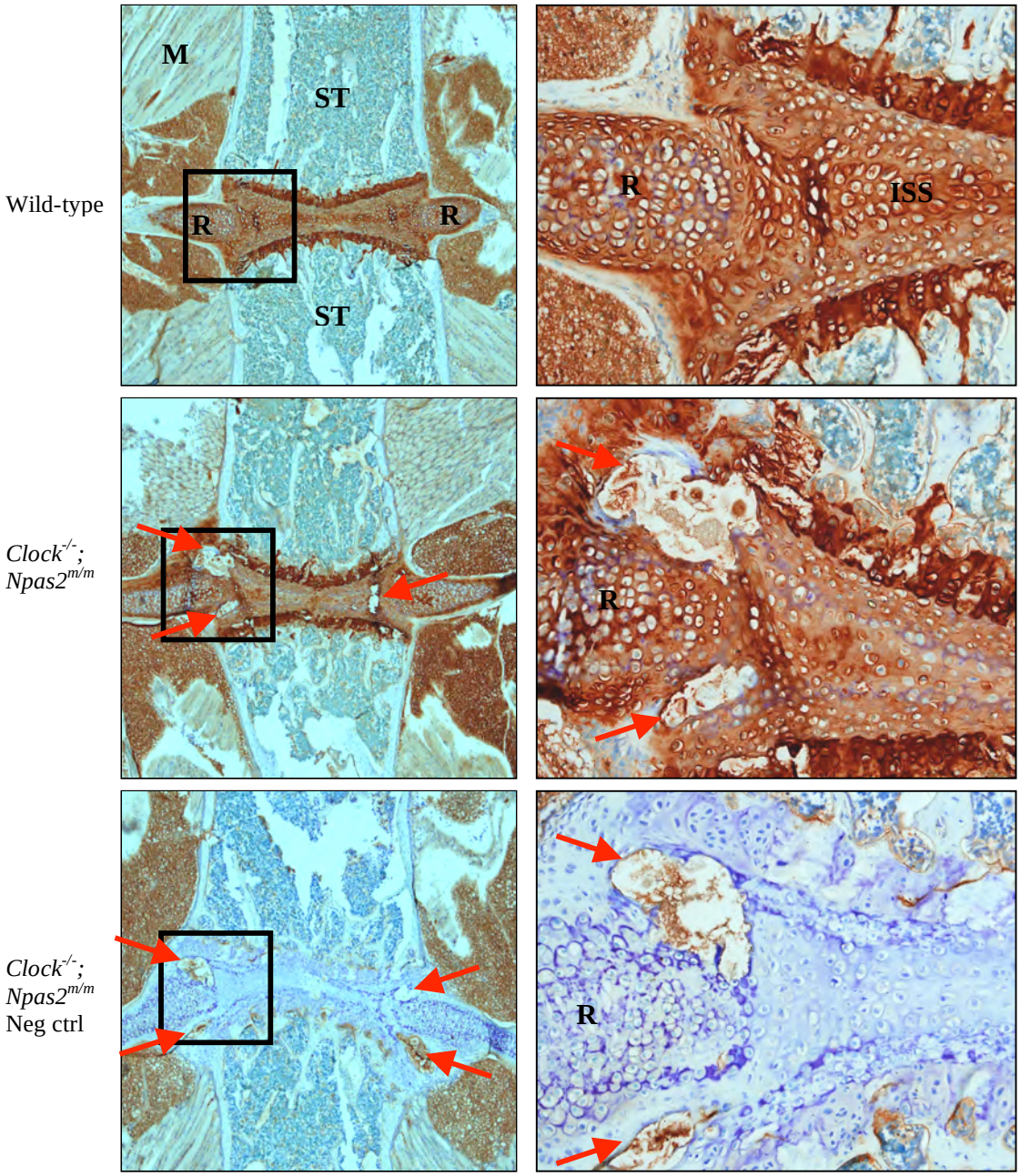

Figure 5.6. Type II collagen IHC of 6-7 week-old *Clock*$^{-/-}$;*Npas2*$^{m/m}$ and wild-type sterna. Wild-type and *Clock*$^{-/-}$;*Npas2*$^{m/m}$ costal cartilage, intersternebral cartilage, and growth plate all stain strongly for type II collagen (brown). The negative control (bottom) shows nonspecific background staining. Images on the right are 20X magnifications of the boxed sections indicated on the 5X images on the left. Red arrows highlight ectopic calcification. Slides are counterstained with toluidine blue made in water. ST: sternebral trabeculae; R: rib cartilage; ISS: intersternebral space; M: muscle.

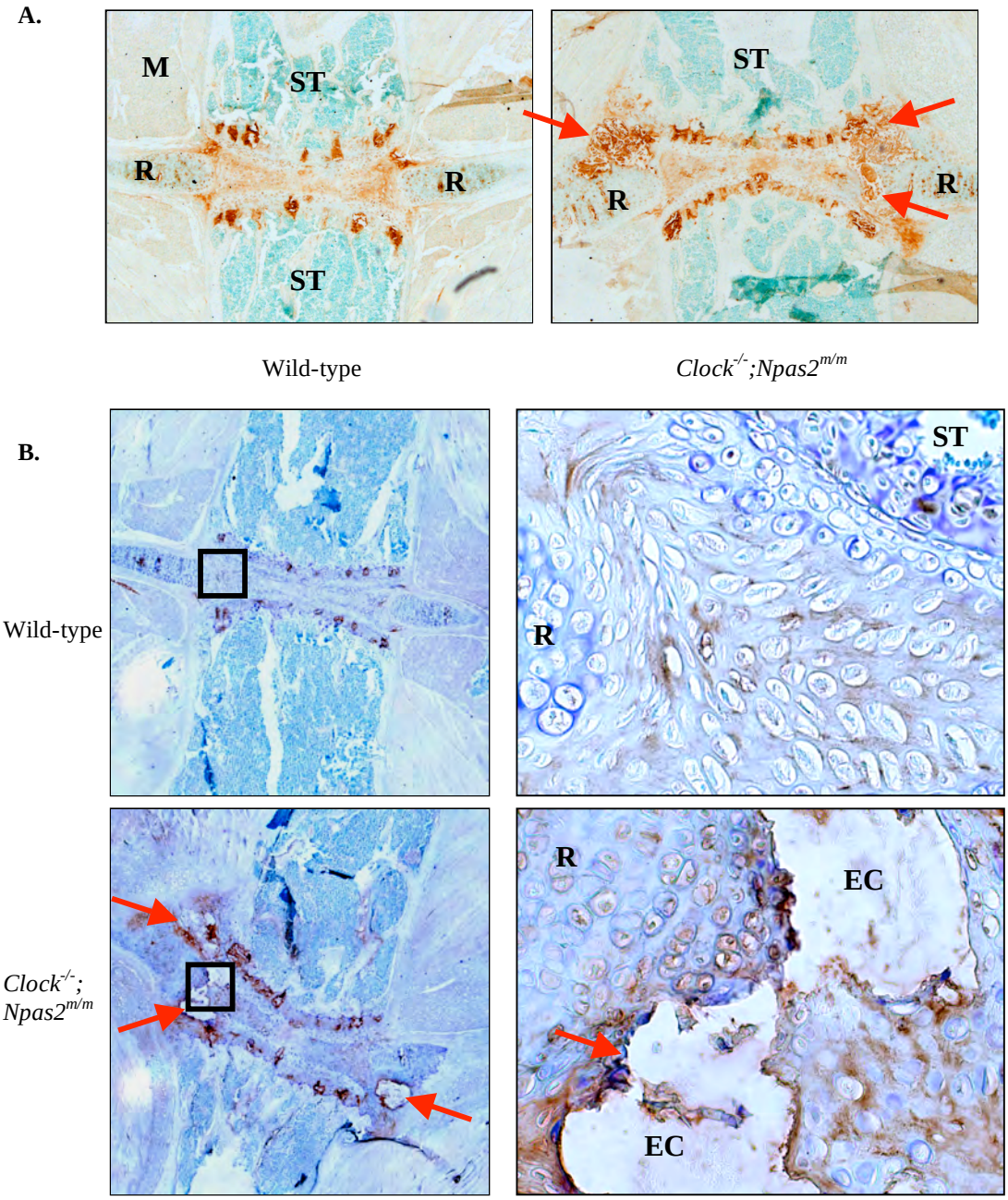

Figure 5.7. Type X collagen IHC of 6-7 week-old *Clock*$^{-/-}$;*Npas2*$^{m/m}$ and wild-type sterna. (A) Wild-type and *Clock*$^{-/-}$;*Npas2*$^{m/m}$ sterna type X collagen IHC (brown) with methyl green counterstain. 5x magnification. (B) Wild-type and *Clock*$^{-/-}$;*Npas2*$^{m/m}$ sterna type X collagen IHC (brown) with toluidine blue (made in distilled water) counterstain. Images on the right are 40X magnifications of the boxed sections indicated on the 5X images on the left. In both type X collagen IHC preparations, costal cartilage, intersternebral cartilage, and growth plate stain for type X collagen. Red arrows highlight ectopic calcification (EC). ST: sternebral trabeculae; R: rib cartilage; M: muscle.

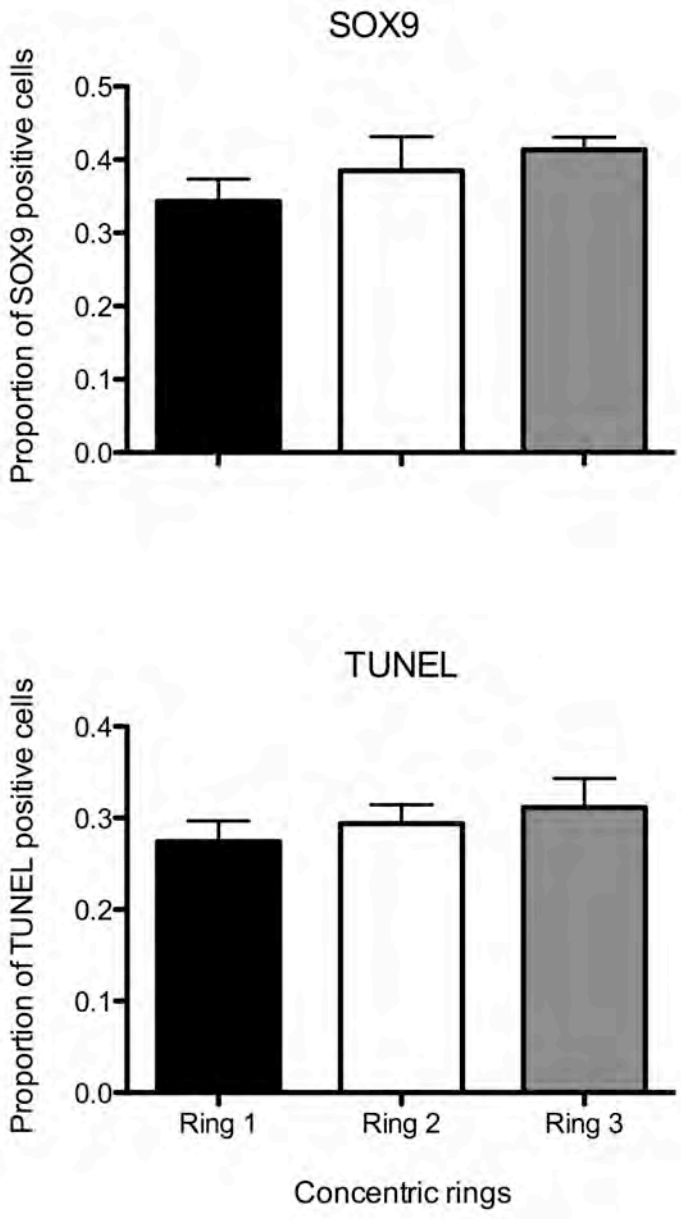

Figure 5.8. Quantitative analysis of SOX9 and TUNEL positive cells around costosternal junction lesions. Quantitative analysis reveals no significant difference in the percentage of positively labeled SOX9 or TUNEL cells distributed around costosternal junction lesions of *Clock*$^{-/-}$;*Npas2*$^{m/m}$ double mutant mice.

Chapter VI

Discussion

Dissertation conclusions

Summary of results

Clock$^{-/-}$*;Npas2*$^{m/m}$ double mutant mice exhibit age-dependent, site-specific ectopic calcification. The two sites with the most prominent arthropathy are the costosternal junction and calcaneal tendon. Costosternal junction ectopic calcifications in a *Bmal1*$^{-/-}$ mouse are composed of CPPD crystals. This arthropathy phenotype is unlikely due to mechanical stress, disruption of centrally regulated circadian rhythms, or metastatic calcification (see Chapter III). *In vitro* micromass culture results suggest that mutant chondrocytes alone do not exhibit irregular differentiation, and RNA analyses of intersternebral tissue suggest that any gene dysregulation associated with arthropathy could be sub-localized to the specific areas that develop calcification. Based on the unaltered distribution of osteoclast and osteoblast markers, these cell types probably do not contribute to the development of ectopic calcification in the costosternal junction, but the presence of chondrocytes suggests that chondrocytes are involved. Chondrocyte-related protein expression in the costosternal junction of *Clock*$^{-/-}$*;Npas2*$^{m/m}$ double mutant mice appears normal. These results together suggest that arthropathy in the costosternal

junction of *Clock*$^{-/-}$;*Npas2*$^{m/m}$ double mutant mice is likely due to dysregulation of genes that have not yet been evaluated, and local factors that could be interacting with systemic factors.

A novel role of the circadian transcriptional activator complex

While the experiments in this dissertation do not identify the mechanism of age-dependent arthropathy in *Clock*$^{-/-}$;*Npas2*$^{m/m}$ double mutant mice, the results nevertheless enable exciting conclusions to be drawn. First, the striking similarity of phenotypes between *Clock*$^{-/-}$;*Npas2*$^{m/m}$ double mutant and *Bmal1*$^{-/-}$ mice strongly suggests that disruption of the transcriptional activator complex (CLOCK/NPAS2:BMAL1) leads to site-specific, age-dependent arthropathy. The absence of such dramatic ectopic calcification in *Per1*$^{-/-}$;*Per2*$^{-/-}$ and *Cry1*$^{-/-}$;*Cry2*$^{-/-}$ double mutant mice further supports this hypothesis, as disrupting the negative repressor complex does not yield the same striking arthropathy [37] (Figure 2.6). However, CLOCK/NPAS2:BMAL1 drive the expression of *Pers* and *Crys*, so presumably *Per* and *Cry* expression is diminished in *Clock*$^{-/-}$;*Npas2*$^{m/m}$ double mutant mice. It is possible that the high bone mass phenotype observed in *Cry1*$^{-/-}$;*Cry2*$^{-/-}$ and *Per1*$^{-/-}$;*Per2*$^{-/-}$ double mutant mice is also present in *Clock*$^{-/-}$;*Npas2*$^{m/m}$ double mutant and *Bmal1*$^{-/-}$ mice. Preliminary attempts to evaluate HBM in distal femur of *Clock*$^{-/-}$;*Npas2*$^{m/m}$ double mutant mice by micro-CT were inconclusive, but future attempts should be made to elucidate any HBM phenotype in *Clock*$^{-/-}$;*Npas2*$^{m/m}$ double mutant mice. The implications of CLOCK/NPAS2:BMAL1 regulating ectopic calcification create a novel role for these core clock transcription factors. It has long been

suggested that core clock genes are involved in non-oscillator functions [119], but data supporting the idea of this particular complex being involved in ectopic calcification is new.

Another reason why this conclusion is so striking is that BMAL1 is capable of forming transcription factor heterodimers with proteins other than CLOCK and NPAS2 [120]. It is this ability to interact with alternate binding partners that probably explains the wide array of phenotypes observed in *Bmal1*$^{-/-}$ mice, which range from premature aging [96] to glucose intolerance [53] to increased sensitivity to chemotherapeutics [59]. BMAL1 can bind to hypoxia inducible factor 1α (HIF-1α) and HIF-2α, which are bHLH-PAS domain-containing transcription factors important for regulating hypoxia responses [120]. Since hypoxia can cause tissue damage that can in turn lead to dystrophic calcification, it seems reasonable to hypothesize that BMAL1's interaction with HIFs could contribute to age-dependent arthropathy. However, the unexpected finding that *Clock*$^{-/-}$*;Npas2*$^{m/m}$ double mutant mice exhibit a very similar arthropathy shows that arthropathy in *Bmal1*$^{-/-}$ mice is due to disruption of the *circadian* transactivator complex, not hypoxia-related ones. CLOCK and NPAS2 are the binding partners of BMAL1 that regulate arthropathy. This conclusion is surprising but strongly suggests that the CLOCK/NPAS2:BMAL1 transactivator complex regulates a pathway involving age-dependent arthropathy.

Another fascinating conclusion is that these results show an overlapping role of *Clock* and *Npas2* in specific peripheral tissues. Previous studies have shown that *Clock* and *Npas2* have overlapping roles in the SCN [39]. Peripheral liver, lung, and fibroblastic tissue from *Clock*$^{-/-}$ mice, when cultured *ex vivo,* are arrhythmic [52], showing that the

presence of *Npas2* in these tissues is insufficient to drive rhythmicity in the absence of imposed rhythmicity from the SCN. A unique feature of ectopic calcification in *Clock*$^{-/-}$*;Npas2*$^{m/m}$ double mutant mice is that it only appears in double mutants, not in single *Clock*$^{-/-}$ or *Npas2*$^{m/m}$ mice. This shows that *Clock* and *Npas2* are capable of compensating for one another's absence to prevent arthropathy. In the SCN, a subset of neurons express *Npas2*, and through network connections are able to maintain rhythmicity in the absence of *Clock* [39, 121, 122]. This sparse distribution of *Npas2*-expressing cells could also be characteristic of peripheral tissues that develop arthropathy. *Npas2* has very low expression in peripheral tissues [37], suggesting that *Npas2*-expressing cells in tissues that can develop arthropathy may form network connections in order to prevent arthropathy in *Clock*$^{-/-}$ mice, or just a few *Npas2*-expressing cells in these tissues is sufficient to prevent arthropathy. Such an overlapping role of *Clock* and *Npas2* has only been otherwise described in the SCN, making peripheral tissues that develop age-dependent arthropathy in *Clock*$^{-/-}$*;Npas2*$^{m/m}$ double mutant mice distinct from other peripheral tissues, such as liver, lung, and fibroblasts. These unique features of peripheral tissues that develop arthropathy add another layer of novelty to this already surprising phenotype.

Local and systemic factors likely regulate calcification in *Clock*$^{-/-}$*;Npas2*$^{m/m}$ double mutant mice

The three most obvious, systemic mechanisms to explain this arthropathy have essentially been ruled out: mechanical stress, centrally-regulated circadian rhythms, and systemic electrolyte imbalance (see Chapter III). This leads to the conclusion that local

factors likely play an important role in the development of ectopic calcification. This conclusion is further supported by the unique site-specificity of arthropathy. Diverse tissues develop ectopic calcification but why certain tissues calcify earlier and more intensely than others is unclear, and is most likely due to local, yet unidentified factors. Differential expression of transcription factors could play a role. If peripheral tissues express varying levels of *Clock, Npas2,* and *Bmal1,* one would expect that tissues that normally express high levels of *Clock, Npas2,* and *Bmal1* would be more severely affected by disruption of those genes than tissues that do not normally express such high levels of *Clock, Npas2,* or *Bmal1*. It would be very interesting to explore expression levels of these three genes in peripheral tissues. If they are most highly expressed in costosternal junction and calcaneal tendon, then that finding would suggest that local, differential expression of these genes in tissues contributes to the site-specificity of arthropathy.

Of the three types of ectopic calcification (metastatic calcification, dystrophic calcification, and heterotopic ossification (HO)), dystrophic calcification is the most likely process behind age-dependent arthropathy in *Clock*$^{-/-}$*;Npas2*$^{m/m}$ double mutant mice. The lack of systemic mineral imbalance in *Clock*$^{-/-}$*;Npas2*$^{m/m}$ double mutant mice rules out metastatic calcification. The presence of osteoblasts would be indicative of ossification, but the lack of alkaline phosphatase staining and characteristic bone morphology in the calcific lesions suggests against HO. Thus, dystrophic calcification remains as a likely mechanism to explain arthropathy in *Clock*$^{-/-}$*;Npas2*$^{m/m}$ double mutant mice. Dystrophic calcification can be caused by trauma, illness, or aging. We have shown

that aging contributes to ectopic calcification in *Clock*$^{-/-}$*;Npas2*$^{m/m}$ double mutant mice. Future studies investigating trauma and illness could explore dystrophic calcification as a mechanism of arthropathy in *Clock*$^{-/-}$*;Npas2*$^{m/m}$ double mutant mice.

To further support the hypothesis of local and systemic factors being involved, the micromass culture experiments show that potential chondrocyte-mediated ectopic calcification is not cell autonomous. The micromass culture results could also be interpreted to mean that chondrocytes are not involved at all, or that the chondrocytes in micromass culture do not represent the type of chondrocytes that cause ectopic calcification. These conclusions mean that other *in vivo* factors most likely interact with chondrocytes to initiate ectopic calcifications, if chondrocytes are the cells mediating arthropathy. Whether these unknown factors are systemic hormones, local signals, or other cell types has yet to be determined. But the micromass culture results show that chondrocytes, in general, are not solely responsible for arthropathy; it is more likely that a combination of systemic and local factors cause ectopic calcification in certain locations. These locations are extremely specific, too. Isolating intersternebral cartilage and analyzing gene expression profiles yielded no significant differences between *Clock*$^{-/-}$*;Npas2*$^{m/m}$ double mutant and wild-type mice, suggesting that any gene dysregulation occurs immediately in the areas that develop calcification and that this dysregulation could be rather subtle. Even IHC is not able to detect noticeable changes in protein expression or cell distribution. Thus, it is likely that a complicated combination of factors, both systemic and very local, interact to initiate ectopic calcification at the costosternal junction of *Clock*$^{-/-}$*;Npas2*$^{m/m}$ double mutant mice.

Additional possible mechanisms

Aging

The finding that *Clock*$^{-/-}$*;Npas2*$^{m/m}$ double mutant mice phenocopy the arthropathy of *Bmal1*$^{-/-}$ mice opens multiple doors of exploration. Many studies have been conducted with *Bmal1*$^{-/-}$ mice studying various aspects of its mutant phenotype, one of which is premature aging. Interestingly, aging can cause dystrophic calcification so it seems likely that premature aging could play a role in age-dependent arthropathy.

Aging is a collection of complex processes coordinated in an organism [123]. It can be defined as the age-related deterioration of physiological functions necessary for survival and fertility of an organism. The exact output measurements to define aging are nebulous, but it is generally accepted that any symptoms characteristic of older populations can be defined as signs of "aging" [123]. These symptoms include, but are not limited to, arteriosclerosis, cancer, dementia, sterility/reduced fertility, ectopic calcification, shortened lifespan, growth retardation, organ atrophy, weight loss, and cataracts [93, 123].

Several studies have linked aging phenotypes with circadian mutant mice. *Bmal1*$^{-/-}$ mice exhibit premature aging characterized by premature death, ectopic calcification, sarcopenia, cataracts, reduced subcutaneous fat stores, organ shrinkage, and altered levels of immune cells in peripheral blood [64, 95, 96]. *Clock*$^{-/-}$ mice have also been shown to exhibit signs of premature aging, such as premature death, cataracts, and skin inflammation [124]. A subset of aging phenotypes have been observed in *Per1*$^{-/-}$*;Per2*$^{-/-}$ double knockout mice

as well: reduced fertility (females) and an increased incidence of spontaneous cancer [67]. Under conditions of irradiation, there is an increased tumor incidence in *Cry1*$^{-/-}$ knockout, *Cry1*$^{-/-}$*;Cry2*$^{-/-}$ double knockout, *Per2*$^{-/-}$ knockout, and *Per1*$^{-/-}$*;Per2*$^{-/-}$ double knockout mice compared to wild-type mice [67]. Clearly, core circadian oscillator genes play a role in aging, although the exact mechanism remains unclear [119, 125, 126].

Our observation that *Clock*$^{-/-}$*;Npas2*$^{m/m}$ double mutant mice exhibit ectopic calcifications similar to that of *Bmal1*$^{-/-}$ mice, and the finding that *Bmal1*$^{-/-}$ mice display signs of premature aging raises the possibility that ectopic calcification in *Clock*$^{-/-}$*;Npas2*$^{m/m}$ double mutant mice could be due to premature aging. In the course of studying *Clock*$^{-/-}$*;Npas2*$^{m/m}$ double mutant mice, it was observed that they also suffer from weight loss, premature death, organ shrinkage, and sterility, all of which are consistent with premature aging (our unpublished data). It would be interesting to investigate whether or not the phenotype observed in *Clock*$^{-/-}$*;Npas2*$^{m/m}$ double mutant mice is due to accelerated aging. Possible future experiments could include thoroughly characterizing the aging phenotype in *Clock*$^{-/-}$*;Npas2*$^{m/m}$ double mutant mice, namely assessing skin and organ atrophy, cataracts, and arteriosclerosis. Evaluating beneficial effects of treating *Clock*$^{-/-}$*;Npas2*$^{m/m}$ double mutant mice with anti-aging therapies, such as caloric restriction [127] could also be done. Antioxidant administration was shown to increase lifespan and decrease weight loss and cataract development, but had no effect on arthropathy in *Bmal1*$^{-/-}$ mice [128], so it is possible that anti-aging therapies will not affect arthropathy.

Osteoclasts

Another possible mechanism of age-dependent arthropathy in *Clock*$^{-/-}$*;Npas2*$^{m/m}$ double mutant mice is osteoclast dysfunction. In the TRAP stain performed, osteoclasts are localized to the sternebral trabecular bone, where they should be located. No TRAP staining is evident around the calcific lesions, suggesting that osteoclasts are not involved because they are not around.

To argue against this conclusion, perhaps the lack of ectopic calcification clearance in *Clock*$^{-/-}$*;Npas2*$^{m/m}$ double mutant mice is due to a defect in macrophage recruitment. Osteoclasts originate from mononuclear, hematopoietic stem cells from which macrophages also differentiate [5]. Circadian oscillators are present in spleen, lymph nodes, and peritoneal macrophages and generate rhythmic secretions of TNFα and IL-6 [129]. Osteoclasts, a type of multi-nucleated macrophage, are not present around calcific lesions. This may be due to a defect in inflammatory immune response, as we do not see other inflammatory cells around the lesions either. Further supporting this idea is the fact that *Bmal1*$^{-/-}$ mice exhibit altered levels of immune cells in peripheral blood [95]. Specifically, 4-5 month-old *Bmal1*$^{-/-}$ mice have significantly lower levels of monocytes (a type of macrophage), lymphocytes, and white blood cells.

In order to test the hypothesis of osteoclast or inflammatory response dysfunction, one could induce an inflammatory response in wild-type and *Clock*$^{-/-}$*;Npas2*$^{m/m}$ double mutant mice and measure changes in inflammatory markers, such as IL-6 and TNFα. If *Clock*$^{-/-}$*;Npas2*$^{m/m}$ double mutant mice are unable to properly respond to the immune challenge, then it is possible that an abnormal immune response could play a role in the

development of arthropathy in these double mutant mice. Alternatively, wild-type mice could be irradiated to see if destroying their immune system is sufficient to induce ectopic calcification. Bone marrow transplants from *Clock*$^{-/-}$;*Npas2*$^{m/m}$ double mutant to wild-type mice could also be performed to assess the effect of the mutant immune system on arthropathy.

FGF23, PHEX, and Klotho

X-linked hypophosphatemia (XLH) is a disease in which people suffer from osteomalacia and rickets. A mouse model, the Hyp mouse, has been developed to study this disease. Hyp mice and XLH patients carry an inactivating mutation in phosphate-regulating gene with homology to endopeptidases on the X chromosome (PHEX) [130]. When PHEX is inactivated, it leads to elevated levels of fibroblast growth factor 23 (FGF23) that causes hypophosphatemia and impaired bone mineralization [131]. Despite having hypophosphatemia, Hyp mice and XLH patients exhibit paradoxical ectopic calcification of tendon and ligament insertion sites. Klotho, a molecule whose disruption leads to an accelerated aging phenotype in mice, facilitates FGF23 binding to its receptor [132]. *FGF23*$^{-/-}$ mice phenocopy *Klotho* mutant mice (*kl/kl*); both mutants exhibit accelerated aging characterized by ectopic soft tissue calcification, hyperphosphatemia, decreased lifespan, osteopenia, emphysema, and arteriosclerosis [93, 98, 133]. The aging phenotype is due to hyperactivity of vitamin D, which FGF23 normally inhibits [134].

The effect of disrupting FGF23 activity is systemic, as serum phosphate level changes are detected in patients and mice with the PHEX mutation, and *kl/kl* mutant and

FGF23$^{-/-}$ mice. However, serology profiles of *Clock*$^{-/-}$*;Npas2*$^{m/m}$ double mutant mice do not show any significant changes in phosphate levels. This suggests that systemic changes in FGF23, PHEX, and Klotho activity are not involved in age-dependent arthropathy. It is possible that local, site-specific changes in FGF23 function contribute to arthropathy in *Clock*$^{-/-}$*;Npas2*$^{m/m}$ double mutant mice, though, particularly in the calcaneal tendon, which is ectopically calcified in Hyp mice and XLH patients [135]. A possible future experiment could be localizing FGF23 receptors in tissues that develop arthropathy in *Clock*$^{-/-}$*;Npas2*$^{m/m}$ double mutant mice. If FGF23 receptors are exclusively disrupted in tissues that develop ectopic calcification, then it would functionally inhibit FGF23 function in a site-specific manner and possibly cause ectopic calcification. FGFR3, an FGF23 receptor, is located in the calcaneal tendon of Hyp mice, which develop ectopic calcification of the calcaneal tendon entheses [135]. It would be interesting to investigate the expression levels of FGF23 receptors in *Clock*$^{-/-}$*;Npas2*$^{m/m}$ double mutant mouse tissues to see if receptors are down regulated in tissues with the most prominent arthropathy.

Future experiments

Based on the results presented in this dissertation, there are many avenues that could be pursued to further investigate age-dependent arthropathy in *Clock*$^{-/-}$*;Npas2*$^{m/m}$ double mutant mice. A few of these possibilities are discussed here.

Chromatin-immunoprecipitation (ChIP)

The overall hypothesis presented in this dissertation is that CLOCK or NPAS2, and BMAL1 form a transcription factor activator complex that drives the expression of a gene that prevents age-dependent arthropathy. The attempts to identify genes dysregulated in *Clock*$^{-/-}$*;Npas2*$^{m/m}$ double mutant mice were specific and focused, but did not yield any promising leads. One way to identify direct targets of CLOCK/NPAS2:BMAL1-mediated transcription is to perform chromatin-immunoprecipitation (ChIP) studies. These studies would not necessarily identify the gene(s) directly involved in calcification, as the calcification pathway could be further downstream, but ChIP could narrow down the list of potential, direct target genes. Such was the rationale behind evaluating *Prrx1* and *Sox7* expression levels, which were identified in a liver *Bmal1* ChIP screen [112]. Isolating tissues that undergo arthropathy and performing ChIP on them may identify direct targets that can be linked to calcification pathways.

Needle-biopsy tissue collection & RNA analysis

The *in vivo* tissue collection technique employed clearly was not localized enough to detect gene dysregulation. In order to better isolate the tissue that could exhibit changes in gene expression, more refined techniques will be needed. Unfortunately, attempts to use laser-capture microscopy to isolate individual cells in costosternal junction tissue were unsuccessful. Another idea is to section tissue and use a blunted needle tip to punch out areas of interest under a dissecting microscope, rather than using a

scalpel to dissect out the entire intersternebral region. Then microarray analysis could be performed, which would survey many genes at once, rather than performing single RT-PCR experiments for individual genes. This tissue isolation technique could be applied to any of the tissue areas that develop arthropathy, not just costosternal junction and calcaneal tendon. Studies investigating arthropathy in other joints affected in *Clock*$^{-/-}$*;Npas2*$^{m/m}$ double mutant mice should be pursued in parallel to determine if separate processes are occurring in different locations.

Osteoblast & chondrocyte cultures (MC3T3 & ATDC5)

Micromass culture of *Clock*$^{-/-}$*;Npas2*$^{m/m}$ double mutant MEFs did not generate an *in vitro* system in which to study arthropathy in *Clock*$^{-/-}$*;Npas2*$^{m/m}$ double mutant mice. However, other *in vitro* systems could be explored, as an *in vitro* system in which to manipulate gene expression would be invaluable to studying this phenotype.

Two cell lines are commonly used to study calcification: MC3T3-E1 and ATDC5. MC3T3-E1 is a clonal osteogenic cell line established from newborn mouse calvaria with high ALP activity that can differentiate into osteoblasts and mineralize *in vitro* [136]. ATDC5 is a clonal cell line derived from a mouse teratocarcinoma stem cell line that, when treated with insulin, undergoes chondrogenesis [137]. It would be very interesting to see if MC3T3-E1 or ATDC5 cells have increased mineralization phenotypes when *Clock* and *Npas2*, or *Bmal1* are knocked down with RNAi. If there is a phenotype *in vitro*, then these cell lines could be used as a model in which to evaluate and manipulate genes involved in arthropathy caused by *Clock* and *Npas2* disruption.

Immunohistochemistry (IHC) and in-situ hybridization (ISH)

The site-specificity of arthropathy suggests that changes in gene or protein expression *in vivo* are best assessed by in-situ hybridization (ISH) or immunohistochemistry (IHC), respectively, as these methods preserve anatomical detail. Our IHC results did not show obvious changes in expression of markers of different cell populations in *Clock*$^{-/-}$*;Npas2*$^{m/m}$ double mutant mice (see Chapter V), but that could be due to the inherent limitations of the technique. ISH can be quantitative and differences in gene expression patterns can be measured as well as visualized anatomically in the tissue. This type of powerful analysis would nicely complement array screens of tissue gene expression.

Specific IHC experiments of interest are localizing CLOCK and NPAS2 expression. Preliminary attempts of CLOCK IHC were unsuccessful (data not shown) so further optimization using this particular CLOCK primary antibody for paraffin-embedded tissue IHC is necessary. The mutant *Npas2* allele contains a LacZ insertion [92] and so assessing β-galactosidase activity is a way to localize mutant *Npas2* expression. Unfortunately, preliminary attempts to detect β-galactosidase activity in *Clock*$^{-/-}$*;Npas2*$^{m/m}$ double mutant costosternal junction and calcaneal tendon tissue were unsuccessful. The expression of β-galactosidase is too low in these tissues, as β-galactosidase activity was detected in brain sections from the same animals processed in parallel. These results suggest that NPAS2 levels are simply too low to measure directly

using IHC. In fact, currently there is not a reliable NPAS2 primary antibody available for IHC on mouse tissues.

An alternative method to identify cells that express *Clock* and *Npas2* is to perform BMAL1 IHC. CLOCK or NPAS2 binds to and stabilizes BMAL1, such that in *Clock*$^{-/-}$ tissue, only cells that contain NPAS2 stain positively for BMAL1 [51]. In the SCN, only a subset of neurons express *Npas2*, and that elite subset is responsible for maintaining behavioral rhythmicity, even in the absence of *Clock*, through SCN network connections [39, 122]. By staining for BMAL1 in *Clock*$^{-/-}$ costosternal juntion or calcaneal tendon tissue, we can identify cells that express *Npas2*, which possibly are a restricted subset of cells that prevent age-dependent arthropathy. Single *Clock*$^{-/-}$ and *Npas2*$^{m/m}$ mice do not develop arthropathy, so the identification of cells that express both *Clock* and *Npas2* is of particular interest.

Calcaneal tendon experiments

Aside from the initial characterization of arthropathy in *Clock*$^{-/-}$*;Npas2*$^{m/m}$ double mutant mice, calcification of the calcaneal tendon has not yet been extensively studied in this mouse model. Future experiments focusing on this tissue are of interest, as pathological calcification of the human calcaneal tendon is a significant health problem [8].

Tendons and ligaments consist of dense connective tissue with a high fibrillar collagen content and minimal vascularization [138]. They contain relatively few fibroblasts and tenocytes but an abundant extracellular matrix. At bone insertion sites, collagen

fibers intertwine with fibrocartilage. This fibrocartilage gradually becomes more mineralized as it inserts into the bone [138].

Primary tendon stem/progenitor cells (TSPCs) can be cultured *ex vivo* and have the ability to undergo osteogenesis, adipogenesis, or chondrogenesis [90]. A potential future experiment could be culturing TSPCs from *Clock*$^{-/-}$*;Npas2*$^{m/m}$ double mutant calcaneal tendon, stimulating chondrogenesis or osteogenesis, and assessing their phenotype. Establishing a cell culture system in which to study tendon differentiation would enable us to knock down and rescue gene expression to test candidate gene effects. If TSPCs contribute to calcaneal tendon calcification in *Clock*$^{-/-}$*;Npas2*$^{m/m}$ double mutant mice, then one could expect to see abnormal chondrogenic or osteogenic differentiation in cell culture.

Safranin-O staining of calcaneal tendon confirms the presence of fibrocartilage at the tendon insertion site to bone (Figure 2.9). However, calcification develops above the insertion site, suggesting that chondrocytes may not be involved in calcaneal tendon calcification. Thus, the pathology of calcification in the calcaneal tendon appears distinct from the hypothesized mechanism in costosternal junction. Investigation of tendon-specific genes is necessary. Tenomodulin and thrombospondin-4 are tendon-specific markers [139]. Tenomodulin is a late marker of tendon differentiation and may play a role in tenocyte proliferation [140] while thrombospondin-4's exact function is unclear, but it may be involved in coupling muscle and tendon formation [141]. We could collect tendon tissues, extract RNA, and perform microarrays to screen for candidate tendon-specific genes dysregulated in *Clock*$^{-/-}$*;Npas2*$^{m/m}$ double mutant tendon. Evaluating the expression

patterns of these types of genes could shed light on the mechanism of age-dependent calcification of the calcaneal tendon in *Clock*$^{-/-}$;*Npas2*$^{m/m}$ double mutant mice.

Health implications

CPPD crystal deposition disease

The identification of CPPD crystals in costosternal junction of a *Bmal1*$^{-/-}$ mouse potentially links this circadian mutant mouse model to human clinical pathology. Calcium pyrophosphate dihydrate crystal deposition disease (CPPD-CDD) is a broad term used to describe abnormal CPPD crystal deposition in articular joints. It occurs most commonly in the elderly, with 10-15% of people 65-75 years old and 30-50% of people 85 years and older suffering from it [23]. While in most cases the process is asymptomatic, in other cases CPPD-CPP can induce or enhance osteoarthritis (OA), cause severe joint destruction, and calcification of spinal tissues can restrict mobility similar to anklyosing spondylitis. The knee is most frequently affected in CPPD-CDD, but CPPD deposition is polyarticular and other sites, such as the wrist, shoulder, ankle, elbow, and hands, are commonly affected as well. CPPD crystal deposition in synovial joint space stimulates phagocytosis of these crystals by monocyte-macrophages and neutrophils [23]. Interestingly, *Bmal1*$^{-/-}$ mice have a significant increase in segmented neutrophils in peripheral blood [95], indicating an inflammatory response. However, the overall changes in the immune system of *Bmal1*$^{-/-}$ mice are relatively mild so it is unclear if the immune response in *Bmal1*$^{-/-}$ mice contributes to arthropathy.

Pseudogout, pyrophosphate arthropathy, and chondrocalcinosis (CC) all fall under CPPD-CDD [142]. Pseudogout is characterized by acute synovitis associated with intraarticular CPPD deposition [23, 142]. It differs from gout in that gout is due to hyperuremia and monosodium urate crystal deposition in synovial joint space [23]. Pyrophosphate arthropathy refers to structurally abnormal cartilage or bone due to articular CPPD deposition, and CC describes any radiographic calcification of articular fibrocartilage or hyaline cartilage [142]. CC could also refer to other types of crystal deposition in joints, not just CPPD.

There are not many effective treatment options for CPPD-CDD. The most common treatments include joint aspiration (to remove the crystals), non-steroidal anti-inflammatory drugs (NSAIDs), or intraarticular glucocorticoid injection to reduce inflammation [23]. Unfortunately, there is no effective way to remove CPPD deposits and in some cases joint replacement is the only solution [23]. The identification of CPPD crystal deposition in the costosternal junction of a *Bmal1*$^{-/-}$ mouse raises the possibility of this circadian mutant mouse model becoming a model in which to study CPPD-CDD, specifically CPPD-CC, for which there is no murine model [143]. There are mutant mice used to study extracellular PP_i levels, which in excess can precipitate CPPD crystal deposition, but none of these models develop ectopic CPPD calcification visible on X-ray, which defines CPPD-CC. Experimenting with different treatments in *Clock*$^{-/-}$*;Npas2*$^{m/m}$ double mutant mice could prove to be a fruitful exploration if it yields therapies applicable to people suffering from CPPD-CDD.

Even though they are not animal models for CPPD-CDD, mutant mice have nonetheless shed light on the regulation of extracellular PP_i. The three genes that regulate PP_i levels are tissue non-specific alkaline phosphatase (*Akp2* that encodes TNAP), ankylosis protein (*Ank* that encodes ANK), and ectonucleotide pyrophosphatase 1 (*Enpp1* that encodes NPP1). *Akp2*$^{-/-}$ mice have high extracellular PP_i levels and hypophosphatasia [79]. *Ank*$^{-/-}$ mice have decreased extracellular PP_i levels and ectopic HA deposition [28]. *Enpp1*$^{-/-}$ mice have ossification of the posterior longitudinal ligament (OPLL) due to low extracellular PP_i levels and HA deposition. Given the phenotypes in mice lacking each of these genes and the identification of CPPD crystal deposits in a *Bmal1*$^{-/-}$ mouse, it seems likely that *Clock*$^{-/-}$*;Npas2*$^{m/m}$ double mutant mice could have dysfunctional TNAP, ANK, or NPP1. Initial studies described in this dissertation were unable to detect changes in alkaline phosphatase activity, or *Ank* or *Enpp1* expression. Closer, more localized inspection of these genes and proteins in calcification sites is necessary to determine if they are involved in age-dependent arthropathy of *Clock*$^{-/-}$*;Npas2*$^{m/m}$ double mutant mice. If these genes are involved, it could identify a novel pathway in which circadian genes contribute to the regulation of extracellular PP_i levels.

DISH, OPLL, and AS

Diffuse idiopathic skeletal hyperostosis (DISH) is a disorder of robust ectopic calcification of the midthoracic spine, specifically of the anterior longitudinal ligament [144]. It is not common in the general population, but is generally seen in the middle-aged and elderly. Pain is usually minimal or absent in DISH, although in some cases

calcification can limit mobility. An important feature of DISH is that the intervertebral disc spaces are preserved, unlike in degenerative spondylitis. DISH can occur in locations other than the spine, such as ligamentous and tendinous insertion sites, particularly the pelvis and calcaneus [144].

Ossification of the posterior longitudinal ligament (OPLL) of the spine causes spinal canal stenosis and myelopathy. OPLL is particularly relevant in the elderly Asian population. It is due to ectopic endochondral ossification of the posterior longitudinal ligament of the cervical spine [145]. The *Enpp1*$^{-/-}$ mouse is the animal model for OPLL, highlighting the importance of extracellular PP_i regulation in ectopic calcification.

Anylosing spondylitis (AS) is an inflammatory disorder of unknown cause that primarily affects the axial skeleton, although peripheral joints, such as sacroiliac joints and costovertebral junctions, are also frequently involved [146]. A classic radiological finding of AS is “bamboo spine”, which is the complete fusion of vertebrae, typically from the lumbar region upwards [145]. The *ank* mutant is an animal model for AS, but despite the similarity of the mutant mouse phenotype remains controversial due to the lack of an association of ANKH mutations with clinical AS [143].

DISH, OPLL, and AS are all age-related, calcific rheumatic diseases that can associate with one another. The fact that *Clock*$^{-/-}$*;Npas2*$^{m/m}$ double mutant mice exhibit profound calcification of their cervical, thoracic, and sacral vertebrae suggest that their pathology may be related to DISH, OPLL, and/or AS. DISH patients can develop calcaneal tendon calcification, similar to *Clock*$^{-/-}$*;Npas2*$^{m/m}$ double mutant mice. Micro-CT images indicate *Clock*$^{-/-}$*;Npas2*$^{m/m}$ double mutant intervertebral spaces appear to

remain intact despite robust costovertebral calcification. Initial attempts to evaluate changes in *Enpp1* and *Ank* expression in sterna of *Clock*$^{-/-}$;*Npas2*$^{m/m}$ double mutant mice did not reveal genotype-specific differences, but it is possible that different processes are occurring in the different tissues affected in *Clock*$^{-/-}$;*Npas2*$^{m/m}$ double mutant mice and that *Enpp1* and/or *Ank* could be dysregulated in the spine. Closer inspection of spinal calcification in *Clock*$^{-/-}$;*Npas2*$^{m/m}$ double mutant mice could link this circadian mutant mouse model to these human pathologies and provide valuable insights to their pathology.

Concluding remarks

Clock$^{-/-}$;*Npas2*$^{m/m}$ double mutant mice exhibit a unique, age-dependent, site-specific arthropathy that, to date, is only shared phenotypically by *Bmal1*$^{-/-}$ mice. Whether this arthropathy is a reflection of premature aging, CPPD-CDD, chondrocyte maturation dysfunction, or processes relevant to human clinical pathology remains to be seen. Future studies are required to elucidate the mechanism of arthropathy in this circadian mutant mouse model. This line of investigation could have profound clinical relevance, as understanding this novel mechanism of regulation of calcification by "circadian genes" may reveal more approaches for treatment of pathological conditions in humans.

REFERENCES

1. Steitz, S. A. *et al*. Osteopontin inhibits mineral deposition and promotes regression of ectopic calcification. *Am. J. Pathol.* **161**, 2035-2046 (2002).

2. Tuohimaa, P. Vitamin D and aging. *J. Steroid Biochem. Mol. Biol.* **114**, 78-84 (2009).

3. de Crombrugghe, B., Lefebvre, V. & Nakashima, K. Regulatory mechanisms in the pathways of cartilage and bone formation. *Curr. Opin. Cell Biol.* **13**, 721-727 (2001).

4. Karsenty, G. Transcriptional control of skeletogenesis. *Annu. Rev. Genomics Hum. Genet.* **9**, 183-196 (2008).

5. Soltanoff, C. S., Yang, S., Chen, W. & Li, Y. P. Signaling networks that control the lineage commitment and differentiation of bone cells. *Crit. Rev. Eukaryot. Gene Expr.* **19**, 1-46 (2009).

6. Pape, H. C., Marsh, S., Morley, J. R., Krettek, C. & Giannoudis, P. V. Current concepts in the development of heterotopic ossification. *J. Bone Joint Surg. Br.* **86**, 783-787 (2004).

7. Shehab, D., Elgazzar, A. H. & Collier, B. D. Heterotopic ossification. *J. Nucl. Med.* **43**, 346-353 (2002).

8. Richards, P. J., Braid, J. C., Carmont, M. R. & Maffulli, N. Achilles tendon ossification: pathology, imaging and aetiology. *Disabil. Rehabil.* **30**, 1651-1665 (2008).

9. Wallis, G. A. Bone growth: coordinating chondrocyte differentiation. *Curr. Biol.* **6**, 1577-1580 (1996).

10. Goldring, M. B., Tsuchimochi, K. & Ijiri, K. The control of chondrogenesis. *J. Cell. Biochem.* **97**, 33-44 (2006).

11. Aigner, T. & Gerwin, N. Growth plate cartilage as developmental model in osteoarthritis research--potentials and limitations. *Curr. Drug Targets* **8**, 377-385 (2007).

12. Bi, W., Deng, J. M., Zhang, Z., Behringer, R. R. & de Crombrugghe, B. Sox9 is required for cartilage formation. *Nat. Genet.* **22**, 85-89 (1999).

13. Bi, W. *et al.* Haploinsufficiency of Sox9 results in defective cartilage primordia and premature skeletal mineralization. *Proc. Natl. Acad. Sci. U. S. A.* **98**, 6698-6703 (2001).

14. Galotto, M. *et al.* Hypertrophic chondrocytes undergo further differentiation to osteoblast-like cells and participate in the initial bone formation in developing chick embryo. *J. Bone Miner. Res.* **9**, 1239-1249 (1994).

15. Bringhurst, F. R., Demay, M. B., Krane, S. M. & Kronenberg, H. M. in *Harrison's Principles of Internal Medicine* (eds Fauci, A. S. et al.), 2008).

16. Kouri, J. B., Aguilera, J. M., Reyes, J., Lozoya, K. A. & Gonzalez, S. Apoptotic chondrocytes from osteoarthrotic human articular cartilage and abnormal calcification of subchondral bone. *J. Rheumatol.* **27**, 1005-1019 (2000).

17. Kirsch, T. Determinants of pathologic mineralization. *Crit. Rev. Eukaryot. Gene Expr.* **18**, 1-9 (2008).

18. Hashimoto, S. *et al.* Chondrocyte-derived apoptotic bodies and calcification of articular cartilage. *Proc. Natl. Acad. Sci. U. S. A.* **95**, 3094-3099 (1998).

19. Adams, C. S. & Horton, W. E.,Jr. Chondrocyte apoptosis increases with age in the articular cartilage of adult animals. *Anat. Rec.* **250**, 418-425 (1998).

20. Mescher, A. L. in *Junqueira's Basic Histology: Text & Atlas* (The McGraw-Hill Companies, Inc., 2010).

21. Fuerst, M. *et al.* Investigation of calcium crystals in OA knees. *Rheumatol. Int.* **30**, 623-631 (2010).

22. Fuerst, M. *et al.* Calcification of articular cartilage in human osteoarthritis. *Arthritis Rheum.* **60**, 2694-2703 (2009).

23. Schumacher, H. R. & Chen, L. X. in *Harrison's Principles of Internal Medicine* (eds Fauci, A. S. & Longo, D. L.) (The McGraw-Hill Companies, Inc., 2008).

24. Orimo, H. The mechanism of mineralization and the role of alkaline phosphatase in health and disease. *J. Nippon Med. Sch.* **77**, 4-12 (2010).

25. Terkeltaub, R. A. Inorganic pyrophosphate generation and disposition in pathophysiology. *Am. J. Physiol. Cell. Physiol.* **281**, C1-C11 (2001).

26. Harmey, D. *et al.* Concerted regulation of inorganic pyrophosphate and osteopontin by akp2, enpp1, and ank: an integrated model of the pathogenesis of mineralization disorders. *Am. J. Pathol.* **164**, 1199-1209 (2004).

27. Hessle, L. *et al.* Tissue-nonspecific alkaline phosphatase and plasma cell membrane glycoprotein-1 are central antagonistic regulators of bone mineralization. *Proc. Natl. Acad. Sci. U. S. A.* **99**, 9445-9449 (2002).

28. Ho, A. M., Johnson, M. D. & Kingsley, D. M. Role of the mouse ank gene in control of tissue calcification and arthritis. *Science* **289**, 265-270 (2000).

29. Gurley, K. A., Reimer, R. J. & Kingsley, D. M. Biochemical and genetic analysis of ANK in arthritis and bone disease. *Am. J. Hum. Genet.* **79**, 1017-1029 (2006).

30. Zaka, R. & Williams, C. J. Role of the progressive ankylosis gene in cartilage mineralization. *Curr. Opin. Rheumatol.* **18**, 181-186 (2006).

31. Hastings, M., O'Neill, J. S. & Maywood, E. S. Circadian clocks: regulators of endocrine and metabolic rhythms. *J. Endocrinol.* **195**, 187-198 (2007).

32. Waterhouse, J. M. & Decoursey, P. J. in *Chronobiology: Biological Timekeeping* (eds Dunlap, J. C., Loros, J. J. & DeCoursey, P. J.) 321-356 (Sinauer Associates, Inc., Sunderland, Massachusetts, U.S.A., 2004).

33. Reppert, S. M. & Weaver, D. R. Coordination of circadian timing in mammals. *Nature* **418**, 935-941 (2002).

34. Balsalobre, A., Damiola, F. & Schibler, U. A serum shock induces circadian gene expression in mammalian tissue culture cells. *Cell* **93**, 929-937 (1998).

35. Welsh, D. K., Yoo, S. H., Liu, A. C., Takahashi, J. S. & Kay, S. A. Bioluminescence imaging of individual fibroblasts reveals persistent, independently phased circadian rhythms of clock gene expression. *Curr. Biol.* **14**, 2289-2295 (2004).

36. Welsh, D. K., Logothetis, D. E., Meister, M. & Reppert, S. M. Individual neurons dissociated from rat suprachiasmatic nucleus express independently phased circadian firing rhythms. *Neuron* **14**, 697-706 (1995).

37. Fu, L., Patel, M. S., Bradley, A., Wagner, E. F. & Karsenty, G. The molecular clock mediates leptin-regulated bone formation. *Cell* **122**, 803-815 (2005).

38. Gekakis, N. *et al*. Role of the CLOCK protein in the mammalian circadian mechanism. *Science* **280**, 1564-1569 (1998).

39. DeBruyne, J. P., Weaver, D. R. & Reppert, S. M. CLOCK and NPAS2 have overlapping roles in the suprachiasmatic circadian clock. *Nat. Neurosci.* **10**, 543-545 (2007).

40. Shearman, L. P. *et al.* Interacting molecular loops in the mammalian circadian clock. *Science* **288**, 1013-1019 (2000).

41. Preitner, N. *et al.* The orphan nuclear receptor REV-ERBalpha controls circadian transcription within the positive limb of the mammalian circadian oscillator. *Cell* **110**, 251-260 (2002).

42. Sato, T. K. *et al.* A functional genomics strategy reveals Rora as a component of the mammalian circadian clock. *Neuron* **43**, 527-537 (2004).

43. Ripperger, J. A. & Schibler, U. Rhythmic CLOCK-BMAL1 binding to multiple E-box motifs drives circadian Dbp transcription and chromatin transitions. *Nat. Genet.* **38**, 369-374 (2006).

44. Lavery, D. J. *et al.* Circadian expression of the steroid 15 alpha-hydroxylase (Cyp2a4) and coumarin 7-hydroxylase (Cyp2a5) genes in mouse liver is regulated by the PAR leucine zipper transcription factor DBP. *Mol. Cell. Biol.* **19**, 6488-6499 (1999).

45. Bunger, M. K. *et al.* Mop3 is an essential component of the master circadian pacemaker in mammals. *Cell* **103**, 1009-1017 (2000).

46. Vitaterna, M. H. *et al.* Mutagenesis and mapping of a mouse gene, Clock, essential for circadian behavior. *Science* **264**, 719-725 (1994).

47. van der Horst, G. T. *et al.* Mammalian Cry1 and Cry2 are essential for maintenance of circadian rhythms. *Nature* **398**, 627-630 (1999).

48. Zheng, B. *et al.* Nonredundant roles of the mPer1 and mPer2 genes in the mammalian circadian clock. *Cell* **105**, 683-694 (2001).

49. Bae, K. *et al*. Differential functions of mPer1, mPer2, and mPer3 in the SCN circadian clock. *Neuron* **30**, 525-536 (2001).

50. King, D. P. *et al*. The mouse Clock mutation behaves as an antimorph and maps within the W19H deletion, distal of Kit. *Genetics* **146**, 1049-1060 (1997).

51. Debruyne, J. P. *et al.* A clock shock: mouse CLOCK is not required for circadian oscillator function. *Neuron* **50**, 465-477 (2006).

52. DeBruyne, J. P., Weaver, D. R. & Reppert, S. M. Peripheral circadian oscillators require CLOCK. *Curr. Biol.* **17**, R538-9 (2007).

53. Marcheva, B. *et al.* Disruption of the clock components CLOCK and BMAL1 leads to hypoinsulinaemia and diabetes. *Nature* **466**, 627-631 (2010).

54. Sadacca, L. A., Lamia, K. A., deLemos, A. S., Blum, B. & Weitz, C. J. An intrinsic circadian clock of the pancreas is required for normal insulin release and glucose homeostasis in mice. *Diabetologia* **54**, 120-124 (2011).

55. Storch, K. F. *et al*. Intrinsic circadian clock of the mammalian retina: importance for retinal processing of visual information. *Cell* **130**, 730-741 (2007).

56. Lamia, K. A., Storch, K. F. & Weitz, C. J. Physiological significance of a peripheral tissue circadian clock. *Proc. Natl. Acad. Sci. U. S. A.* **105**, 15172-15177 (2008).

57. Sato, Y., Seo, N. & Kobahashi, E. The dosing-time dependent effects of intravenous hypnotics in mice. *Anesth. Analg.* **101**, 1706-1708 (2005).

58. Gachon, F., Olela, F. F., Schaad, O., Descombes, P. & Schibler, U. The circadian PAR-domain basic leucine zipper transcription factors DBP, TEF, and HLF modulate basal and inducible xenobiotic detoxification. *Cell. Metab.* **4**, 25-36 (2006).

59. Gorbacheva, V. Y. *et al*. Circadian sensitivity to the chemotherapeutic agent cyclophosphamide depends on the functional status of the CLOCK/BMAL1 transactivation complex. *Proc. Natl. Acad. Sci. U. S. A.* **102**, 3407-3412 (2005).

60. Dallmann, R., DeBruyne, J. P. & Weaver, D. R. *Functional Activity of the Liver Circadian Clock Revealed by Assessing Pentobarbital Sleep Time* (Society for Research on Biological Rhythms, 2008).

61. Hinoi, E. *et al.* Up-regulation of per mRNA expression by parathyroid hormone through a protein kinase A-CREB-dependent mechanism in chondrocytes. *J. Biol. Chem.* **281**, 23632-23642 (2006).

62. Zvonic, S. *et al.* Circadian oscillation of gene expression in murine calvarial bone. *J. Bone Miner. Res.* **22**, 357-365 (2007).

63. Zheng, L., Papagerakis, S., Schnell, S. D., Hoogerwerf, W. A. & Papagerakis, P. Expression of clock proteins in developing tooth. *Gene Expr. Patterns* **11**, 202-206 (2011).

64. Bunger, M. K. *et al*. Progressive arthropathy in mice with a targeted disruption of the Mop3/Bmal-1 locus. *Genesis* **41**, 122-132 (2005).

65. Andrews, J. L. *et al.* CLOCK and BMAL1 regulate MyoD and are necessary for maintenance of skeletal muscle phenotype and function. *Proc. Natl. Acad. Sci. U. S. A.* **107**, 19090-19095 (2010).

66. Maronde, E. *et al*. The clock genes Period 2 and Cryptochrome 2 differentially balance bone formation. *PLoS One* **5**, e11527 (2010).

67. Lee, S., Donehower, L. A., Herron, A. J., Moore, D. D. & Fu, L. Disrupting circadian homeostasis of sympathetic signaling promotes tumor development in mice. *PLoS One* **5**, e10995 (2010).

68. McDearmon, E. L. *et al*. Dissecting the functions of the mammalian clock protein BMAL1 by tissue-specific rescue in mice. *Science* **314**, 1304-1308 (2006).

69. Okawa, A. *et al*. Mutation in Npps in a mouse model of ossification of the posterior longitudinal ligament of the spine. *Nat. Genet.* **19**, 271-273 (1998).

70. Sakamoto, M., Hosoda, Y., Kojimahara, K., Yamazaki, T. & Yoshimura, Y. Arthritis and ankylosis in twy mice with hereditary multiple osteochondral lesions: with special reference to calcium deposition. *Pathol. Int.* **44**, 420-427 (1994).

71. Furusawa, N., Baba, H., Imura, S. & Fukuda, M. Characteristics and mechanism of the ossification of posterior longitudinal ligament in the tip-toe walking Yoshimura (twy) mouse. *Eur. J. Histochem.* **40**, 199-210 (1996).

72. Johnson, K. *et al*. Linked deficiencies in extracellular PP(i) and osteopontin mediate pathologic calcification associated with defective PC-1 and ANK expression. *J. Bone Miner. Res.* **18**, 994-1004 (2003).

73. Sweet, H. O. & Green, M. C. Progressive ankylosis, a new skeletal mutation in the mouse. *J. Hered.* **72**, 87-93 (1981).

74. Hakim, F. T. *et al*. Hereditary joint disorder in progressive ankylosis (ank/ank) mice. I. Association of calcium hydroxyapatite deposition with inflammatory arthropathy. *Arthritis Rheum.* **27**, 1411-1420 (1984).

75. Mahowald, M. L., Krug, H. & Halverson, P. Progressive ankylosis (ank/ank) in mice: an animal model of spondyloarthropathy. II. Light and electron microscopic findings. *J. Rheumatol.* **16**, 60-66 (1989).

76. Sampson, H. W. & Davis, J. S. Histopathology of the intervertebral disc of progressive ankylosis mice. *Spine (Phila Pa. 1976)* **13**, 650-654 (1988).

77. Gurley, K. A. *et al*. Mineral formation in joints caused by complete or joint-specific loss of ANK function. *J. Bone Miner. Res.* **21**, 1238-1247 (2006).

78. Narisawa, S., Frohlander, N. & Millan, J. L. Inactivation of two mouse alkaline phosphatase genes and establishment of a model of infantile hypophosphatasia. *Dev. Dyn.* **208**, 432-446 (1997).

79. Fedde, K. N. *et al.* Alkaline phosphatase knock-out mice recapitulate the metabolic and skeletal defects of infantile hypophosphatasia. *J. Bone Miner. Res.* **14**, 2015-2026 (1999).

80. Vega, R. B. *et al*. Histone deacetylase 4 controls chondrocyte hypertrophy during skeletogenesis. *Cell* **119**, 555-566 (2004).

81. Jenuwein, T. & Allis, C. D. Translating the histone code. *Science* **293**, 1074-1080 (2001).

82. Etchegaray, J. P., Lee, C., Wade, P. A. & Reppert, S. M. Rhythmic histone acetylation underlies transcription in the mammalian circadian clock. *Nature* **421**, 177-182 (2003).

83. Ueta, C. *et al*. Skeletal malformations caused by overexpression of Cbfa1 or its dominant negative form in chondrocytes. *J. Cell Biol.* **153**, 87-100 (2001).

84. Luo, G. *et al*. Spontaneous calcification of arteries and cartilage in mice lacking matrix GLA protein. *Nature* **386**, 78-81 (1997).

85. Schinke, T., McKee, M. D. & Karsenty, G. Extracellular matrix calcification: where is the action? *Nat. Genet.* **21**, 150-151 (1999).

86. Munroe, P. B. *et al*. Mutations in the gene encoding the human matrix Gla protein cause Keutel syndrome. *Nat. Genet.* **21**, 142-144 (1999).

87. Sharma, P. & Maffulli, N. Tendon injury and tendinopathy: healing and repair. *J. Bone Joint Surg. Am.* **87**, 187-202 (2005).

88. Alsalameh, S., Amin, R., Gemba, T. & Lotz, M. Identification of mesenchymal progenitor cells in normal and osteoarthritic human articular cartilage. *Arthritis Rheum.* **50**, 1522-1532 (2004).

89. Dowthwaite, G. P. *et al*. The surface of articular cartilage contains a progenitor cell population. *J. Cell. Sci.* **117**, 889-897 (2004).

90. Bi, Y. *et al*. Identification of tendon stem/progenitor cells and the role of the extracellular matrix in their niche. *Nat. Med.* **13**, 1219-1227 (2007).

91. Crawley, J. N. in *What's Wrong With My Mouse?* 47 (Wiley-Liss, Inc., United States of America, 2000).

92. Garcia, J. A. *et al*. Impaired cued and contextual memory in NPAS2-deficient mice. *Science* **288**, 2226-2230 (2000).

93. Kuro-o, M. *et al*. Mutation of the mouse klotho gene leads to a syndrome resembling ageing. *Nature* **390**, 45-51 (1997).

94. Klement, J. F. *et al*. Targeted ablation of the abcc6 gene results in ectopic mineralization of connective tissues. *Mol. Cell. Biol.* **25**, 8299-8310 (2005).

95. Sun, Y. *et al*. The mortality of MOP3 deficient mice with a systemic functional failure. *J. Biomed. Sci.* **13**, 845-851 (2006).

96. Kondratov, R. V., Kondratova, A. A., Gorbacheva, V. Y., Vykhovanets, O. V. & Antoch, M. P. Early aging and age-related pathologies in mice deficient in BMAL1, the core componentof the circadian clock. *Genes Dev.* **20**, 1868-1873 (2006).

97. Fitzgerald, P. A. in *CURRENT Medical Diagnosis & Treatment* (eds McPhee, S. J. & Papadakis, M. A.) (The McGraw-Hill Companies, Inc., 2011).

98. Shimada, T. *et al*. Targeted ablation of Fgf23 demonstrates an essential physiological role of FGF23 in phosphate and vitamin D metabolism. *J. Clin. Invest.* **113**, 561-568 (2004).

99. Sitara, D. *et al*. Homozygous ablation of fibroblast growth factor-23 results in hyperphosphatemia and impaired skeletogenesis, and reverses hypophosphatemia in Phex-deficient mice. *Matrix Biol.* **23**, 421-432 (2004).

100. Harri, M. *et al*. Effect of access to a running wheel on behavior of C57BL/6J mice. *Lab. Anim. Sci.* **49**, 401-405 (1999).

101. Chaudhry, F. A. *et al*. The vesicular GABA transporter, VGAT, localizes to synaptic vesicles in sets of glycinergic as well as GABAergic neurons. *J. Neurosci.* **18**, 9733-9750 (1998).

102. Oishi, K. *et al*. Genome-wide expression analysis of mouse liver reveals CLOCK-regulated circadian output genes. *J. Biol. Chem.* **278**, 41519-41527 (2003).

103. Miller, B. H. *et al.* Circadian and CLOCK-controlled regulation of the mouse transcriptome and cell proliferation. *Proc. Natl. Acad. Sci. U. S. A.* **104**, 3342-3347 (2007).

104. Panda, S. *et al.* Coordinated transcription of key pathways in the mouse by the circadian clock. *Cell* **109**, 307-320 (2002).

105. Mescher, A. L. in *Junqueira's Basic Histology: Text & Atlas* (ed Mescher, A. L.) (The McGraw-Hill Companies, Inc., United States of America, 2010).

106. Loeser, J., R.F. & Delbono, O. in *Hazzard's Geriatric Medicine and Gerontology* (eds Halter, J. B. et al.).

107. Lengner, C. J. *et al.* Primary mouse embryonic fibroblasts: a model of mesenchymal cartilage formation. *J. Cell. Physiol.* **200**, 327-333 (2004).

108. Gaur, T. *et al.* Secreted frizzled related protein 1 regulates Wnt signaling for BMP2 induced chondrocyte differentiation. *J. Cell. Physiol.* **208**, 87-96 (2006).

109. Denker, A. E., Haas, A. R., Nicoll, S. B. & Tuan, R. S. Chondrogenic differentiation of murine C3H10T1/2 multipotential mesenchymal cells: I. Stimulation by bone morphogenetic protein-2 in high-density micromass cultures. *Differentiation* **64**, 67-76 (1999).

110. Schmitt, B. *et al.* BMP2 initiates chondrogenic lineage development of adult human mesenchymal stem cells in high-density culture. *Differentiation* **71**, 567-577 (2003).

111. Zeng, L., Kempf, H., Murtaugh, L. C., Sato, M. E. & Lassar, A. B. Shh establishes an Nkx3.2/Sox9 autoregulatory loop that is maintained by BMP signals to induce somitic chondrogenesis. *Genes Dev.* **16**, 1990-2005 (2002).

112. Rey, G. *et al*. Genome-wide and phase-specific DNA-binding rhythms of BMAL1 control circadian output functions in mouse liver. *PLoS Biol.* **9**, e1000595 (2011).

113. Lu, X. *et al*. Identification of the homeobox protein Prx1 (MHox, Prrx-1) as a regulator of osterix expression and mediator of tumor necrosis factor alpha action in osteoblast differentiation. *J. Bone Miner. Res.* **26**, 209-219 (2011).

114. Martin, J. F., Bradley, A. & Olson, E. N. The paired-like homeo box gene MHox is required for early events of skeletogenesis in multiple lineages. *Genes Dev.* **9**, 1237-1249 (1995).

115. Zhang, Y. *et al*. SOX7, down-regulated in colorectal cancer, induces apoptosis and inhibits proliferation of colorectal cancer cells. *Cancer Lett.* **277**, 29-37 (2009).

116. Oltvai, Z. N., Milliman, C. L. & Korsmeyer, S. J. Bcl-2 heterodimerizes in vivo with a conserved homolog, Bax, that accelerates programmed cell death. *Cell* **74**, 609-619 (1993).

117. Rozen, S. & Skaletsky, H. J. in *Bioinformatics Methods and Protocols: Methods in Molecular Biology.* (eds Krawetz, S. & Misener, S.) 365-386 (Humana Press, Totowa, NJ, 2000).

118. Spandidos, A., Wang, X., Wang, H. & Seed, B. PrimerBank: a resource of human and mouse PCR primer pairs for gene expression detection and quantification. *Nucleic Acids Res.* **38**, D792-9 (2010).

119. Kondratov, R. V. & Antoch, M. P. The clock proteins, aging, and tumorigenesis. *Cold Spring Harb. Symp. Quant. Biol.* **72**, 477-482 (2007).

120. Hogenesch, J. B., Gu, Y. Z., Jain, S. & Bradfield, C. A. The basic-helix-loop-helix-PAS orphan MOP3 forms transcriptionally active complexes with circadian and hypoxia factors. *Proc. Natl. Acad. Sci. U. S. A.* **95**, 5474-5479 (1998).

121. Liu, A. C. *et al*. Intercellular coupling confers robustness against mutations in the SCN circadian clock network. *Cell* **129**, 605-616 (2007).

122. Debruyne, J. P. Oscillating perceptions: the ups and downs of the CLOCK protein in the mouse circadian system. *J. Genet.* **87**, 437-446 (2008).

123. Miller, R. A. in *Hazzard's Geriatric Medicine and Gerontology* (eds Halter, J. B. et al.), 2009).

124. Dubrovsky, Y. V., Samsa, W. E. & Kondratov, R. V. Deficiency of circadian protein CLOCK reduces lifespan and increases age-related cataract development in mice. *Aging (Albany NY)* **2**, 936-944 (2010).

125. Kondratov, R. V. A role of the circadian system and circadian proteins in aging. *Ageing Res. Rev.* **6**, 12-27 (2007).

126. Yu, E. A. & Weaver, D. R. Disrupting the circadian clock: Gene-specific effects on aging, cancer, and other phenotypes. *Aging (Albany NY)* (2011).

127. Weindruch, R., Walford, R. L., Fligiel, S. & Guthrie, D. The retardation of aging in mice by dietary restriction: longevity, cancer, immunity and lifetime energy intake. *J. Nutr.* **116**, 641-654 (1986).

128. Kondratov, R. V., Vykhovanets, O., Kondratova, A. A. & Antoch, M. P. Antioxidant N-acetyl-L-cysteine ameliorates symptoms of premature aging associated

with the deficiency of the circadian protein BMAL1. *Aging (Albany NY)* **1**, 979-987 (2009).

129. Keller, M. *et al.* A circadian clock in macrophages controls inflammatory immune responses. *Proc. Natl. Acad. Sci. U. S. A.* **106**, 21407-21412 (2009).

130. Strom, T. M. *et al.* Pex gene deletions in Gy and Hyp mice provide mouse models for X-linked hypophosphatemia. *Hum. Mol. Genet.* **6**, 165-171 (1997).

131. Liu, S. *et al.* Regulation of fibroblastic growth factor 23 expression but not degradation by PHEX. *J. Biol. Chem.* **278**, 37419-37426 (2003).

132. Urakawa, I. *et al.* Klotho converts canonical FGF receptor into a specific receptor for FGF23. *Nature* **444**, 770-774 (2006).

133. Lanske, B. & Razzaque, M. S. Premature aging in klotho mutant mice: cause or consequence? *Ageing Res. Rev.* **6**, 73-79 (2007).

134. Razzaque, M. S. & Lanske, B. Hypervitaminosis D and premature aging: lessons learned from Fgf23 and Klotho mutant mice. *Trends Mol. Med.* **12**, 298-305 (2006).

135. Liang, G., Katz, L. D., Insogna, K. L., Carpenter, T. O. & Macica, C. M. Survey of the enthesopathy of X-linked hypophosphatemia and its characterization in Hyp mice. *Calcif. Tissue Int.* **85**, 235-246 (2009).

136. Sudo, H., Kodama, H. A., Amagai, Y., Yamamoto, S. & Kasai, S. In vitro differentiation and calcification in a new clonal osteogenic cell line derived from newborn mouse calvaria. *J. Cell Biol.* **96**, 191-198 (1983).

137. Atsumi, T., Miwa, Y., Kimata, K. & Ikawa, Y. A chondrogenic cell line derived from a differentiating culture of AT805 teratocarcinoma cells. *Cell Differ. Dev.* **30**, 109-116 (1990).

138. Gupta, R., Caiozzo, V. & Skinner, H. B. in *CURRENT Diagnosis & Treatment in Orthopedics* (ed Skinner, H. B.) (The McGraw-Hill Companies, Inc., The United States of America, 2006).

139. Jelinsky, S. A., Archambault, J., Li, L. & Seeherman, H. Tendon-selective genes identified from rat and human musculoskeletal tissues. *J. Orthop. Res.* **28**, 289-297 (2010).

140. Docheva, D., Hunziker, E. B., Fassler, R. & Brandau, O. Tenomodulin is necessary for tenocyte proliferation and tendon maturation. *Mol. Cell. Biol.* **25**, 699-705 (2005).

141. Baumeister, A., Arber, S. & Caroni, P. Accumulation of muscle ankyrin repeat protein transcript reveals local activation of primary myotube endcompartments during muscle morphogenesis. *J. Cell Biol.* **139**, 1231-1242 (1997).

142. Richette, P., Bardin, T. & Doherty, M. An update on the epidemiology of calcium pyrophosphate dihydrate crystal deposition disease. *Rheumatology (Oxford)* **48**, 711-715 (2009).

143. Couto, A. R. & Brown, M. A. Genetic factors in the pathogenesis of CPPD crystal deposition disease. *Curr. Rheumatol. Rep.* **9**, 231-236 (2007).

144. Dixit, R. K. in *CURRENT Rheumatology Diagnosis & Treatment* (eds Imboden, J. B., Hellmann, D. B. & Stone, J. H.) (The McGraw-Hill Companies, Inc., The United States of America, 2007).

145. Hu, S. S., Tribus, C. B., Tay, B. K. & Bhatia, N. N. in *CURRENT Diagnosis & Treatment in Orthopedics* (ed Skinner, H. B.) (The McGraw-Hill Companies, Inc., The United States of America, 2006).

146. Taurog, J. D. in *Harrison's Principles of Internal Medicine* (eds Fauci, A. S. et al.) (The McGraw-Hill Companies, Inc., The United States of America, 2008).

147. Anderson, H. C., Hsu, H. H., Morris, D. C., Fedde, K. N. & Whyte, M. P. Matrix vesicles in osteomalacic hypophosphatasia bone contain apatite-like mineral crystals. *Am. J. Pathol.* **151**, 1555-1561 (1997).

148. Eicher, E. M., Southard, J. L., Scriver, C. R. & Glorieux, F. H. Hypophosphatemia: mouse model for human familial hypophosphatemic (vitamin D-resistant) rickets. *Proc. Natl. Acad. Sci. U. S. A.* **73**, 4667-4671 (1976).

149. Komori, T. *et al*. Targeted disruption of Cbfa1 results in a complete lack of bone formation owing to maturational arrest of osteoblasts. *Cell* **89**, 755-764 (1997).

150. St-Jacques, B., Hammerschmidt, M. & McMahon, A. P. Indian hedgehog signaling regulates proliferation and differentiation of chondrocytes and is essential for bone formation. *Genes Dev.* **13**, 2072-2086 (1999).

151. Rosati, R. *et al*. Normal long bone growth and development in type X collagen-mice. *Nat. Genet.* **8**, 129-135 (1994).

152. Peacock, J. D., Levay, A. K., Gillaspie, D. B., Tao, G. & Lincoln, J. Reduced sox9 function promotes heart valve calcification phenotypes in vivo. *Circ. Res.* **106**, 712-719 (2010).